Fiammetta Venuti

Crowd-Structure Interaction in lively footbridges

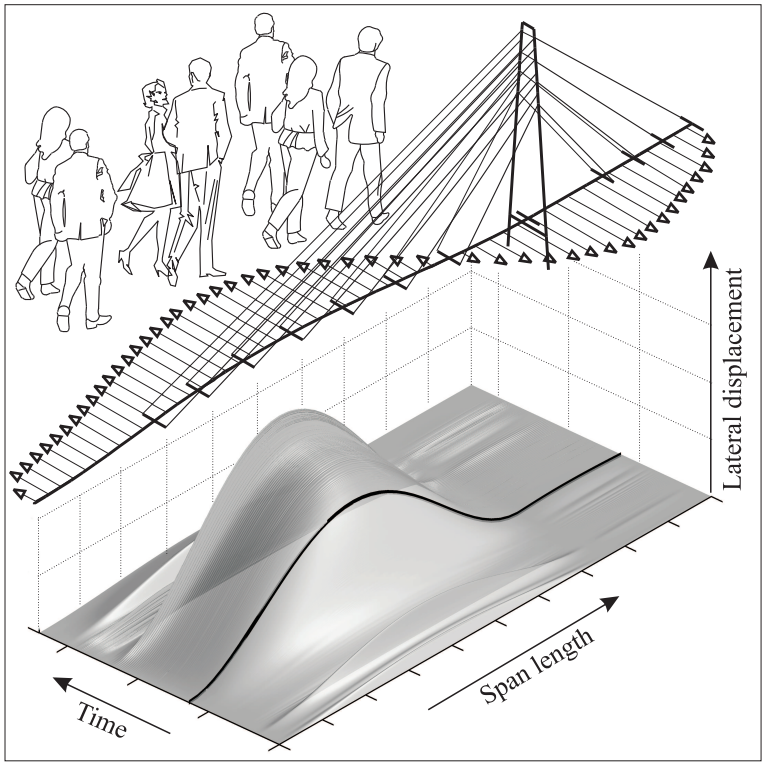

Dottorato di Ricerca in Ingegneria delle Strutture
Politecnico di Torino

Fiammetta Venuti

Crowd-Structure Interaction in lively footbridges

Tesi per il conseguimento del titolo di Dottore di Ricerca
XX Ciclo (A.A. 2005, 2006, 2007)

Dottorato di Ricerca in Ingegneria delle Strutture
Politecnico di Torino

Dicembre 2007

Dottorato di Ricerca in Ingegneria delle Strutture
Politecnico di Torino, Corso Duca degli Abruzzi 24, 10129, Torino

Tutori:	Prof. Paolo Napoli (ICAR/09)
	Prof. Nicola Bellomo (MAT/07)
Coordinatore:	Prof. Alberto Carpinteri

Ringraziamenti

Desidero in primo luogo ringraziare Luca Bruno, che ha seguito il mio percorso degli ultimi anni con grande determinazione, assiduità ed entusiasmo.

Un ringraziamento speciale è rivolto a Walter Ceretto, docente eccezionale, per avermi trasmesso una piccola parte della sua trascinante passione per le strutture.

Grazie agli amici del Dipartimento di Ingegneria Strutturale, Davide Bigaran, Mario Sassone, Alberto Spadafora, Roberto Spadavecchia e l'insostituibile Fernanda, per avere contribuito a creare un ambiente di lavoro stimolante, spensierato e privo di competizione.

Grazie agli amici dottorandi del Dipartimento di Matematica, Davide Fransos e Andrea Tosin, per le ore dedicate ad introdurmi ai misteri delle equazioni iperboliche.

Infine, non posso non ringraziare i miei tutori, Paolo Napoli, per la fiducia incondizionata che ha sempre riposto nelle mie capacità, e Nicola Bellomo, prezioso consulente scientifico senza il quale questo lavoro non sarebbe stato possibile.

Sommario

Il presente lavoro di tesi affronta il problema della modellazione matematica e computazionale di fenomeni di interazione folla-struttura sulle passerelle pedonali. In particolare, si fa riferimento al fenomeno di *eccitazione laterale sincronizzata*, recentemente portato all'attenzione della comunità scientifica internazionale in seguito alla chiusura del Millennium Bridge di Londra il giorno della sua inaugurazione. Il fenomeno, osservato a partire dagli anni Settanta anche su ponti stradali occasionalmente attraversati dalla folla, può interessare qualunque ponte con frequenza laterale prossima a quella laterale del passo (≈ 1 Hz), caricato con un sufficiente numero di pedoni.

Il problema è stato finora affrontato con un approccio empirico, attraverso prove di laboratorio su tapis-roulant per misurare la forzante laterale esercitata da un pedone, attraverso prove *in situ* su passerelle pedonali o tramite l'osservazione di video registrati in occasione di grande affollamento. I risultati ottenuti sono serviti a comprendere meglio l'evoluzione del fenomeno, che è dovuto all'insorgere di due tipi di sincronizzazione: la prima tra pedoni, in presenza di elevata densità di folla che ne limita la libertà di movimento; la seconda tra pedoni e struttura (lock-in), quando i pedoni per mantenere l'equilibrio camminano inconsciamente con la stessa frequenza di oscillazione del ponte. Entrambi i tipi di sincronizzazione hanno l'effetto di produrre un incremento della forzante esercitata dai pedoni, con conseguente aumento delle oscillazioni. Il fenomeno, quindi, si autoalimenta ma, fortunatamente, è autolimitato: infatti, quando le oscillazioni superano una certa intensità, i pedoni si fermano per l'impossibilità di mantenere l'equilibrio. È per questo motivo che l'eccitazione laterale sincronizzata difficilmente implica problemi di sicurezza strutturale, ma riguarda prevalentemente problemi di comfort per gli utenti.

I codici e le linee guida internazionali affrontano il problema principalmente fissando dei criteri di comfort e proponendo modelli di carico da utilizzare in fase progettuale. I modelli di forza finora proposti hanno, però, delle limitazioni: non distinguono i due tipi di sincronizzazione sopracitati; non permettono di modellare l'innesco del lock-in e la successiva autolimitazione della forzante; non tengono in conto di eventuali fenomeni non-lineari di traffico dovuti alla disomogeneità della distribuzione spaziale della folla.

Il presente lavoro si propone di ovviare ad alcuni dei problemi enunciati, tramite la proposta di un modello accoppiato di interazione folla-struttura, che possa descrivere il fenomeno in modo sufficientemente accurato e fornire un utile strumento

in fase di progettazione. La complessità del problema affrontato ha richiesto un approccio multidisciplinare, che ha portato a svolgere questo lavoro in cotutela con il Dipartimento di Matematica. Il modello proposto si basa sul disaccoppiamento del sistema complesso in sottosistemi interagenti tra loro. Il sottosistema Folla è descritto da un modello macroscopico basato sulla scrittura e chiusura dell'equazione di conservazione della massa, sfruttando l'analogia idrodinamica. Il sottosistema Struttura è descritto da un modello agli elementi finiti, la cui risposta nel tempo è rappresentata dalla soluzione dell'equazione del moto. I termini di interazione sono rappresentati da un lato dall'equazione di chiusura che lega la velocità di camminata alla densità della folla e alle oscillazioni del ponte, e dall'altro dal modello di forzante esercitata dai pedoni. Il modello matematico concepito è stato implementato in un codice di calcolo utilizzato per le simulazioni computazionali.

Nel **Capitolo 1** viene presentata un'introduzione al fenomeno studiato e alle problematiche finora insolute.

Il **Capitolo 2** presenta lo stato dell'arte degli studi relativi al comportamento del singolo pedone, alla dinamica delle folle e ai fenomeni di interazione folla-struttura dal punto di vista dell'analisi fenomenologica, dei modelli e delle normative internazionali.

Nel **Capitolo 3** viene fornita una descrizione dettagliata del modello matematico proposto in tutte le sue componenti.

Il **Capitolo 4** è dedicato all'approccio computazionale utilizzato per risolvere numericamente le equazioni che governano i sottosistemi Folla e Struttura.

Il **Capitolo 5** riporta i risultati delle simulazioni computazionali condotte. Le prime sono relative alla sola dinamica della folla per studiare le proprietà dell'equazione di chiusura adottata. Successivamente viene presentata un'applicazione del solo modello di forza a due casi studio e i risultati sono confrontati con quelli ottenuti da modelli in letteratura. Infine, il modello completo di interazione viene applicato alla simulazione di un evento reale occorso sul T-bridge in Giappone e lo stesso caso studio è utilizzato per condurre uno studio parametrico sulle diverse componenti del modello.

Le conclusioni e le prospettive di ricerca sono infine discusse nel **Capitolo 6**.

Gli aspetti originali di questo lavoro possono essere così sintetizzati:

- il modello matematico del sistema accoppiato folla-struttura si basa su un framework generale che può essere caratterizzato nelle singole componenti per simulare problemi specifici di interazione;

- la folla non è intesa semplicemente come un carico ma viene modellata come un sistema dinamico che evolve in spazio e tempo e interagisce con la struttura;

- il modello di forza proposto permette di tenere conto dei diversi tipi di sincronizzazione, dell'innesco del lock-in e dell'autolimitazione della forzante;

- il codice di calcolo sviluppato permette di valutare la risposta della struttura simulando casi reali o ipotizzando diversi scenari di comportamento e distribuzione della folla.

Summary

The topic of this work is the mathematical and computational modelling of crowd-structure interaction phenomena in lively footbridges. The problem of *synchronous lateral excitation* is addressed. This phenomenon has recently attracted scientific attention after the Millennium Bridge in London was closed the day it opened (June 2000), but it has been observed from the Seventies, even on road bridges that are occasionally crossed by crowds and it can occurr on any footbridge that has a natural frequency close to the lateral walking frequency (≈ 1 Hz) and which is loaded with a sufficient number of pedestrians.

The problem has so far been tackled with an empirical approach, by means of laboratory tests on treadmills to measure the lateral force exerted by one pedestrian, *in situ* tests on footbridges or the observation of videos recorded during crowd events. The obtained results have permitted the phenomenon to be better understood. The lateral vibrations are due to two kinds of synchronization: the first among pedestrians, when free walking is constrained by high crowd density; the second between pedestrians and the structure (lock-in), when pedestrians unconsciously walk with the same frequency as the structure in order to maintain balance. As a consequence, the force exerted by pedestrians increases, and in turn the vibrations grow. The phenomenon is therefore self-sustained, but fortunately it is also self-limited, that is, when the vibrations exceed a threshold value, pedestrians stop walking causing the vibrations to diminish. For this reason, synchronous lateral excitation has never caused structural failure, but only discomfort for the users.

International codes and guidelines treat the problem of human-induced lateral vibrations by proposing comfort requirements and load models. The latter have so far experienced some difficulties in taking into account some important features: the existence of two kinds of synchronization, triggering of the lock-in and its self-limited nature, modelling of non-linear traffic phenomena due to inhomogeneous distribution of the crowd density.

The aim of this work is to propose a coupled crowd-structure interaction model, which is able to take some of the aforementioned features of the phenomenon into account. The model aims at describing the problem with sufficient accuracy and proving a useful tool for footbridge designers. The complexity of the topic has required a multidisciplinary approach, and has been tackled with the support of the Department of Mathematics. The proposed model is based on the partitioning of the complex system into interacting subsystems. The Crowd subsystem is described by a macroscopic

model based on the derivation and closure of the mass conservation equation, in analogy to the principles of fluid dynamics. The Structure subsystem is described by a finite element model and its dynamic response is given by the solution of the equation of motion. The interacting terms are represented, on one hand, by the closure equation that links the walking velocity to the crowd density and deck lateral motion and, on the other hand, by the load model of the pedestrian lateral force. The mathematical model has been implemented in a code in order to perform computational simulations.

An introduction to the problem is presented in **Chapter 1**.

Chapter 2 is devoted to a review of the state-of-the-art concerning the behaviour of one pedestrian, the crowd dynamics and the crowd-structure interaction phenomena, as far as the phenomenological analysis, the models and the international codes are concerned.

A detailed analysis of the mathematical model in each of its parts is given in **Chapter 3**.

Chapter 4 is devoted to the computational approach used to solve the equations governing the two subsystems.

Chapter 5 illustrates the results of the performed computational simulations. The first ones only concern the crowd dynamics, in order to study the properties of the adopted closure equation. Then, the load model is applied to two case studies and the results are compared to those obtained with force models found in literature. Finally, the complete interaction model is applied to a real event that occurred on the T-bridge in Japan and the same benchmark is used to perform a sensitivity study on the model parameters.

Finally, the conclusions and research perspectives are discussed in **Chapter 6**.

The original features of this work can be summarized as follows:

- the mathematical model of the coupled system is based on a general framework that can be characterized by its components in order to simulate a specific interaction problem;
- the crowd is not simply viewed as a load, but is modelled as a dynamical system which evolves in space and time and interacts with the structure;
- the proposed force model allows the two kinds of synchronization, triggering of the lock-in and self-limitation of the force to be taken into account;
- the developed code allows the structural response to be calculated either through the simulation of actual cases or due to different scenarios of crowd behaviour and density.

Nomenclature

A	cross-section area
B	width of the footbridge road deck
C	structural damping
d	forward distance among walking pedestrians
d_0	body depth of a motionless pedestrian
d_c	characteristic dimension of a cluster of pedestrians
d_s	sensory distance
E	modulus of elasticity
F	lateral force exerted by pedestrians
F_{pp}	lateral force component due to pedestrians synchronized among each other
F_{ps}	lateral force component due to pedestrians synchronized with the structure
F_{rms}	root mean square value of $F(t)$
F_s	lateral force component due to uncorrelated pedestrians
$\bar{F}_s$	lateral force exerted by a single pedestrian on motionless deck
f_p	step frequency
f_{pl}	lateral step frequency
f_r	frequency ratio f_{pl}/f_s
f_s	structural natural frequency of interest
g	corrective factor that sensitises v to the deck motion
I_y, I_z	cross section moments of inertia
K	structural stiffness
L	length of the footbridge span
l_p	step length
M	mass of the crowd-structure system
M_c	crowd mass
M_s	structural mass
n	total number of pedestrians
n_{pp}	number of pedestrians synchronised to each other
n_{ps}	number of pedestrians synchronised to the structure
n_s	number of uncorrelated pedestrians
q	crowd flow
q_{ca}	capacity flow

S	area occupied by a walking pedestrian
S_0	area occupied by a motionless pedestrian
S_{pp}	coefficient of synchronization among pedestrians
S_{ps}	coefficient of synchronization between the pedestrians and the structure
$s, \dot{s}, \ddot{s}$	structural displacements, velocities and accelerations
T	axial force in cables
T_c	crowd characteristic time
T_s	period of the structural mode
t	time
t_r	time at which pedestrians stop because of excessive deck vibrations
u	crowd density
u_c	critical density, upper limit for unconstrained free walking
u_{ca}	capacity density
u_M	jam density
u_{sync}	crowd density corresponding to complete synchronization among pedestrians
v	pedestrian velocity
v_M	free speed
$\bar{v}_M$	average free speed
w	lateral width occupied by a walking pedestrian
w_0	lateral width occupied by a motionless pedestrian
x	space coordinate along the footbridge length
$z, \dot{z}, \ddot{z}$	deck lateral displacement, velocity and acceleration
$\dot{z}_c, \ddot{z}_c$	thresholds of motion perception
$\dot{z}_M, \ddot{z}_M$	maximum values of the deck lateral velocity and acceleration
$\dot{z}_s, \ddot{z}_s$	serviceability limits on the deck lateral velocity and acceleration
α_G, α_T	coefficients of geography and travel affecting v_M
β_G, β_T	coefficients of geography and travel affecting S
Δt_r	stop-and-go time interval
δ	space dislocation in the closure equation
γ	parameter of travel purpose in the Kladek closure equation
ν	envelope of $\dot{z}(t)$
ρ	mass density
τ	time delay
ζ	envelope of $\ddot{z}(t)$
ξ	damping ratio

Contents

1 Introduction **1**

2 State-of-the-art **5**

2.1 Phenomenological observation 5

2.1.1 Single pedestrian behaviour on motionless platforms 5

2.1.2 Crowd behaviour 8

2.1.3 Crowd-structure interaction: the synchronous lateral excitation phenomenon 14

2.2 Physical-mathematical models 21

2.2.1 Structural models 21

2.2.2 Crowd models 23

2.2.3 Force models 27

2.2.4 Coupled mechanical systems 31

2.3 Design codes and guidelines 33

3 Crowd-Structure Interaction (CSI) Model **35**

3.1 The Structure subsystem 36

3.2 The Crowd subsystem 36

3.3 Structure-to-Crowd action: the closure equation 37

3.3.1 Physical-based model of the pedestrian fundamental relation . 37

3.3.2 Comparison with fundamental laws revisited 42

3.3.3 Space dislocation and time delay 45

3.4 Crowd-to-Structure action: the force model 47

4 Computational approach **53**

4.1 Partitioned simulation strategies 53

4.2 Space and time grids 54
4.3 Computational Structural Dynamics (CSD) solver 56
4.4 Computational Crowd Dynamics (CCD) solver 58
4.4.1 Grid effects on a model equation 60

5 Applications and results 63
5.1 Crowd dynamics on a motionless platform 63
5.2 Application of the force model 64
5.3 Complete computational simulation on the T-bridge (Japan) 72
5.3.1 Description of the case study 72
5.3.2 Simulation of an actual event 77
5.3.3 Sensitivity studies on the model parameters 84

6 Conclusions 103

A The derivation of the mass conservation equation 105
A.1 Integral and differential forms 105
A.2 Scalar conservation laws 106
A.3 Burgers' equation 107

Chapter 1

Introduction

The problem of lateral vibrations induced by pedestrians who walk on crowded footbridges has attracted increasing public attention in the last few decades (Živanović et al., 2005) from the earliest cases in the nineties (Fujino et al., 1993) up to the well-known case of the London Millennium Bridge which was opened on 10 June 2000 (Dallard et al., 2001). The growing frequency of occurrence of these phenomena is primarily due to the increasing strength of new structural materials and the longer spans of new footbridges, accompanied by aesthetic requirements for greater slenderness. Up to date, such kinds of dynamic lateral loads have never involved structural failure, but have often caused discomfort for the users and the temporary closure of the footbridges. Neverthless, this reduced serviceability represents a severe problem for its economic and social outcomes, bearing in mind that these structures often represent a "visiting card" of the town where they are built and that large crowds generally gather during the opening day of a structure. The aforementioned reasons have motivated recent and intense research activities, to date mainly developed in the field of civil engineering and structural dynamics. The extensive scientific literature published in recent years, and recently reviewed by Živanović et al. (2005), testifies this effort and provides a useful background to comment on the approaches that are actually employed and to introduce the one proposed in this work.

The problem has generally been tackled using an empirical approach. The studies can roughly be classified according to the addressed scales of the phenomenological observation of the system: the small scale (i.e. the behaviour of the single pedestrian) and the large scale (i.e. the crowd-structure interaction and the structural response).

The measurements of the forces exerted by one pedestrian walking on a fixed or moving platform belong to the first class of studies. Walking forces on motionless platforms have been extensively studied in the field of biomechanics together with that of footbridge dynamics (e.g. Andriacchi et al., 1997).
Laboratory tests involving a single pedestrian walking on platforms or treadmills

forced to move laterally (e.g. in Dallard et al. 2001, McRobie et al. 2003, Pizzimenti and Ricciardelli 2005) allow important data about the relationship between the platform motion and the lateral force component to be obtained. In an attempt to maintain body balance on the laterally moving platform, the pedestrian adapts his step frequency to that of the platform (lock-in) and he walks with his legs more widespread. Hence, the lateral motion of the upper part of the torso increases and the resulting force in turn grows. The same tests point out that different pedestrians can show different sensitivities to platform motion, so that a factor is introduced to describe the degree of synchronization, i.e. to estimate the mean probability that individuals will synchronise their footfall rates to the swaying rate of the platform (Dallard et al., 2001).

As far as the second class of studies is concerned, observation of videos recorded during crowd events has made it possible to qualitatively point out the great complexity of the overall mechanical system, mainly due to the two-way interaction between the crowd and the structure and to the non homogeneous crowd distribution along the deck (density, velocity). In particular, the motion of each pedestrian is affected by the presence of the surrounding people, especially by the flow of the pedestrians in front. The higher the crowd density, the more likely it is that pedestrians can see each other, walk shoulder-to-shoulder and subconsciously synchronize their pacing rate. Hence, a second kind of synchronization takes place, apart from the one between each pedestrian and the structure. An attempt to take into account the effects of the crowd density on synchronization among pedestrians was made by Grundmann et al. (1993): three human-induced force models, which correspond to different but spatially homogeneous pedestrian densities and that have to be separately considered, were proposed. Hence, the problem of actual non homogeneous crowd still remains open.

According to the author, the models proposed so far encountered some difficulties in taking some important aspects of the problem into account, i.e. the self-organization effects that occur in pedestrian flow. These effects could be induced due to the features of the deck (e.g. shape, slope, presence of obstacles) or to the deck vibrations. They may involve discontinuities of the crowd density and velocity along the deck up to obstructions, traffic jams or stop-and-go phenomena. From this point of view, pedestrians cannot be simply described by means of a given force model but need to be directly modelled as a part of the complex dynamic system.

Traffic dynamics have been extensively analysed and modelled for vehicular flows in the field of applied mathematics and transportation engineering since the beginning of the 1970s. A useful background of the field of research is provided by Prigogine and Herman (1971), Leutzbach (1988), Bellomo et al. (2002) and Helbing et al. (2002). Generally speaking, the models developed in literature describe the evolution in time and space of the flow conditions, i.e. car density and velocity. The first task in modelling granular traffic flows is to select the correct observation and representation scale, the choice of which determines three different framework classes. A

microscopic description corresponds to modelling the dynamics of each single vehicle under the action of the surrounding vehicles. A statistical or mesoscale description, in a framework close to the one of the kinetic theory of gases, consists of the derivation of an evolution equation for the probability distribution function on the position and velocity of a vehicle along a road. A macroscopic description, which is analogous to that of fluid dynamics, refers to the derivation, on the basis of conservation equations and material models, of an evolution equation for the mass density, linear momentum and energy, regarded as macroscopic observable quantities of the flow of vehicles assumed to be continuous. All the above mentioned approaches have been extended to the simulation of crowd dynamics in recent years (Helbing, 2001). Macroscopic modelling has been applied since the pioneering works of Henderson (1974). Hoogendoorn and Bovy (2000), among others, applied the mesoscale description to pedestrian traffic. A relevant number of models have been developed in recent years in the framework of the microscopic description, such as the social force model (Helbing, 1991) or the cellular automata model (Blue and Adler, 1998). In the last decade, special attention has been devoted to the microsimulation of pedestrian crowds, since it is more flexible and may be easily applied to panic conditions and emergency evacuation. To the best of the author's knowledge, up to now none of the three previously mentioned frameworks has been applied to crowd-structure interaction.

This work deals with the proposal of a mathematical model of crowd-structure interaction and its implementation in a computational code. The model aims at representing the complex multiphysical non-linear dynamic system to give, on one hand, a detailed description of the crowd flow along the deck and its effects on the structural dynamics and, on the other, to obtain synthetic results that are useful for engineers and designers. The general modelling framework is based on the mathematical and numerical partitioning of the coupled system into two subsystems, the Crowd and the Structure, which interact between each other by means of suitably defined interacting terms: the structure-to-crowd action develops through the constitutive law that links pedestrian velocity to crowd density and deck motion; the crowd-to-structure action takes place through the definition of a force model. Each part of the framework is characterized in order to simulate the synchronous lateral excitation phenomenon. In particular, the proposed force model is conceived in order to take into account both kinds of synchronization, the triggering of the lock-in and the self-limited nature of the pedestrian lateral force. Furthermore, the modelling of the crowd as part of the overall dynamical system allows the aforementioned effects of pedestrian self-organization to be taken into account.

Chapter 2

State-of-the-art

This chapter is not intended to be an exhaustive treatment of the great number of studies found in literature, which belong to different research fields and to different scales of the phenomenological observation of the system. The aim is to provide a brief review of the main topics, addressed to the development of the work proposed in this thesis. In order to provide a clear exposition, the chapter is organized into the following sections:

- Phenomenological observation;
- Models;
- Design codes and guidelines.

2.1 Phenomenological observation

This section is devoted to a brief review of the studies concerning the phenomenological description of the crowd-structure interaction phenomenon, named synchronous lateral excitation. In the following they are roughly classified into three categories, corresponding to the different scales of observation: the studies concerning the behaviour of a single pedestrian, those relative to the crowd behaviour and the ones concerning crowd-structure interaction.

2.1.1 Single pedestrian behaviour on motionless platforms

When a pedestrian walks, he produces a dynamic time varying force which has components in all three directions: vertical, horizontal-lateral and horizontal-longitudinal. Many studies have focused on the measurement of the single pedestrian walking force

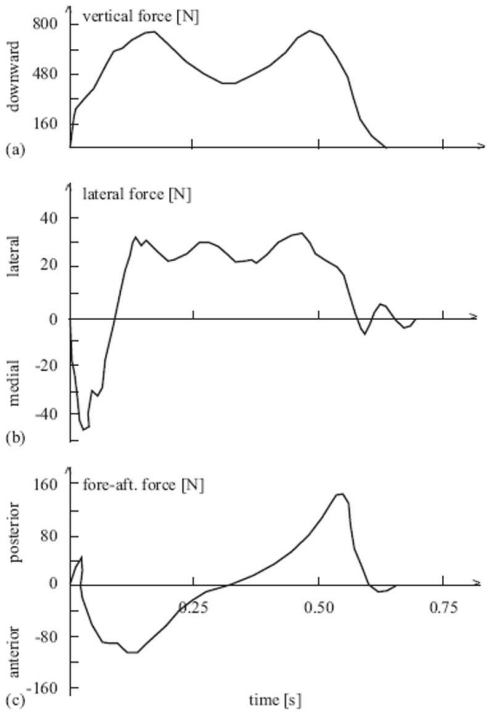

Figure 2.1. Typical shapes of walking force in (a) vertical, (b) lateral and (c) longitudinal direction (after Andriacchi et al., 1997)

by means of force plates or treadmills, in particular on the vertical component, which has the highest magnitude. Since a complete review of these studies can be found in Živanović et al. (2005), only a brief summary is made in the following, with particular attention to those related to the lateral force component.

A lot of research on bipedal locomotion and walking forces has been carried out in the field of biomechanics (e.g. Andriacchi et al. 1997; Belli et al. 2001; Bauby and Kuo 2000; Ebrahimpour and Fitts 1996; Ebrahimpour et al. 1996; Masani et al. 2002; Vaughan 2003). For instance, Andriacchi et al. (1997) measured single step walking forces in all three directions by means of a force plate (Fig. 2.1). They reported that step length and peak force magnitude increase with incresing walking velocity. A similar conclusion was also reached by Wheeler (1982), who stressed that, with increasing step frequency, the peak amplitude, step length and velocity increase (Fig. 2.2).

The importance of establishing a relationship between the walking frequency, velocity and step length is therefore clear. As for the walking frequency, we refer to a vertical frequency, that is, the number of times a foot touches the ground in a time

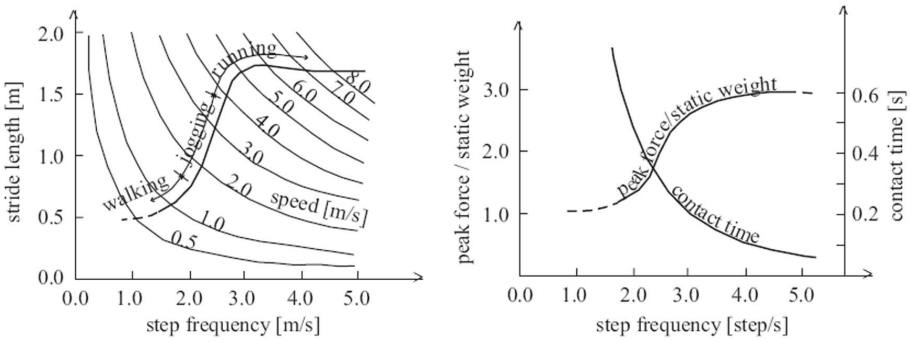

Figure 2.2. Dependance of stride length, velocity, peak force and contact time on different pacing rates (after Wheeler, 1982)

unit, and a horizontal frequency, that is, the number of times the same foot touches the ground. The lateral step frequency is therefore half the vertical frequency. A reliable statistical description was given by Matsumoto et al. (1978), who analyzed a sample of 505 people, and concluded that the vertical frequencies follow a normal distribution, with a mean of 2 Hz and a standard deviation of 0.173 Hz. Similar investigations were performed by Pachi and Ji (2005), who measured the walking frequency and velocity of 800 people walking unobserved: they found different values of step length, speed and walking frequency depending on the kind of floor (shopping centre floors or footbridges) and on the sex. Walking velocity is linked to the walking frequency f and step length l by the simple relation $v = fl$. Bertram and Ruina (2001) obtained different walking speed-frequency relations under different constrained circumstances (fixed v, f or l). This result stresses the complexity of pedestrian walking behaviour once more.

If we assume the perfect periodicity of the force, both the vertical and the lateral component can be represented by a Fourier series , respectively:

$$F_v(t) = F_0 + \sum_i F_{i,v}(2\pi i f t - \varphi_i) \tag{2.1}$$

$$F_h(t) = \sum_i F_{i,h}(2\pi i \frac{f}{2} t - \varphi_i) \tag{2.2}$$

Many researches have tried to quantify the Dynamic Load Factors (DLFs), i.e. the ratio of the force amplitude to the weight of a person, of the vertical component first harmonics, but only a few have reported results concerning the lateral component. Among them, it is worth citing Bachmann and Ammann (1987), who measured the first five harmonics for the lateral direction and reported a dominance of the first and third harmonics ($DLF_1 = 0.039$, $DLF_2 = 0.01$, $DLF_3 = 0.043$, $DLF_4 = 0.012$, $DLF_5 = 0.015$). Sétra (2006) recommends taking into account the first four harmonics

to achieve a loading function that is sufficiently close to the force measurements. After the London Millennium Bridge opening, various attempts have been made to characterize the lateral force component. One of the most recent studies in this direction is that of Pizzimenti (2005). In his PhD thesis, Pizzimenti measured the lateral force of a sample of 66 pedestrians walking on a treadmill, and showed that the hypothesis of perfect periodicity is unlikely.

2.1.2 Crowd behaviour

It is widely accepted that the behaviour of a pedestrian walking within a crowd is different from that of a pedestrian walking alone. Walking velocity is affected by crowd density, which means that the higher the crowd density, the lower the walking velocity. Another important aspect is that, when a pedestrian's walking is constrained because of high density, people tend to walk with the same frequency and a null relative phase angle, that is, they synchronize to each other. While the latter feature has not yet been deeply investigated or understood, many studies have been directed to the determination of a law that links the walking velocity to the crowd density. Most of these studies belong to the tranportation research field, with the aim of controlling the layout and dimensions of pedestrian walking facilities (e.g. Weidmann 1993, Daamen 2004). In recent years, research has been directed to the study of crowd flow patterns in emergency situations (e.g. Fang et al., 2003).

Let us consider a stationary and homogeneous pedestrian traffic flow. For each type of flow, the so-called *fundamental relation* is valid:

$$q = uv \tag{2.3}$$

where q is the flow, intended as the number of pedestrians passing a cross-section of an area in a unit of time [ped/ms]; u is the crowd density [ped/m^2]; v is the average walking velocity [m/s]. The three variables are macroscopic characteristics of the flow: the graphical representations of their relations are called the *fundamental diagrams*. Looking at the flow-density diagram in Fig. 2.3, some relevant quantities can be identified (Daamen, 2004):

- free speed v_M: the slope of the function $q(u)$ at the origin that corresponds to the mean velocity if $q = 0$ ped/ms and $u = 0$ ped/m^2;
- critical density u_c: the lower bound for unconstrained free walking. For $u < u_c$, pedestrians walk with constant free speed $v = v_M$ (*stable region*); for $u > u_c$, the walking speed decreases with increasing density (*unstable region*);
- capacity speed v_{ca} and density u_{ca}: the speed and density when $q = q_{ca}$, that is, the maximum flow. The region of density under u_{ca} is called *free flow region*, while the *congestion region* corresponds to a higher density than the capacity density;

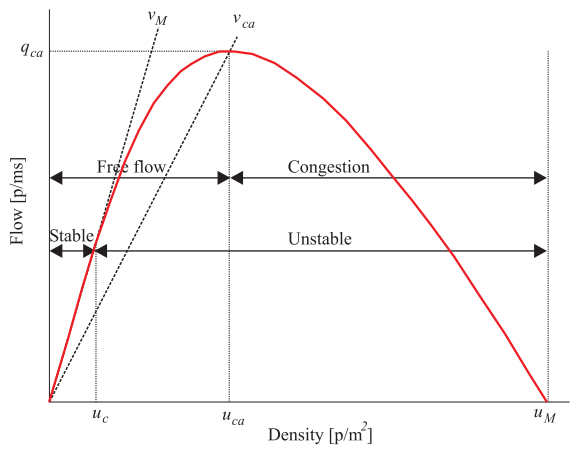

Figure 2.3. Flow-density fundamental diagram

- jam density u_M: the maximum admissible density corresponding to null speed and flow.

It is worth noting that, in the flow-density fundamental diagram, the walking speeds can be read by evaluating the slope of the straight lines passing through the origin.

The determination of the values of the aforementioned variables is not a simple task, since walking behaviour is influenced by a great number of factors, such as age, culture, gender, travel purpose, type of infrastructure and walking direction, as pointed out by Weidmann (1993) and Daamen (2004). In particular, several studies have been directed to the determination of free speeds. According to Weidmann, the observed free walking speeds appear to follow a normal distribution with an estimated mean of 1.34 m/s and a standard deviation of 0.37 m/s (Daamen 2004, Buchmueller and Weidmann 2006). As an example, Table 2.1 classifies the free speeds as a function of the travel purpose and the cultural and ratial differences, respectively.
It is worthwhile pointing out that the observed free speeds are almost always underestimated, since they are determined by extrapolating the found speed-density relation to the null density area, as highlighted by Daamen and Hoogendoorn (2006).They in fact estimated, with a new method, higher free speeds than those found in literature (1.57 m/s istead of 1.49 m/s for unidirectional flow).

As far as the jam densities are concerned, they have been estimated to vary between 4 and 5.4 ped/m^2 (see Table 12 in Buchmueller and Weidmann, 2006). The average human body in the world has a width of 45.6 cm and a depth of 28.2 cm (see Table 1 in Buchmueller and Weidmann, 2006). These dimensions refer to a motionless pedestrian. The maximum pedestrian density could be derived from the minimum average body surface (0.13 m^2): this leads to a density of 7.69 ped/m^2, that is diffi-

Table 2.1. Example of classification of free speeds [m/s] (Buchmueller and Weidmann 2006, Daamen 2004)

Geographic area	**Free speed**	**Travel purpose**	**Free speed**
Europe	1.41	Business district	1.45 ÷ 1.61
United States	1.35	Commuters	1.34 ÷ 1.49
Australia	1.44	Shoppers	1.04 ÷ 1.16
Asia	1.24	Leisure	0.99 ÷ 1.10

cult to obtain in practice, since people can hardly move at densities over 5 ped/m^2. When pedestrians are walking they require more lateral and forward space than a motionless person. The required lateral additional space has been estimated to be about 62% of the average width of pedestrians. The required forward space (distance among pedestrians d) instead depends on the walking velocity: a linear relation has been proposed by Seyfried et al. (2005), as a fitting to experimental data (Fig. 2.4), which is valid in the $0.1 < v < 1$ m/s domain:

$$d = 0.36 + 1.06v. \tag{2.4}$$

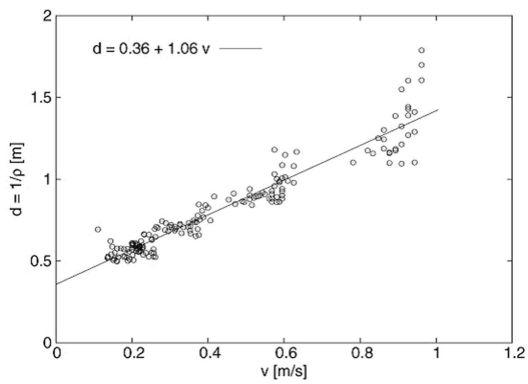

Figure 2.4. Relation between d and v, after (Seyfried et al., 2005)

Because of the great number of factors affecting pedestrian flows, rather different fundamental diagrams can be found in literature. A complete review of the

speed-density relations proposed so far can be found in Daamen (2004) and Buchmueller and Weidmann (2006). They are graphically represented in Fig.s 2.5 and 2.6: the experimental data classified with respect to the kind of pedestrian traffic (from Oeding 1963, Fang et al. 2003, Seyfried et al. 2005) (Fig. 2.5); the linear relations (from Daamen 2004, Buchmueller and Weidmann 2006) (Fig.2.6a); the non-linear laws (from Weidmann, 1993, Hughes, 2002) (Fig.2.6b). The proposed relations are also summarized in Tables 2.2 and 2.3.

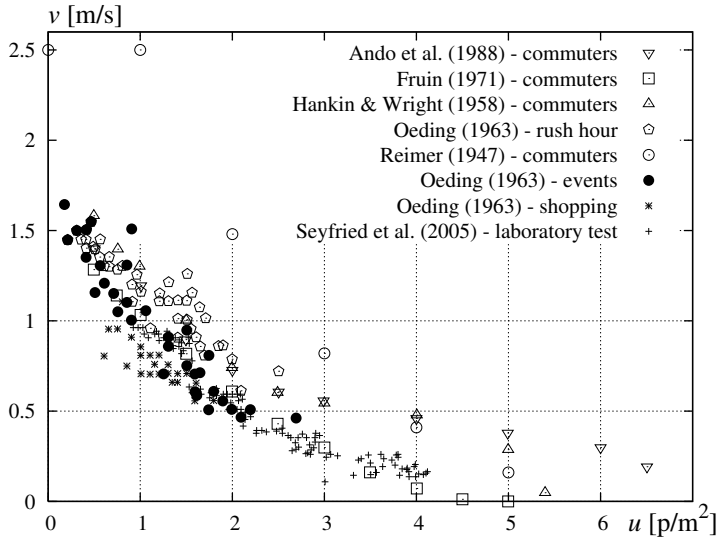

Figure 2.5. Speed-density relation: experimental data

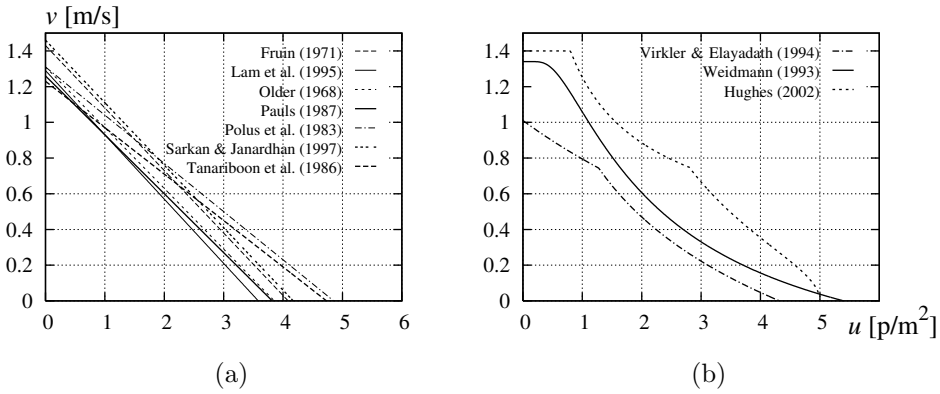

Figure 2.6. Speed density relations in literature: linear (a) and non linear (b)

Table 2.2. Speed-density linear relations (Buchmueller and Weidmann 2006, Daamen 2004)

Source	**Location**	**Relation**
Fruin (1971)	Peak hour flow at commuter bus terminal	$v = 1.43 - 0.35u$
Lam et al. (1995)	Indoor walking in Hong Kong	$v = 1.29 - 0.36u$
Older (1968)	Shopping streets	$v = 1.31 - 0.34u$
Pauls (1987)	Stairs in total evacuation of office buildings	$v = 1.26 - 0.33u$
Polus et al. (1983)	Sidewalks in central business district in Israel	$v = 1.31 - 0.27u$
Sarkan & Janardhan (1997)	Calcutta Metropolitan transfer area	$v = 1.46 - 0.35u$
Tanariboon et al. (1986)	Singapore	$v = 1.23 - 0.26u$

Table 2.3. Speed-density non-linear relations (Buchmueller and Weidmann 2006, Daamen 2004, Hughes 2002)

Source	**Location**	**Relation**
Hughes (2002)	-	$v = \begin{cases} 1.4 & u < 0.8 \\ 1.4\sqrt{(0.8/u)} & 0.8 < u < 2.8 \\ 1.4\frac{\sqrt{5-u}}{u} & 2.8 < u < 5 \end{cases}$
Virkler & Elayadath (1994)	Pedestrian tunnel after University of Missouri football games	$v = \begin{cases} 1.01\exp(-u/4.17) & u < 1.07 \\ 0.61\ln(4.32/u) & u > 1.07 \end{cases}$
Weidmann (1993)	Kladek formula	$v = 1.34\left[1 - \exp\left(-1.913\left(\frac{1}{u} - \frac{1}{5.4}\right)\right)\right]$

One of the first studies was developed by Oeding (1963). He proposes an in-

teresting diagram (Fig. 2.7), recently recovered by Schlaich (2002) and FIB (2005), which graphs the capacity of pedestrian walkways as a function of density and traffic type. In particular he distinguishes four types of pedestrian traffic (shopping, event, rush hour and factory traffic), corresponding to increasing walking velocity and capacity. The diagram also allows a classification of walking regimes to be outlined, that is: free ($u < 0.3$ ped/m^2); acceptable ($0.3 < u < 0.6$ ped/m^2); dense ($0.6 < u < 1$ ped/m^2); very dense ($1 < u < 1.5$ ped/m^2); crowded ($u > 1.5$ ped/m^2).

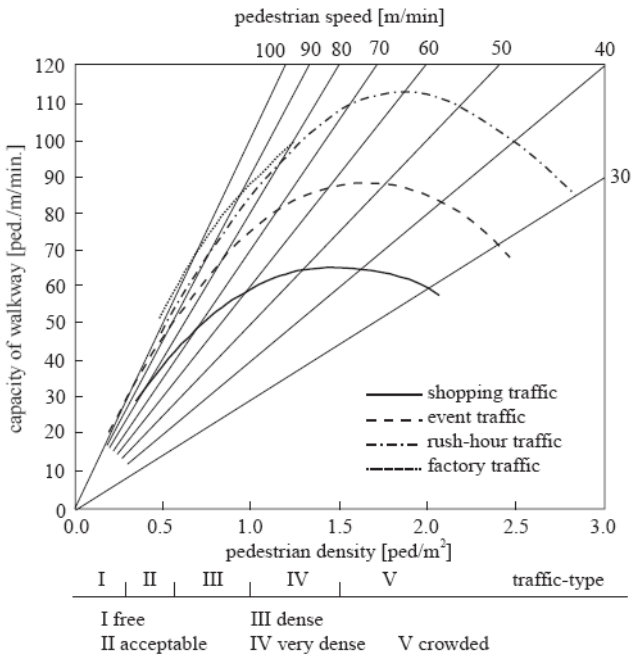

Figure 2.7. Relationship between bridge capacity, pedestrian density and their velocity, after Oeding (1963)

Many of the studies report a linear relationship between velocity and density (Fig. 2.6a), according to the following form:

$$v = v_{max} - \alpha u;\ \alpha > 0. \tag{2.5}$$

Other authors have proposed non linear laws (e.g. Weidmann, 1993) or multi-regime models (e.g. Hughes, 2002). The non-linear multi-regime models (e.g. Hughes, 2002) are certainly more accurate than the linear laws, since they better capture the almost constant speed at low densities and they have the upward concave form that better fits the observation data. The unrealistic discontinuity in the Hughes' diagram is of no interest, since he observes that it would be difficult for such a flow to occur in

practice.

Looking at the experimental data (Fig. 2.5), it is clear that the Reimer's measurements, reported by Oeding (1963), are clearly different from the other ones, since they refer to fast pedestrian transit in train stations and the author himself refers to them as exceptional cases: it is odd that a recent design guideline (FIB, 2005) only reports Reimer's diagram.

It is worthwhile pointing out that the proposed speed-density relations refer to a one-directional flow. In a bi-directional flow, the effects due to passing pedestrians lead to a reduction of the flow capacity. Weidmann (1993) reports a capacity loss of about 4-9% in the case of equal flows in both directions (50%/50%) and a higher capacity loss (about 14.5%) for a directional ratio of 10%/90%.

Finally, it is worth drawing some considerations about flow dimensionality. Many of the proposed relations refer to pedestrian movement on a plane. Seyfried et al. (2005) showed that the measurement of the speed-density relation for a single-file movement of pedestrians leads to results in complete agreement with Weidmann's diagram: this means that specific two-dimensional features, such as internal friction and lateral interference, do not have a strong influence on the fundamental diagram in the considered density range.

In conclusion, it can be stated that it is not possible to determine a universally valid speed-density relation, since there are too many parameters that affect such a relation. For this reason, a specific law has to be tuned in order to characterize a particular problem. Furthermore, it should be borne in mind that the fundamental diagrams are derived in steady state conditions: this means that the quantities characterizing the system vary slowly with respect to space and time. Therefore, the fundamental diagrams are not suitable for use in unsteady conions, such as emergency or panic situations.

2.1.3 Crowd-structure interaction: the synchronous lateral excitation phenomenon

When a pedestrian walks on a laterally moving surface, because of the attempt to maintain body balance, he walks with his legs more widespread and adapts his lateral frequency and phase to that of the moving surface, that is, he synchronizes with the structure. Hence, the lateral motion of the upper part of the torso increases and the resulting lateral force grows in turn. This phenomenon is amplified if the pedestrian walks in a crowd, since synchronization among pedestrians increases the effects of the pedestrian-structure synchronization. The phenomenon, called *synchronous lateral excitation* by Dallard et al. (2001), can occur in any bridge with a lateral frequency below 1.3 Hz that is loaded with a sufficient number of pedestrians. So far, the phenomenon has never led to structural failure since it has a self-limited nature, that is, when the vibrations exceed a limit value pedestrians stop walking or touch the handrails, causing the vibrations to decay. Nevertheless, the resulting reduced com-

fort for the users has often led to a temporary closure of the footbridge in order to provide proper countermeasures, with consequent economic and social repercussions. This is exacly what happened on the famous London Millennium Bridge, which was closed the day it opened (10 June 2000) because of excessive lateral vibrations. The event gave rise to investigations in order to explain what had happened, and it resulted that the phenomenon had already occurred in the past but had not been fully investigated.

The growing frequency of occurrence of these phenomena is primarily due to the increasing strength of new structural materials and longer spans of new footbridges, accompanied by the aesthetic requirements for greater slenderness (Bachmann, 2002). Most of the footbridges that suffer from this phenomenon are, in fact, characterized by a reduced structural mass, so that the ratio between the mass of pedestrians and the structural mass is no longer negligible, and also by a very low damping. A sample of the bridges that experienced the phenomenon is summarized in Table 2.4 and Fig. 2.8. It should also be pointed out that a road bridge, like the Auckland Harbour Bridge in New Zealand, also experienced this kind of lateral vibration, showing that the problem is not related to a specific structural type or to technical innovations.

Table 2.4. Examples of bridges that have experienced human-induced lateral vibration

Bridge	**Year**	**Type**	**Span [m]**	**Lateral freq. [Hz]**
Auckland Harbour Bridge, north span (New Zealand)	1975	Steel box girder	190	0.67
Groves Bridge (Chester, UK)	1977	Suspension	100	-
T-Bridge (Japan)	1993	Cable-stayed	178	0.90
Solferino Bridge (Paris, F)	1999	Steel arch	106	0.71
Millennium Bridge (London, UK)	2000	Suspension	81 (north)	1.00
			144 (centre)	0.5
			108 (south)	0.8
M-bridge (Japan)	2003	Suspension	320	0.88

In the last few years, many studies have been devoted to the measurement of the lateral force exerted by one pedestrian walking on a moving surface. The first

Auckland Harbour Bridge
(New Zealand)

Groves Bridge
(Chester, UK)

T-bridge
(Japan)

M-bridge
(Japan)

Solferino Footbridge
(Paris, F)

London Millennium Bridge
(London, UK)

Figure 2.8. Examples of bridges that have experienced human-induced lateral vibration

laboratory experiments were carried out at London Imperial College and at the University of Southampton to explain what had happened on the London Millennium Bridge (Dallard et al., 2001). The tests at the University of Southampton involved a person walking "on the spot" on a small shaking table. The tests at Imperial College involved persons walking along a 7.2m-long platform which could be driven laterally at different frequencies and amplitudes. Even though these tests did not permit the behaviour of people walking in a crowd to be investigated, they allowed important results to be obtained about the behaviour of a single pedestrian and the probability that he would synchronise his footfall rate to the frequency of the swaying platform (lock-in). Fig. 2.9 reports the DLFs of the first harmonic and the probability of lock-in, both of which increase for increasing platform amplitudes.

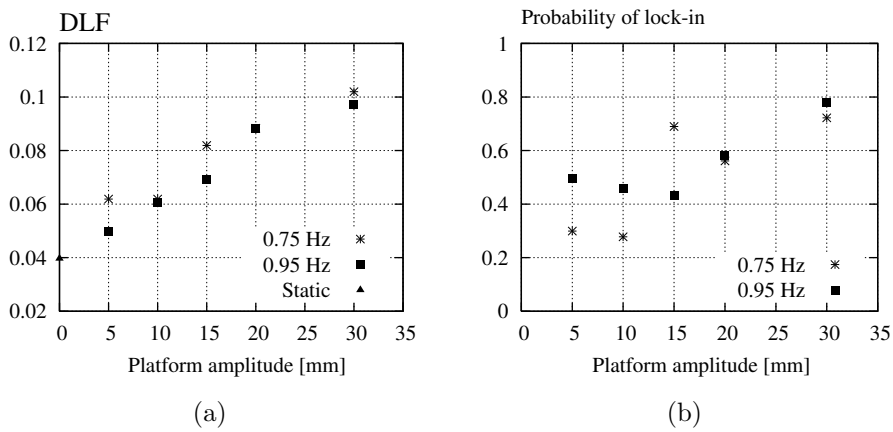

Figure 2.9. DLFs of the first harmonic (a) and probability of lock-in, after Dallard et al. (2001)

In France, Sétra (2006) built a 7-m long and 2-m wide slab on 4 flexible blades moving laterally, in order to measure the horizontal load of pedestrians (Fig. 2.10a). The device was provided with access and exit ramps in order to maintain walking continuity. These tests showed that there is an acceleration threshold above which some synchronization arises and causes uncomfortable vibrations (> 0.6 m/s^2). Similar tests on a moving treadmill were also performed by Pizzimenti (2005). The specially built treadmill (Fig. 2.10b) was laterally driven at 15 different amplitude configurations ($z = \pm 15$, ± 30, ± 45 mm) and frequency configurations (f_s =0.6, 0.7, 0.75, 0.82, 0.92 Hz). The DLFs of the force component at the same frequency as the platform are reported in Fig. 2.11: the dashed line refers to the mean value obtained from the static tests discussed in §2.1.1.

Other suggestions come from the observation of the videos recorded during crowd events. Fujino et al. (1993) were the first to observe the phenomenon of syn-

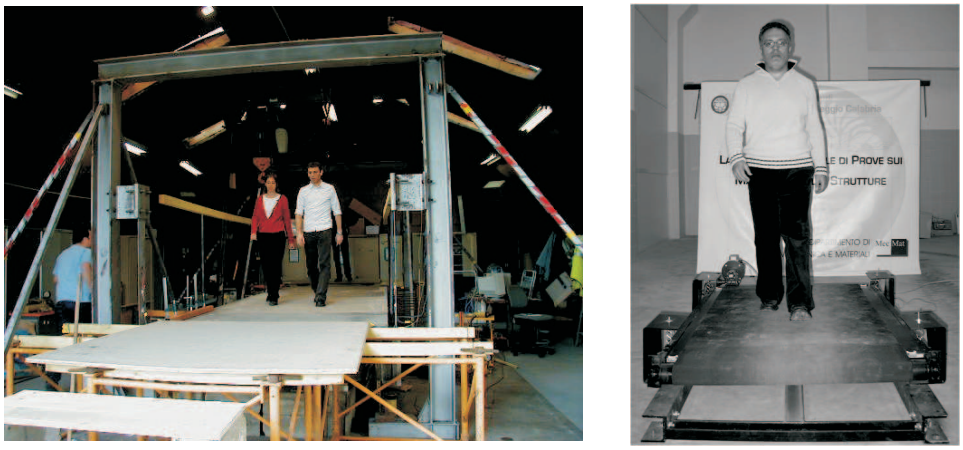

(a) (b)

Figure 2.10. Example of treadmills after Sétra (2006) and Pizzimenti (2005)

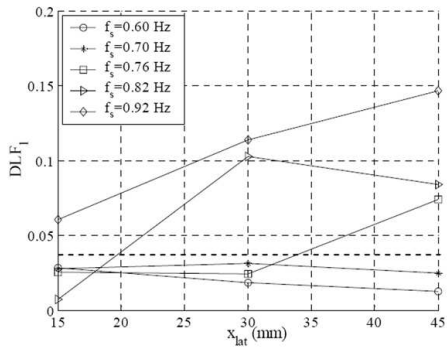

Figure 2.11. DLFs of the force component at the frequency f_s, after Pizzimenti (2005)

chronous lateral excitation on the T-bridge in Japan and recorded human passage during a congested period. The motion of a selected number of pedestrian heads were digitized from the video by means of a microcomputer (Yoshida, 2002). The head motion time histories showed a surprising similarity, i.e. they were synchronized although the amplitudes were different. Fujino et. al estimated a percentage of synchronized pedestrians of about 20%. They explained the phenomenon as follows: first a small lateral vibration is induced by random pedestrian forces and some pedestrians synchronize with the structure; then the deck vibration increases because of the resonant force and more pedestrians become syncronized. The vibration is therefore self-excited, but it does not go to infinity because of the adaptive nature of men, who

stop walking when the vibration is excessive.

The phenomenon has also been studied by means of tests performed on the structure. The tests carried out on the Millennium Bridge in July and December 2000 (Dallard et al., 2001) (Fig. 2.12) evidenced an almost linear dependence of the pedestrian force on the deck lateral velocity. In addition, the deck acceleration abruptly increased when the number of pedestrians exceeded a critical value. The triggering number of people was defined as

$$N_L = \frac{8\pi c f M}{k}, \tag{2.6}$$

where c, M and f are the modal damping, mass and lateral frequency, while $k = 300$ Ns/m in the frequency range 0.5-1.0 Hz. The critical number of people likely to induce synchronous lateral excitation was also estimated by Roberts (2003), assuming a single-span simply-supported deck and a uniform crowd distribution along the span L:

$$N_p = \frac{\rho L}{m_p \Omega^2 D}, \tag{2.7}$$

where ρ is the bridge mass per unit length, m_p is the average mass of a single pedestrian, Ω is the ratio between the step frequency and the frequency of the dominant mode of vibration, D is the dynamic amplification factor which is equal to:

$$D = \sqrt{\frac{1}{(1-\Omega^2)^2 + (2\xi\Omega)^2}}, \tag{2.8}$$

and ξ is the damping ratio. Roberts (2003) also extended his model to the more general case of pedestrians uniformly distributed over n discrete regions of length $\alpha L/n$. Both Eq.s (2.6) and (2.7) can be used to predict the required damping for a given density in order to avoid synchronous lateral excitation. The damping required to ensure stability has also been estimated by other authors, e.g Barker (2002) and Newland (2003). According to the latter, the stability criterion is defined as:

$$2\xi > \alpha\beta m/M, \tag{2.9}$$

where α is the ratio between the body movement and the amplitude of deck vibration, β is the percentage of synchronised pedestrians, m is the pedestrian modal mass and M the modal mass of the dominant mode of vibration.

Several test campaigns were also carried out on the Solferino footbridge (Sétra, 2006), leading to the following conclusions: the lock-in occurred for the first lateral mode and appeared to start and develop more easily when the step lateral frequency was lower than the deck lateral frequency; lock-in occurs beyond a particular threshold, that can be determined in terms of critical number of pedestrians (as proposed by Dallard et al., 2001) or critical value of acceleration, which seems more relevant; below 0.1 m/s^2, pedestrian behaviour may be considered random.

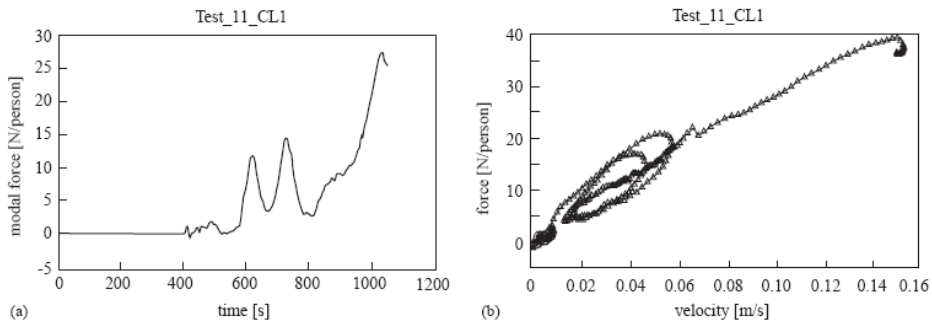

Figure 2.12. (a) Peak amplitude of the lateral modal force per person per vibration cycle. (b) Lateral force per person per vibration cycle vs deck velocity, after Dallard et al. (2001)

Field measurements were also conducted in November 2002 by Nakamura (2003) on the M-bridge in Japan. Accelerometers in the lateral direction were attached to the base of the handrails at five positions of L/8, L/4, 3L/8, L/2 and 9L/16 (L: span length), and accelerometers were also attached to the waist belt of a person, who walked on the bridge among other pedestrians. The measurements confirmed that the pedestrian walked at the same frequency as the girder and showed that the pedestrian phase is between 120° and 160° ahead of the girder. A comparison between the time histories of the girder and pedestrian lateral motion also showed that the pedestrian was sometimes no longer tuned to the structure (Fig. 2.13): this means that he lost his balance because of large girder vibrations and temporarily stopped walking. By analizing the behaviour of the three aforementioned footbridges (Millennium Bridge, T-bridge and M-bridge), Nakamura proposed a serviceability limit for lateral vibration, that is, a displacement of 45 mm (a velocity of about 0.25 m/s and an acceleration of about 1.35 m/s^2). Nakamura also observed that synchronization is unlikely to occur at a deck natural frequency under 0.6 Hz.

Finally, other interesting suggestions to better understand the phenomenon come from wind engineering. Several authors (e.g. McRobie et al. 2003, Newland 2003, Pizzimenti and Ricciardelli 2004) observed some similarities with an interaction phenomenon between fluid flow and structures that is widely studied in wind engineering and commonly known as lock-in. In this case, the cross-flow oscillations of a bluff structure are due to and interact with the shedding of vortices in its wake. Even though the vortex-induced and crowd-induced oscillations differ in their causes, they show analogous features about the structural response. In a given range of the incoming wind velocity (the so-called lock-in region), the vortex-shedding frequency is in fact constant and equal to the frequency at which the structure oscillates, rather than being a linear function of the wind velocity, as stated by the Strouhal law. In other terms, the structural motion affects the wind flow (or crowd flow) so that

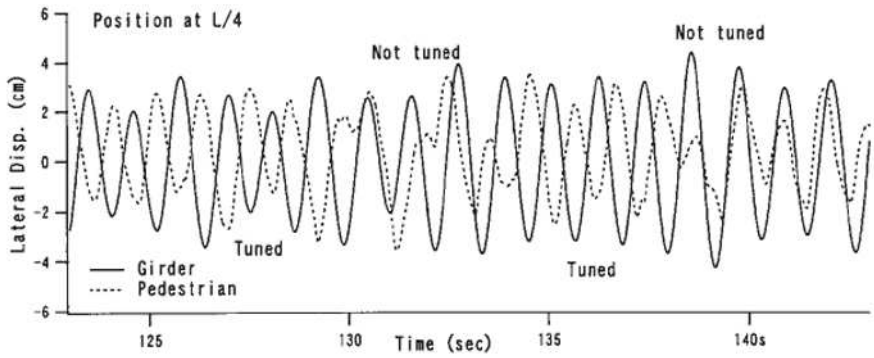

Figure 2.13. M-bridge: lateral displacements of girder and pedestrian at the L/4 position, after Nakamura (2003)

synchronization occurs and the resonance condition takes place. Furthermore, both phenomena are self-limited, in the sense that structural oscillations do not proceed to divergent amplitudes but enter a limit cycle even though the structural damping is null. The tendency for vortex shedding to induce wind-excited structural vibrations is measured by the Scruton number, which is a product of damping and the ratio of structural and fluid masses. According to this analogy, Newland (2003) proposed the definition of a Pedestrian Scruton number defined, with the same notation as Eq. (2.9), as:

$$S_{cp} = 2\xi M/m. \tag{2.10}$$

Therefore, by substituting Eq. 2.10 in (2.9), the required condition for stability is:

$$S_{cp} > \alpha\beta. \tag{2.11}$$

2.2 Physical-mathematical models

This Section, like the previous one, is organized according to the different scales of observation of the coupled system. Therefore, the models referring to the different components of the overall dynamical system (i.e. the structure, the crowd, the force exerted) are reviewed first; then, a few hints of coupled-systems modelling are given.

2.2.1 Structural models

The modelling of structures is usually performed through the Finite Element (FE) approach. This means that the real structure with an infinite number of DOFs is discretised into FEs, which are interconnected at a limited number of points (nodes) with a resulting finite number of degrees-of-freedom (DOFs). The dynamic response

of the structure is given by the well-known equation of motion of a multi-degree-of-freedom (MDOF) system (Clough and Penzien, 1987):

$$\mathbf{M}\ddot{\mathbf{X}}(t) + \mathbf{C}\dot{\mathbf{X}}(t) + \mathbf{K}\mathbf{X}(t) = \mathbf{F}(t), \tag{2.12}$$

where $\mathbf{M}$, $\mathbf{C}$ and $\mathbf{K}$ are the mass, damping and stiffness matrices, while $\ddot{\mathbf{X}}$, $\dot{\mathbf{X}}$, $\mathbf{X}$ and $\mathbf{F}$ are the acceleration, velocity, displacement and external force vectors.

The mass and stiffness matrices are determined by assembling the mass and stiffness element matrices, that are calculated according to the geometrical and material properties of the structure. The damping mechanisms are very difficult to model. If the system is linear, a typical way of expressing viscous damping is in terms of the modal damping ratios ξ_n, where n is the number of DOFs. According to this hypothesis, Eq. 2.12 can be uncoupled into n equations, that is, into n single-degree-of-freedom (SDOF) systems:

$$\ddot{y}_n(t) + 2\xi_n\omega_n\dot{y}_n(t) + \omega_n^2 y_n(t) = F_n(t)/m_n, \tag{2.13}$$

where $\ddot{y}_n$, $\dot{y}_n$ and y_n are the generalized or modal acceleration, velocity and displacement, ω_n is the natural circular frequency for the nth mode of vibration, while F_n and m_n are the modal force and mass for the same mode. The total response of the system can then be obtained by a linear combination of the mode shape vectors ϕ_n:

$$\mathbf{x}(t) = \sum_{i=1}^{n} \phi_i y_i(t). \tag{2.14}$$

If the system is non linear, the damping cannot be expressed by means of damping ratios, but an explicit damping matrix is needed. One of the easiest ways of determining a proportional damping matrix is to make it proportional to either the mass, the stiffnes matrix or a combination of the two:

$$\mathbf{C} = \alpha\mathbf{M} + \beta\mathbf{K}. \tag{2.15}$$

This is the so-called Rayleigh damping and it leads to the following relation:

$$\xi_n = \frac{\alpha}{2\omega_n} + \frac{\beta\omega_n}{2}. \tag{2.16}$$

The evaluation of the two Rayleigh coefficients can be made by solving a pair of simultaneous equations if the damping ratios ξ_n and ξ_m associated to two different frequencies are known. This is unlikely in practice, therefore the same damping ratio $\xi = \xi_n = \xi_m$ is used for both control frequencies and the coefficients are given as:

$$\left\{ \begin{array}{c} \alpha \\ \beta \end{array} \right\} = \frac{2\xi}{\omega_m + \omega_n} \left\{ \begin{array}{c} \omega_m\omega_n \\ 1 \end{array} \right\} \tag{2.17}$$

It is recommended to take ω_m as the fundamental frequency and ω_n as the higher frequency of the modes which significantly contribute to the dynamic response (Clough

and Penzien, 1987).

Thanks to the computational power of personal computers and sophisticated FE software that is currently available, it is possible to perform dynamic analysis of very complex structures. However, when one mode dominates, as often happens in footbridges, the dynamic response can be estimated with sufficient accuracy using a generalized single-DOF (SDOF) model for the appropriate mode (Clough and Penzien, 1987), with a great reduction of computational cost. In other words, the total response is given by:

$$\mathbf{x}(t) = \phi_i y_i(t), \tag{2.18}$$

where ϕ_i is the selected mode shape and the generalized properties are determined as follows:

$$\begin{aligned} m_i &= \phi_i^T \mathbf{M} \phi_i \\ c_i &= \phi_i^T \mathbf{C} \phi_i \\ k_i &= \phi_i^T \mathbf{K} \phi_i \\ F_i &= \mathbf{F} \phi_i. \end{aligned} \tag{2.19}$$

2.2.2 Crowd models

The crowd, as well as the structure, can be seen as a dynamical system. Crowd dynamics modelling is quite recent and is mainly derived from vehicular traffic modelling, which has been widely analysed in the field of applied mathematics since the beginning of the Seventies. Pedestrian and vehicular flows have some common features: they are both granular flows; even though the psychological human component greatly affects people's behaviour, in normal condition, pedestrians and drivers do not act in a chaotic way, but they develop self-organized behaviour that is predictable; in congested situations, some synchronization occurs due to high correlated motion. On the other hand, drivers are more sensitive to velocity and try to avoid crashes. In addition, vehicular flows can be more easily modelled as monodimensional flows, since cars are always organized in lanes, while pedestrians can choose different paths more freely.

What follows refers to the vehicular traffic theory, which has been adapted to pedestrian traffic. Traffic models can be classified into three categories (Bellomo et al., 2002; Bellomo and Coscia, 2005): microscopic, statistical and macroscopic models. Once the representation scale has been chosen, it is useful to express all the variables involved in the problem in dimensionless form and they are therefore scaled with respect to characteristic quantities, that is:

- L is the length of the footbridge span;
- u_M is the maximum admissible density of the crowd, which is also called jam density;

- v_M is the maximum mean velocity of the crowd, which is also called free speed.

Let us also introduce a characteristic time $T_c = L/v_M$, defined as the time necessary to cover the footbridge span L walking at the maximum mean velocity v_M.

We can now define the independent and dependent dimensionless variables (the subscript r refers to the variable dimensional value):

- $t = t_r/T_c$ is the time independent variable;
- $x = x_r/L$ is the space independent variable;
- $u = u_r/u_M$ is the crowd mass density;
- $v = v_r/v_M$ is the crowd velocity;
- $q = u \cdot v$ is the linear mean flow.

In the following, we refer to a one-dimensional flow of pedestrians along a walkway of length L.

Microscopic models

Microscopic models describe the dynamics of each single pedestrian under the action of the surrounding people. The state of the system is described by the position and velocity of each pedestrian as a function of time. Pedestrian behaviour in different situations is described by a set of rules. Models developed at a microscopic scale are generally described by ordinary differential equations. Then, similarly to the Newtonian mechanics for systems of particles, one has to solve a large system of equations. Mean quantities, such as density and mass velocity, are then obtained by an averaging process. If $N(t)$ is the number of pedestrians, each characterized by a position x_i and a velocity v_i, the density can be calculated as the number of pedestrians which, at the time t, are in the tract $[x - \Delta x, x + \Delta x]$, say:

$$u(t, x) \cong \frac{N(t)}{2\Delta x u_M} \tag{2.20}$$

and, similarly, the mean velocity is

$$v(t, x) \cong \frac{1}{N(t) v_M} \sum_{i=1}^{N(t)} v_i(t). \tag{2.21}$$

A large number of microscopic models have been developed in literature, e.g. the social force models by Helbing and Molnár (1995) and Seyfried et al. (2006), the cellular automata model by Blue and Adler (1998) and the microscopic models by Hoogendoorn and Bovy (2004).

Statistical models

Statistical or gas-kinetic models consist of the derivation of an evolution equation for the distribution function on the position and velocity of the pedestrians along the walkway. The state of the system is still identified by the position and velocity of the pedestrians, however their identification does not refer to each individual but to a suitable probability distribution:

$$f = f(t, x, v) \tag{2.22}$$

where $f\ dxdv$ is the number of pedestrians who at time t are in the phase domain $[x, x + dx] \times [v, v + dv]$. Macroscopic observable quantities can be obtained, under suitable integrability assumptions, as momenta of the distribution f, normalized with respect to the maximum density u_M (see Bellomo et al., 2002). The kinetic models are described by integro-differential equations that are similar to the Boltzmann equation.

Gas-kinetic models have been proposed e.g. by Hoogendoorn and Bovy (2000).

Macroscopic models

Macroscopic models, in analogy with the principles of fluid dynamics, refer to the derivation, on the basis of conservation equations and material models, of an evolution equation for the mass density, linear momentum and energy, regarded as macroscopic observable quantities of the flow of pedestrians assumed to be continuous. Macrosopic modelling has been extensively developed for vehicular traffic flow (e.g. Bellomo et al. 2003; Bertotti and Bellomo 2003; Bonzani and Mussone 2003). The macroscopic description, in the case of pedestrian or a vehicular flow, represents only a rough approximation of the physical reality, since the flow of pedestrians is regarded as a fluid. We are in fact dealing with a granular flow, which means that distances among pedestrians may not be negligible with respect to the length of the walkway. The general mathematical framework is given by the three partial differential equations (PDEs), that express the conservation of mass, momentum and energy:

$$\begin{aligned} \frac{\partial u}{\partial t} + \frac{\partial (uv)}{\partial x} &= 0 && (a) \\ \frac{\partial v}{\partial t} + v\frac{\partial v}{\partial x} &= f[u, v, e] && (b) \\ \frac{\partial e}{\partial t} + v\frac{\partial e}{\partial x} &= g[u, v, e] && (c) \end{aligned} \tag{2.23}$$

where f defines the acceleration referring to each particle and g is an energy production term. In order to solve the system (2.23) it is necessary to define the constitutive assuptions, that is, how the production terms f and g depend on their argument. According to the specific constitutive assumption, different models can be derived that involve only some of the three equations in (2.23). They can be classified as follows:

- scalar or first order models: only described by a mass conservation equation and by a closure equation $v = v[u]$ that links the local velocity to the crowd density (e.g. Hughes, 2002);
- second order models: obtained from mass and linear momentum conservation equations with the addition of a phenomenological relation that describes the psycho-mechanic action $f = f[u, v]$ on the pedestrians;
- higher order models: use all the equations in (2.23), with a suitably defined energy density e.

The presented classification involves increasing accuracy in the description of crowd dynamics, but also increasing complexity. Higher order models introduce more parameters that have to be identified and therefore they are very difficult to handle and compare with the experimental observation. Therefore, in the following, more attention is paid to the description of first order models.

Some considerations about the closure of the mass conservation equation should be made. Different models can be proposed to describe the phenomenological relation between density and velocity. The simplest model simply substitutes one of the expressions of $v(u)$, reported in §2.1.2, in equation (2.23)-a. Equation (2.23)-a becomes:

$$\frac{\partial u}{\partial t} + f(u)\frac{\partial u}{\partial x} = 0 \tag{2.24}$$

where $f(u) = \partial q/\partial u$ represents the flow propagation speed. The above equation is hyperbolic and shows unrealistic shock wave phenomena which are not experimentally observed. These phenomena occur each time the density is greater than the capacity density u_{ca}, that is, when the propagation speed is negative (congested regime). This inconsistency is due to the fact that conditions which correspond to steady uniform flow are instantaneously imposed in unsteady conditions. This problem can be solved by introducing a small diffusion term into the closure equation, so that the model becomes parabolic. This can be achieved, for instance, by using an apparent density model (Bellomo and Coscia, 2005) which is based on the concept that the pedestrian feels an apparent density u^*, which is larger than the real one, if the local density gradient is positive (trend to jam conditions), while it is smaller than the real one if the gradient is negative (trend to vacuum). The apparent density can be expressed as follows:

$$u^* = u\left[1 + \eta(1-u)\frac{\partial u}{\partial x}\right] \tag{2.25}$$

where η is a positive parameter.

Finally, it is worth citing the delay models (Bellomo and Coscia, 2005), which assume that the pedestrian reaction time is finite, so that the velocity at which the pedestrian walks refers to a density earlier in time, as:

$$v(\bar{u}) = v(u(x, t-\tau)), \tag{2.26}$$

where τ is a small parameter compared to the unit, that corresponds to a relatively large time, thus introducing a retarded adaptation of the pedestrian to the actual traffic conditions. In their research, Bellomo and Coscia (2005) proposed an improvement of the above model by introducing a space dislocation in Eq. 2.26, that becomes:

$$v(\bar{u}) = v(u(x - |\delta|, t - \tau)), \tag{2.27}$$

where the dislocation parameter $|\delta|$ is small compared to the unit.

2.2.3 Force models

According to Živanović et al. (2005), the load models can be divided into two categories: time-domain and frequency-domain force models. In the following, the models that can be ascribed to the first category are described, since they are the ones that are mainly used in practice. In addition, only the load models concerning the horizontal component are retained for the scope of this work.

Force models in literature

Most of the load models proposed so far are deterministic time-domain models, based on the assumption that both feet produce exactly the same periodic force. According to this hypothesis, the force exerted by a single pedestrian can be represented by a Fourier series (Eq.s 2.2).

Generally, the force exerted by a number of n pedestrians is described by multiplying the force of a single pedestrian by a coefficient that could be considered as a synchronization factor. One of the first attempts in this direction was made by Matsumoto et al. (1978). Assuming that pedestrians arrive on the bridge following a Poisson distribution, the total response can be obtained by multiplying a single pedestrian's response by the multiplication factor $\sqrt{n}$. In other words, this means that pedestrians are absolutely uncorrelated, therefore the model is not suitable for use in the presence of synchronization phenomena.

Grundmann et al. (1993) proposed three models corresponding to different pedestrian density configurations on a footbridge that should be considered separately, based on the derivation of a synchronization coefficient S from probabilistic considerations:

- *Model 1: bridges with low pedestrian density*
  Pedestrians walk in small group with the same speed v and slightly different step frequencies f_p and step length l_p. In such cases, some synchronisation between these people is expected, but only when the bridge frequency is within the normal walking frequency range. The synchronization coefficient can be found according to the graph in Fig. 2.14, which shows that, for the frequency

range between 1.5 and 2.5 Hz, the force exerted is three times that of a single pedestrian.

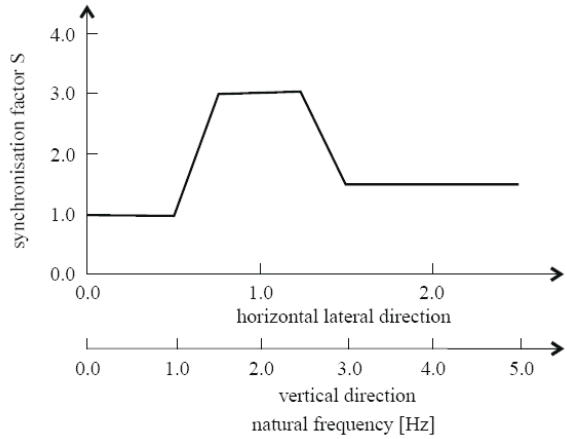

Figure 2.14. Synchronization factor for low densities after Grundmann et al. (1993)

- *Model 2: bridges with a random stream of low density pedestrian traffic*
  If the density is below 0.6 ped/m^2, pedestrians can walk freely. S is defined as follows:
  $$S = \begin{cases} 0.225N_r & 1.5 < f_{1,v} < 2.5Hz \\ \sqrt{N_r} & f_{1,v} < 1.5 \cap > 2.5Hz \\ 0.225 \cdot 0.5N_r & 3.5 < f_{1,v} < 4.5Hz \end{cases}, \tag{2.28}$$
  where the number of pedestrians on the bridge deck N_r is given by the product of the crowd density, the deck surface and a weighting factor K, which accounts for the variable point of application of loading. It should be noted that the second equation in (2.28) recovers Matsumoto et al.'s model.

- *Model 3: bridges with a stream of high density pedestrian traffic*
  For a crowd density above 0.6 ped/m^2, the synchronization coefficient can again be calculated according to Eq. (2.28). This model accounts for synchronization among pedestrians due to high crowd density, but does not account for pedestrian-structure synchronization.

The laboratory and field tests performed on the Millennium Bridge led Dallard et al. (2001) to observe a linear relationship between the lateral force and the local velocity of the deck $\dot{z}$, after the pedestrians had synchronized to the structure:

$$F(t) = k\dot{z}(t), \tag{2.29}$$

where the proportionality factor k has to be determined experimentally and for the Millennium Bridge is equal to 300 Ns/m. This means that moving pedestrians act as negative dampers (i.e. amplifiers) increasing the response of the structure until they have to stop because they loose balance. It should be stressed that this load model only refers to the crowd behaviour after the lock-in occurs.

Different load models have been proposed by Fujino and coworkers, based on the observation of the human-induced lateral vibrations on two Japanese footbridges, the T-bridge and the M-bridge. First, Fujino et al. (1993) showed, by means of a SDOF model of the T-bridge, that the total lateral force exerted by pedestrians was equal to 0.2 times the force of a single pedestrian, which means that 20 % of pedestrians were synchronized. Later on, Nakamura and Kawasaki (2006) proposed a more sophisticated model, where the total force is expressed as:

$$F(t) = k_1 k_2 H(\dot{z}) G(f_{1,h}) M_p g, \tag{2.30}$$

where:
- k_1=0.04;
- k_2=0.2 is the percentage of synchronized pedestrians;
- $H(\dot{z}) = \dfrac{\dot{z}(t)}{k_3 + |\dot{z}(t)|}$ is a function used to describe the pedestrian synchronization nature. At a low deck velocity $\dot{z}$, pedestrians synchronize proportionally with $\dot{z}$; when the velocity increases, pedestrians feel unsafe and stop walking, therefore the girder response is limited. The value of k_3 is determined by trial and error and was set to 0.01 for the T-bridge;
- $G(f_{1,h}) = 1$ describe how pedestrians synchronize with the bridge's first lateral frequency $f_{1,h}$;
- $M_p g$ is the self-weight of the pedestrians.

This model has the merit of accounting for the self-limited nature of the phenomenon by means of the function $H(\dot{z})$. Hence, it represents an improvement of Dallard et al.'s model, in which the force grows linearly with the velocity, causing the structural response to go to infinity (Fig. 2.15).

Force models in international codes and design guidelines

Eurocode 1, Part 1, "Live loads on bridges", includes a load model that allows for synchronization effects. This model is divided into three parts corresponding to different pedestrian configurations. In the following, only the horizontal component is reported:

- *Single pedestrian load model*
  $F_h = 70 \sin(2\pi f_h t)$ [N]
  The action should be applied on the most unfavourable position on the bridge. The same model is also reported in British Standard BS5400, Part 2, and in Ontario Highway Bridge Design Code OHBDC ONT 83 (FIB, 2005).

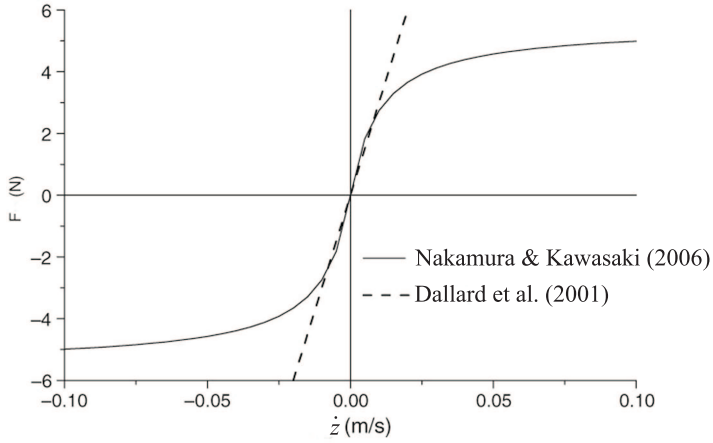

Figure 2.15. Comparison between the models of Dallard et al. (2001) and Nakamura and Kawasaki (2006)

- *Load model for a pedestrian group*
  $F_h = 70k_h(f_h)\sin(2\pi f_h t)$ [N]
  where k_h is a synchronization factor that accounts for random synchronized pedestrians within the group. It can be graphically determined as a function of the structural frequency f_h.

- *Load model for a continuous pedestrian stream*
  $q_h = 3.2k_h(f_h)\sin(2\pi f_h t)$ [N/m^2]
  The load should be applied to the relevant areas of the bridge, according to the excited mode shape.

Finally, it is worth citing the load model proposed in the French design guidelines drawn up by Sétra (2006). The model consists in deriving an equivalent number of pedestrians N_{eq}, which - evenly distributed, at the same frequency of the footbridge and in phase, with the loading sign related to the mode sign - will produce the same effect as random pedestrians. N_{eq} was obtained by performing 500 tests with a fixed number of pedestrians. The following two laws are retained:

- *Sparse or dense crowd*: random phases and frequencies with Gaussian law distribution
  $N_{eq} = 10.8\sqrt{n\xi}$, where ξ is the critical damping ratio;

- *Very dense crowd*: random phases and all pedestrians at the same frequency
  $N_{eq} = 1.85\sqrt{n}$.

The total force is equal to N_{eq} multiplied by the force of a single pedestrian, whose amplitude is equal to 0.05 times the pedestrian weight.

Concluding remarks

Many of the lateral force models proposed so far have the advantage of being synthetic and conceived for practical use. On the other hand, they have experienced some difficulties in taking into account some non negligible aspects of the problem, that is:

- the dependence of the pedestrian lateral force on the two-way interaction between two systems, the crowd and the structure. All the reviewed models, in fact, assume that the state variables of the two systems (i.e. number of pedestrians, crowd density, deck velocity or acceleration) are given;
- the possibility of an inhomogeneous distribution of the crowd along the deck due to bottlenecks, congested traffic or other non-linear traffic phenomena;
- the existence of two kinds of synchronization, one between the pedestrians and the structure and the other among the pedestrians;
- the presence of different frequency components in the overall force;
- triggering of the lock-in phenomena and the resulting self-limited oscillations.

In addition, some of the aforementioned models have been conceived specifically for a particular footbridge (e.g. the ones of Fujino et al., Nakamura and Kawasaki and Dallard et al.), and they therefore lack of generality.

2.2.4 Coupled mechanical systems

The analysis of coupled mechanical systems can be performed according to the so-called *partitioned approach*. The approach, first proposed by Park and Felippa (1983), is widely used in the Aerospace, Mechanical and Civil Engineering fields, e.g. in the modelling of fluid-structure interaction, but so far it has never been applied to crowd-structure interaction. This section is a brief summary of the method described in Park et al. (1999).

Basic terminology

System (according to the American Heritage Dictionary): a functionally related group of components forming, or regarded as, a collective entity.

Coupled system: a system in which physically or computationally heterogeneous mechanical components interact dynamically. The interaction is multiway in the sense

that the response has to be obtained by solving simultaneously the coupled equations which model the system.

Partitioning: the process of spatial separation of a discrete model into interacting components, called *partitions* or *fields*.

System decomposition

Systems are analyzed through decomposition or partitioning. The decomposition can be done according to physical, functional or computational considerations. The common practice in modelling is based on the following partition hierarchy: coupled system (top-level), structure, substructure, subdomain and element. For instance, a top-level partition driven by physics is into fluid and structure models.

At the first level of the hierarchy, two types of subsystems (or fields) are possible:

- *Physical subsystems*, when their mathematical model is described by field equations. Examples are mechanical and non-mechanical objects treated by continuum theories (e.g. fluid, solids, heat);
- *Artificial subsystems*, that are used for computational purposes, for instance to facilitate information transfer between two subsystems.

Computational approach

The main advantages of the partitioned approach lie in the computational treatment of coupled systems, for which fields are discretized in space and time. In particular, in *algebraic* partitioning, the coupled system is spatially discretized first, and then decomposed, while in *differential* partitioning the decomposition is done first and each field then discretized separately. The differential partitioned approach allows:

- *Customization*: each field can be treated by discretization techniques and solution algorithms that are known to perform well for the isolated system;
- *Independent modelling*: the use of non-matching models is facilitated, as in the case of fluid-structure interaction;
- *Software reuse*: the use of existing codes is permitted;
- *Modularity*: new methods and models may be introduced in a modular fashion.

On the other hand, the partitioned approach requires careful formulation and implementation to avoid degradation in stability and accuracy.

2.3 Design codes and guidelines

The problem of vibration is usually handled by international codes by providing comfort requirements, that can be divided into two categories:

- Limit values for structural frequencies, that should fall outside the pedestrian frequency ranges in order to avoid resonance loading;
- Limit values of accelerations: if the limit on structural frequencies is not respected, a dynamic calculation is required and the resulting accelerations are limited to ensure pedestrian comfort.

As observed in FIB (2005), in practice, many footbridges exceed the limits of comfort reported in literature and codes, but users have seldom complained. Users, instead, very often enjoy these structures because of their liveliness.

The following tables provide a summary of the limit values for horizontal frequencies and accelerations provided in international codes (FIB 2005).

Table 2.5. Limit values for horizontal frequencies in international codes (after FIB, 2005)

Code/Standard	**Limit values [Hz]**
Eurocode 2 (ENV 1992-2)	0.8 - 1.2
Eurocode 5 (ENV 1995-2)	< 2.5
SIA 260 (Switzerland)	< 1.3

Table 2.6. Limit values for horizontal accelerations in international codes (after FIB, 2005)

Code/Standard	**Limit values [m/s^2]**	
Eurocode 1	$min \begin{cases} 0.14\sqrt{f_h} \\ 0.15 \end{cases}$	for f_h =0.5-1.5 Hz for f_h =1.5-2.5 Hz: check dependant on case from f_h =2.5 Hz: no check necessary
Eurocode 5	0.2	for $f < 2.5$ Hz (for standing individuals)

A horizontal vibration limit for footbridges is also recommended in ISO 10137,

which reports a perception curve in term of RMS acceleration (Fig. 2.16): this base curve should be multiplied by a factor of 60. The peak acceleration can be obtained by multiplying the RMS value by $\sqrt{2}$ (Živanović et al., 2005). For a frequency of 1 Hz, the peak acceleration limit is about 0.3 m/s^2. Willford (2002) reports that near normal walking can be sustained until the lateral acceleration level exceeds about 0.25 m/s^2 (referring to experiments on the perception of vibration in high buildings).

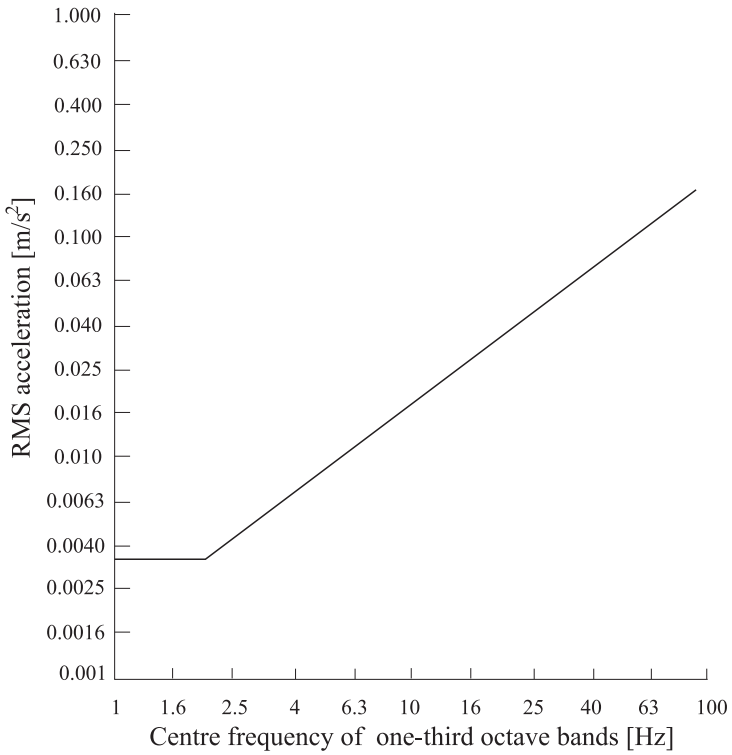

Figure 2.16. Acceptability of horizontal vibration after ISO 10137

It should be pointed out that FIB (2005) suggests a lock-in threshold for lateral vibrations which corresponds to an acceleration of 0.08 m/s^2 for a frequency of 1 Hz. This value has also been suggested by Bachmann (2002), who recommends a limit displacement of about 2 mm in order to avoid the lock-in effect. This value is well below the comfort thresholds reported in Table 2.6.

Chapter 3

Crowd-Structure Interaction (CSI) Model

The main features of the proposed model lie in the mathematical and numerical partitioning of the coupled system into two physical subsystems and in the two-way interaction between them (Park et al., 1999) (Fig. 3.1). The two subsystems, the Crowd and the Structure, will be referred to with the subscripts c and s, respectively.

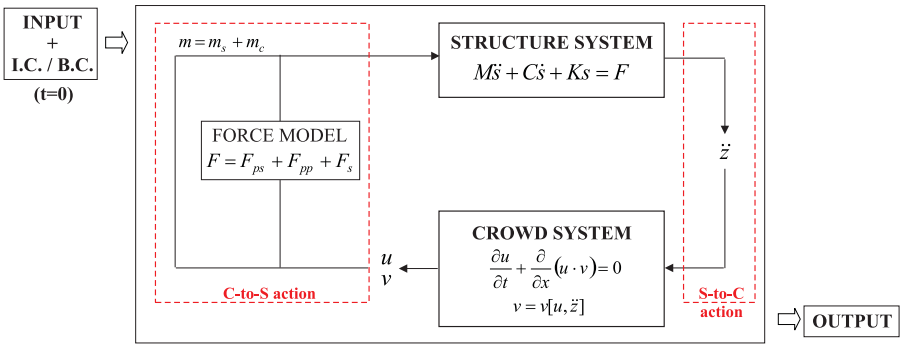

Figure 3.1. Scheme of the time-domain coupled model

In the following, each part of the model is described referring to the framework schematized in Fig. 3.1. It is worth stressing that the model is herein expressed in its dimensional form in order to better point out the physical meaning of its components. Neverthless, the dimensionless form can be obtained by scaling all the variables with respect to reference quantities (Bellomo and Coscia, 2005), that is, the maximum

mean pedestrian velocity v_M, the maximum admissible crowd density u_M and the footbridge length L. In order to ease the notation, the subscript r that refers to the variable dimensional value is omitted in the following.

3.1 The Structure subsystem

The Structure subsystem is modelled by a 3D model. The structural dynamics is described by the non-linear equation of motion:

$$[M_s + M_c(u)]\ddot{s} + C\dot{s} + Ks = F(u, \ddot{z}), \tag{3.1}$$

where s are the structural displacements; M_s, C and K are the structural mass, damping and stiffness; M_c is the crowd mass; F is the applied load; $\ddot{z}$ is the deck lateral acceleration.

It should be noticed that the Ordinary Differential Equation (ODE) (3.1) is non-linear for two reasons: first, the forcing term F is a function of both the crowd density and the lateral acceleration of the deck; second, the overall mass M is given by the sum of the structure and the crowd mass, which derives from the solution of the equation governing the Crowd subsystem, in turn dependent on the solution of the ODE (3.1), as will be explained in the next sections.

3.2 The Crowd subsystem

As stated in Section 2.2, mathematical modelling of crowd dynamics can be developed according to three different mathematical frameworks, respectively based on microscopic, statistical and macroscopic description. In particular, first order macroscopic modelling refers to the derivation of an evolution equation for the mass density, regarded as a macroscopic quantity of the flow assumed to be continuous. Such a representation implies an approximation of the physical reality, since the distances among the pedestrians can be large enough to be in contrast with the continuity assumption of the hydrodynamic model, expecially in case of very low crowd density. On the other hand, a relatively simple model is preferable to study the complexity of the crowd-structure coupled system. Hence, a first order hydrodynamic model in the one-dimensional (1D) spatial domain is developed in the following.

It follows that the reference framework describing the crowd dynamics is given by the 1D mass conservation equation in its Eulerian dimensional form (see A.1), closed by a phenomenological relation that links the mean velocity to the mass density and the deck lateral motion:

$$\begin{aligned} &\frac{\partial u}{\partial t} + \frac{\partial}{\partial x}(uv) = 0 \\ &v = v[u, \ddot{z}] \end{aligned} \tag{3.2}$$

It is worth stressing that, among the three variables describing the structural response (i.e. displacement, velocity, acceleration), it has been generally accepted that acceleration is the vibration parameter which should be used to describe the problem (Živanović et al., 2005). One of the key reasons is that acceleration is convenient to be measured and serviceability criteria reported by most of the design codes make reference to acceleration values. Neverthless, several authors (e.g. Yoneda, 2002) retained the velocity as the parameter which mostly affect pedestrian behaviour.

3.3 Structure-to-Crowd action: the closure equation

In the following an interpretative model of the pedestrian fundamental relation is proposed and compared with some experimental laws herein rivisited.

3.3.1 Physical-based model of the pedestrian fundamental relation

The fundamental relation that links crowd density to walking velocity is usually expressed in the direct form $v = v(u)$. In this section, a phenomenological relation that links pedestrian velocity v to crowd density u and deck acceleration $\ddot{z}$ is proposed in the inverse form $u = u(v, \ddot{z})$. Bearing in mind that crowd density u [ped/m^2] is a scarcely intuitive quantity, its reciprocal Pedestrian Area Module (PAM) (Fruin, 1987), i.e. the surface S occupied by a pedestrian, is used as a more manageable unit [m^2]. Hence, the proposed relation is based on some phenomenological considerations about $S(v, \ddot{z})$. Obviously, once the latter is obtained, the density can be calculated as the reciprocal of $S(v)$, and the speed-density relation can be recovered as an inverse relation.

Among the various factors that can affect walking behaviour, two are specifically retained, that is, the geographic area and the travel purpose: the related coefficients are respectively named with the subscripts G and T. These factors are assumed to affect both free speed v_M and PAM S through the coefficients α and β, respectively.

The free speed is expressed in the general form:

$$v_M = \bar{v}_M \, \alpha_G \, \alpha_T \, g(\zeta), \tag{3.3}$$

where $\bar{v}_M = 1.34$ m/s is the average free speed (Buchmueller and Weidmann, 2006); the coefficients α_G and α_T were determined analyzing the data reported in Buchmueller and Weidmann (2006) as the ratio between the proposed free speeds and $\bar{v}_M$, and they are reported in Table 3.1; ζ is the envelope of the deck acceleration time history $|\ddot{z}(t)|$; the corrective factor $g(\zeta)$ takes into account the sensitivity of v to the deck acceleration and has a qualitative trend, based on the following hypothesis:

- the lateral motion of the deck reduces the walking velocity;
- after the pedestrians have stopped because of excessive lateral vibrations at time t_s, a stop-and-go time interval Δt_r should elapse before they start walking again.

It follows:

$$g = \begin{cases} 1 & \zeta \leq \ddot{z}_c \cap t \geq t_s + \Delta t_r \\ [\ddot{z}_M - \zeta(x,t)]/(\ddot{z}_M - \ddot{z}_c) & \ddot{z}_c < \zeta < \ddot{z}_M \cap t \geq t_s + \Delta t_r \\ 0 & \zeta \geq \ddot{z}_M \cap t_s < t < t_s + \Delta t_r \end{cases}, \tag{3.4}$$

where $\ddot{z}_c \cong 0.2$ m/s^2 (ISO 10137, 1992) corresponds to the threshold of motion perception and $\ddot{z}_M = 2.1$ m/s^2 (Nakamura, 2003) is the maximum acceptable acceleration above which pedestrians stop walking.

Table 3.1. Coefficients of geographic area and travel purpose that affect the free speed v_M

Geographic area α_G			**Travel purpose** α_T		
Europe	USA	Asia	Rush hour/ Business	Commuters/ Events	Leisure/ Shopping
1.05	1.01	0.92	1.20	1.11	0.84

The PAM occupied by a motionless pedestrian can be calculated considering an elliptical or a rectangular form. According to the latter hypothesis, the average surface occupied by a motionless pedestrian is $S_0 = w_0 d_0$, where w_0 and d_0 are the average lateral width and depth of a human body (Fig. 3.2). When a pedestrian is walking, a greater surface is required, that is, $S = wd$ (Fig. 3.2). Both the terms w and d can be expressed as a function of the walking velocity v. In addition, the lateral width could be made sensitive to the deck acceleration, since pedestrians tend to walk with their legs more widespread when the surface is laterally moving, as stressed by various authors (Dallard et al. 2001, Fujino et al. 1993).
The required forward distance d can be expressed as the sum of two terms: l_p, the step length, which is a function of the walking velocity and step frequency f_p; d_s, the sensory distance, which is defined by Fruin (1987) as *the area required by the pedestrian for perception, evaluation and reaction.* While the former can be physically measured, the latter depends to a great extent on cultural and psycological factors and is, therefore, hard to evaluate. As for the lateral width w, even though the same distinction can be made between pacing and sensory zones, a unique width is retained because of the lack of available data. Therefore, S takes the form

$$S(v,\zeta) = S_p + S_s = w(v,\zeta)l_p(v) + w(v,\zeta)d_s(v), \tag{3.5}$$

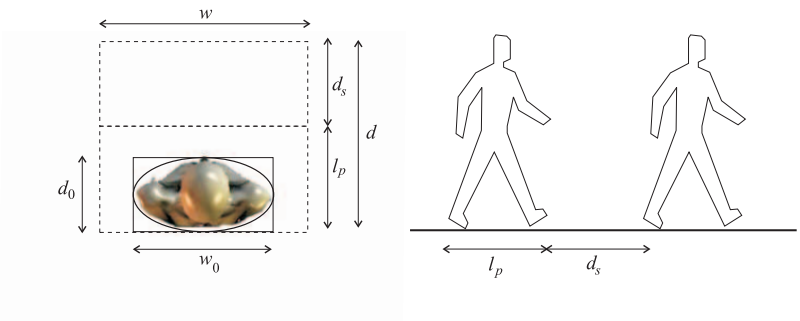

Figure 3.2. Human body dimensions: motionless and walking pedestrian

where S_p and S_s are the pacing zone and the sensory zone, respectively. It is supposed that β_G only affects the pacing zone, since the geographic area is mainly related to the body dimensions (width and step length), while β_T only concerns the sensory zone, since the travel purpose can be connected to psycological factors. Therefore, equation (3.5) can be rewritten as

$$S = w(\beta_G l_p + \beta_T d_s). \tag{3.6}$$

It is worthwhile recalling that the value of the maximum admissible density can be calculated as $u_M = 1/S(0)$, while the critical density is $u_c = 1/S(v_M)$.

All the parameters introduced in the modelling framework are characterized in the following on the basis of several experimental data coming from various research fields such as transportation, biomechanics, safety and structural engineering.

The lateral width $w(v)$ is expressed in the additive form $w(v, \zeta) = w(v) + w_r(\zeta)$, where $w_r(\zeta)$ is the peak-to-peak value of the relative lateral displacement of the torso between adjacent pedestrians. According to Buchmueller and Weidmann (2006), in a free walking regime a pedestrian requires a lateral additional space equal to about 62 % of his average width. Therefore, the simplest expression for $w(v)$ is the linear relation

$$w(v) = w_0 \left(1 + 0.62 \frac{v}{\bar{v}_M}\right), \tag{3.7}$$

where $w_0 = 0.45$ m (Buchmueller and Weidmann, 2006) (Fig. 3.3). The relative lateral displacement of the torso considers the fact that, the higher the platform motion, the higher the synchronization between pedestrians and the platform and therefore, the lower the relative displacement among pedestrians. Hence, the relative displacement can be expressed as

$$w_r(\zeta) = w(\zeta)\,(1 - S_{ps})\,, \tag{3.8}$$

where the relation between w and ζ can be inferred by fitting experimental data recorded on actual lively footbridges (Fig. 3.4a) (Fujino et al. 1993, Nakamura 2003):

$$w(\zeta) = 0.0375\,(\zeta - \ddot{z}_c)^{1/3} \qquad \zeta \geq \ddot{z}_c, \tag{3.9}$$

while $S_{ps}(\zeta)$ is the pedestrian-platform synchronization coefficient (Fig. 3.4b) obtained by fitting the data of Dallard et al. (2001), that will be detailed in §3.4. From Fig.s 3.3 and 3.4a it is clear that the value of the term $w_r(\zeta)$ is two orders of magnitude less than $w(v)$. Therefore, it is not retained in the following.

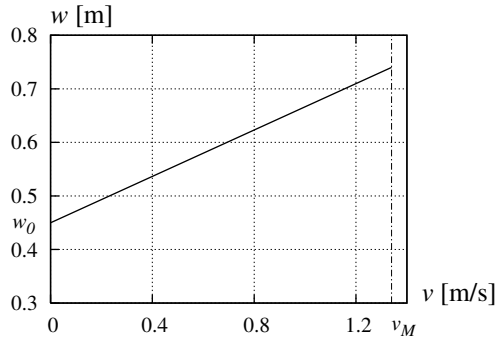

Figure 3.3. $w(v)$ law

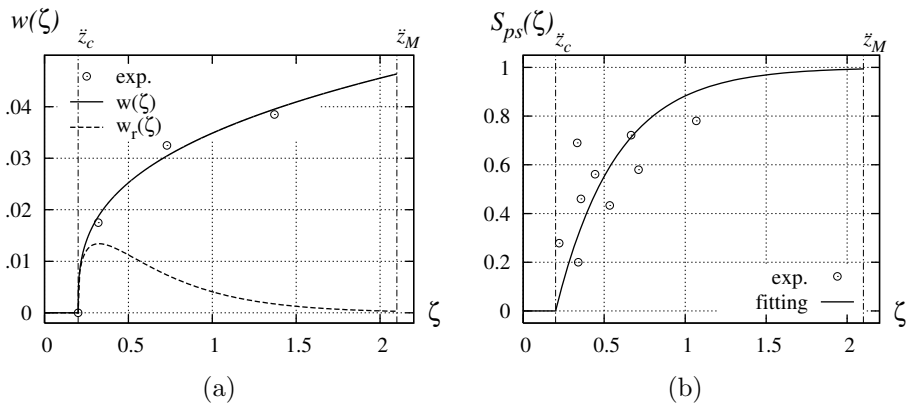

Figure 3.4. $w(\zeta)$ and $S_{ps}(\zeta)$ laws

The relation between the step length l_p and the velocity v can be derived from the relation between the step frequency f_p and v, since $l_p = v/f_p$ (Fig. 3.5b). The frequency-speed relation is derived from a cubic fitting to the Bertram and Ruina (2001) experimental data (Fig. 3.5a) coming from laboratory tests on a treadmill with fixed velocity:

$$f_p = 0.35v^3 - 1.59v^2 + 2.93v. \tag{3.10}$$

Fig. 3.5b shows that, when a pedestrian is motionless ($v = 0$), the body depth d_0, whose value is set equal to $d_0 = 0.36$ m according to Seyfried et al. (2005), takes the

place of the step length.

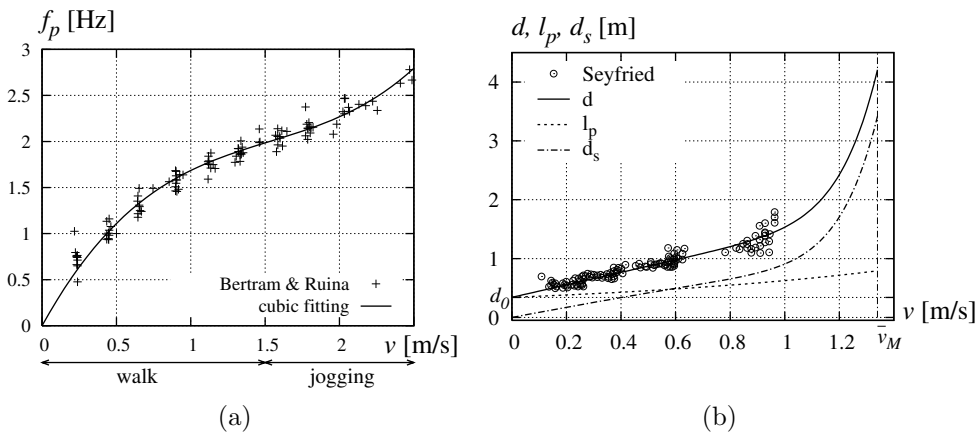

Figure 3.5. Proposed f_p [Hz]-v [m/s] (a) and d, l_p, d_b [m]-v (b) relations

The sensory distance d_s (Fig. 3.5b) can be obtained as $d - l_p$, since some experimental data concerning the $d - v$ relation are available in literature (Seyfried et al., 2005). The data have been fitted according to the law

$$d(v) = d_0 + 1.06v + bv^{10}, \tag{3.11}$$

where $b = (2.08v_M - d_0)/v_M^{10}$, so that $d(v_M)$ takes the value for which $u_c \cong 0.3$ ped/m^2, as proposed by Oeding (1963). It should be pointed out that, according to Seyfried et al. (2005), the almost linear trend of the $d - v$ relation at low velocities is due to synchronization phenomena among pedestrians (e.g. marching in lock-step) which reduce the sensory distance d_s.

The geographic area coefficient β_G is derived, considering the dimension occupied by the human body in different countries (Table 1 in Buchmueller and Weidmann, 2006), as the ratio between the surface averaged per geographic area and the mean surface S_0. It results that β_G equals 1.075 for the European and American case, while it equals 0.847 for Asian countries. The travel purpose coefficient β_T is determined by fitting the reciprocal of equation (3.6) to the experimental data reported by Oeding (1963) and Fruin (1987) (Fig. 3.6 and Table 3.2). It can be noticed that β_T monotonically decreases for increasing free speeds v_M associated to travel purposes.

In order to evaluate the sensitivity of the model to the different parameters of interest, the proposed model has been applied with different combinations of the latter. Some results are represented in Fig. 3.7 in terms of fundamental diagrams. In Fig. 3.7a, the model is applied with a fixed geographic area (Europe), varying the travel purpose; in Fig. 3.7b, the travel purpose is fixed (commuters) and the geographic area varies.

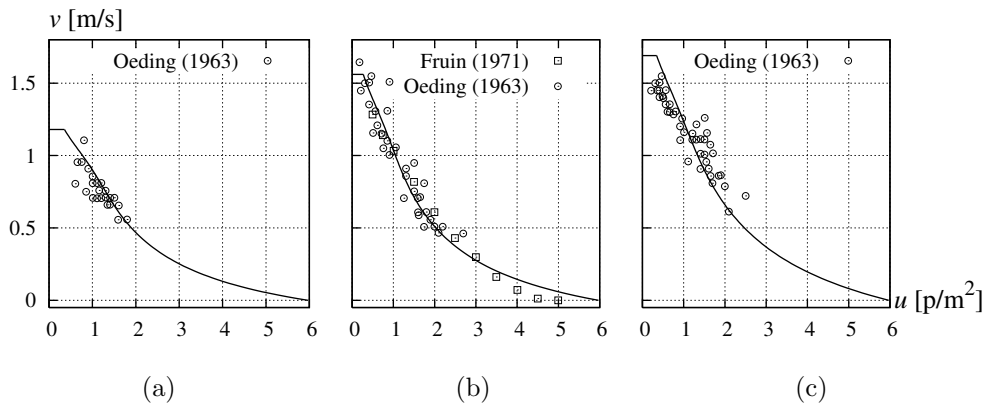

Figure 3.6. Fitting to the experimental data: leisure/shopping (a); commuters/events (b); business/rush hour (c)

Table 3.2. Coefficients β_T

	Leisure/Shopping	Commuters/Events	Rush hour/Business
v_M [m/s]	1.18	1.56	1.69
β_T	1.07	0.93	0.55

The following considerations can be made: i) the effects of the travel purpose can be seen above all in the variation of v_M and β_T, which determines different values of u_c and u_{ca}. It should be noticed that neither u_c nor u_{ca} grow monotonically with the free speed; ii) the geographic area has the effect of varying the jam density u_M. While Europe and the USA have practically the same diagram, Asia shows a higher u_M and capacity flow q_{ca}, which is in agreement with data in literature (Buchmueller and Weidmann, 2006).

3.3.2 Comparison with fundamental laws revisited

The above physical-based relation is compared to two laws previously proposed in literature in the direct form $v = v(u)$: the first one is the Kladek formula, proposed by Weidmann (1993), while the second one is recovered from the vehicular traffic theory (Bellomo and Coscia, 2005). Both are reported in their original (O) dimensional form in Table 3.3.

In order to make these relations sensitive to the walking features considered in this work, the two laws are rewritten in a revisited form (R), where v_M, u_c and u_M are

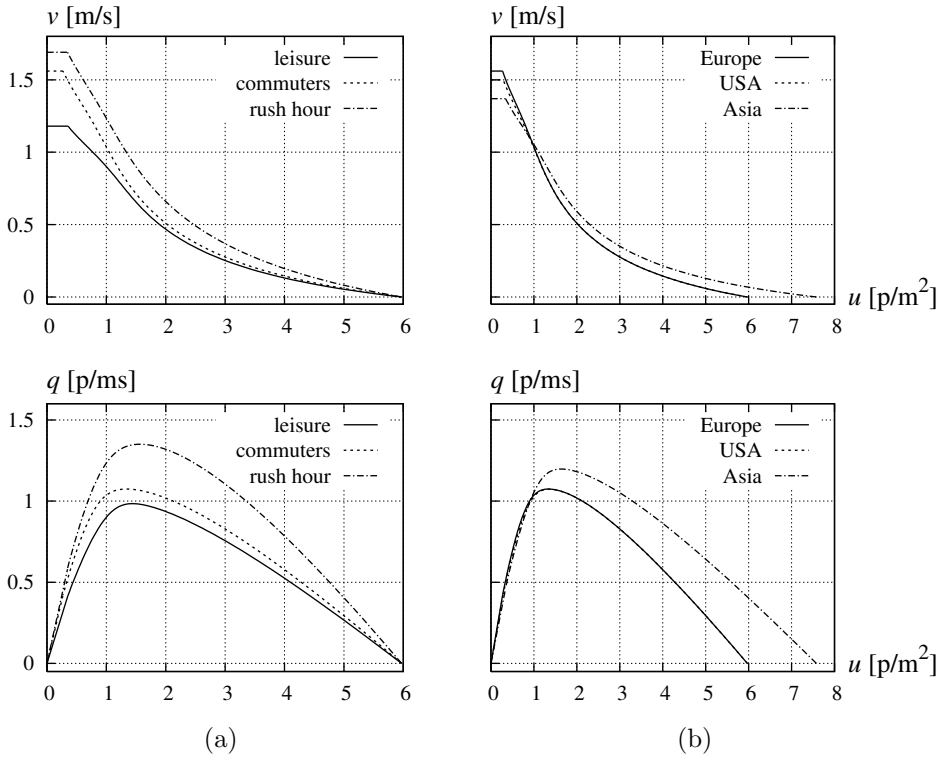

Figure 3.7. Fundamental diagrams varying the travel purpose (a) and the geographic area (b)

Table 3.3. Original (O) and revisited (R) fundamental laws proposed in literature

Kladek formula	$v = v_M \left\{1 - \exp\left[-1.913\left(\frac{1}{u} - \frac{1}{5.4}\right)\right]\right\}$	O
	$v = v_M \left\{1 - \exp\left[-\gamma\left(\frac{1}{u} - \frac{1}{u_M}\right)\right]\right\}$	R
Vehicular law	$v = v_M \exp\left(-\alpha \frac{u}{u_M - u}\right)$	O
	$v = \begin{cases} v_M & u \leq u_c \\ v_M \exp\left(-\gamma \frac{u - u_c}{u_M - u}\right) & u > u_c \end{cases}$	R

determined according to the principles explained in the previous section (see Eq. 3.3, 3.6) and γ is the fitting free parameter determined referring to the same experimental

data (Oeding 1963, Fruin 1987) selected on the basis of the travel purpose. The results of the fitting are reported in Table 3.4: it should be pointed out that the coefficients γ do not show a monotonic trend for increasing free speeds. The revisited laws and the interpretative model are plotted in Fig. 3.8 in the case of Europe and leisure/shopping.

The vehicular traffic law shows a good correspondence with the other two for densities lower than 2 ped/m^2, while it underestimates the velocities for higher densities: this behaviour is stressed in the flow diagram. It can be explained recalling that, in the case of vehicular traffic, the driver tends to reduce speed more quickly for high densities, in order to avoid crashes. As can be noticed, the physical-based

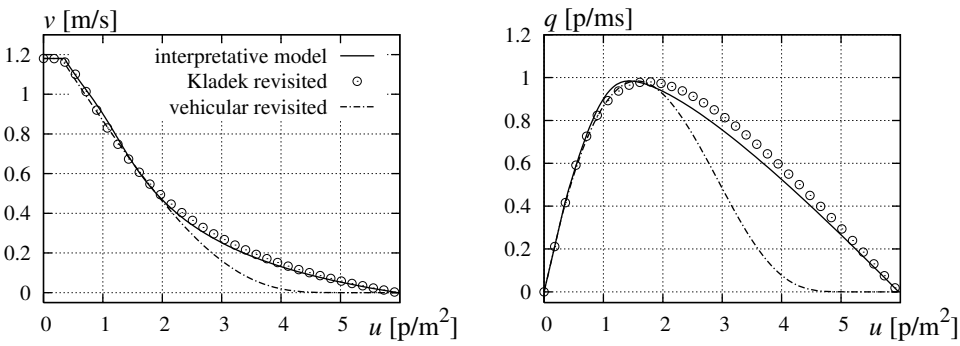

Figure 3.8. Velocity and fundamental diagrams for the three laws in the case of Europe and leisure/shopping

model shows a surprising agreement with the revisited Kladek formula, even though the same results are obtained through different approaches, i.e. based on microscopic interpretative modelling and fitting to macroscopic observation data, respectively. The physical-based model represents a complementary tool to shed some light on the role that microscopic walking phenomena play in the macroscopic fundamental relation, while the revisited Kladek formula, because of its continuity and compact direct form, is more suitable for practical use and will be retained in the following.

Table 3.4. Coefficients γ in the revisited fundamental laws

γ	Leisure/Shopping	Commuters/Events	Rush hour/Business
Kladek revisited	$0.245u_M$	$0.214u_M$	$0.273u_M$
Vehicular law	2.191	2.340	1.788

3.3.3 Space dislocation and time delay

As stressed in §2.2.2, an improvement of the main framework (3.2) can be achieved by introducing in the closure equation a space dislocation δ and a time delay τ (see Eq. 2.27). From a phenomenological point of view, they can be explained as follows:

- the pedestrians react according to what they see in a suitable stretch of road in front of them, and this length is dependent on the walking speed. A similar assumption is made by Delitala and Tosin (2007) for a kinetic vehicular model, where δ is referred to as *visibility length*. In the case of pedestrian traffic, the dislocation parameter δ can be interpreted as the sensory distance d_s discussed in §3.3.1. It has to be noticed that d_s is a microscopic distance, since it refers to one pedestrian, while δ is related to a cluster of pedestrians at the macroscopic scale. Bearing in mind this analogy, δ can be obtained as:

$$\delta = d_s \, d_c/d_0, \tag{3.12}$$

  where d_c has to be intended as the characteristic dimension of a cluster of pedestrians;

- the pedestrians adjust their step to the deck motion with a synchronization time delay τ. Generally speaking, the time delay is expected to be greater than the time interval between two succeeding footfalls.

According to these hypothesis, the closure equation can be rewritten in the form:

$$v(u, \zeta) = v[u(x + \delta, t), \zeta(x, t - \tau)]. \tag{3.13}$$

In the following, only the space dislocation will be considered in order to study the qualitative properties of the model, that is:

$$v(u) = v[u(x + \delta, t)], \;\; \delta > 0. \tag{3.14}$$

A first order Taylor expansion of u gives:

$$u(x + \delta, t) \cong u(x, t) + \frac{\partial u}{\partial x}(x, t)\delta, \tag{3.15}$$

so that:

$$\begin{aligned} v(u(x + \delta, t)) &\cong v\left(u(x, t) + \frac{\partial u}{\partial x}(x, t)\delta\right) \\ &\cong v(u(x, t)) + v'(u(x, t))\frac{\partial u}{\partial x}(x, t)\delta \\ &= v(u) + v'(u)\delta\frac{\partial u}{\partial x}. \end{aligned} \tag{3.16}$$

Let us substitute Eq. (3.16) in the mass conservation equation:

$$\frac{\partial u}{\partial t} + \frac{\partial}{\partial x}\left(uv(u) + uv'(u)\delta\frac{\partial u}{\partial x}\right) = 0, \tag{3.17}$$

that is:

$$\frac{\partial u}{\partial t} + \frac{\partial}{\partial x}(uv(u)) + \frac{\partial}{\partial x}\left[(uv'(u))\left(\delta\frac{\partial u}{\partial x}\right)\right] = 0. \tag{3.18}$$

The parameter δ is a function of the pedestrian velocity v, that is, of the crowd density, $\delta = \delta(u)$. Lets now consider the last term of Eq. (3.18). It can be rewritten as follows, by introducing $G(u) = uv'(u)\delta(u)$:

$$\begin{aligned}\frac{\partial}{\partial x}\left[G(u)\frac{\partial u}{\partial x}\right] &= \frac{\partial}{\partial x}G(u)\frac{\partial u}{\partial x} + G(u)\frac{\partial^2 u}{\partial x^2} \\ &= G'(u)\left(\frac{\partial u}{\partial x}\right)^2 + G(u)\frac{\partial^2 u}{\partial x^2}.\end{aligned} \tag{3.19}$$

Coming back to Eq. (3.18) and assuming:

$$\frac{\partial}{\partial x}(uv(u)) = q'(u)\frac{\partial u}{\partial x}, \tag{3.20}$$

where $q = uv(u)$ is the flow and $q'(u) = v(u) + uv'(u)$ is the propagation speed, we finally have:

$$\frac{\partial u}{\partial t} + q'(u)\frac{\partial u}{\partial x} = -G'(u)\left(\frac{\partial u}{\partial x}\right)^2 - G(u)\frac{\partial^2 u}{\partial x^2}. \tag{3.21}$$

The first member of Eq. (3.21) is the well-known convection term that would be obtained with a closure equation without space dislocation $v = v(u)$, while the second member introduces a diffusive term that has the effect of turning the hyperbolic equation into a parabolic one.

Eq. (3.21) can be particularised for a specific $v - u$ relation. The revisited Kladek formula is chosen as the most suitable and is rewritten in a dimesionless form:

$$v = 1 - exp\left[-\gamma\left(\frac{1}{u} - 1\right)\right]. \tag{3.22}$$

Therefore, the terms $q'(u)$, $G(u)$ and $G'(u)$ become:

$$q'(u) = 1 - \left(1 + \frac{\gamma}{u}\right)\exp\left\{-\gamma\left(\frac{1}{u} - 1\right)\right\}, \tag{3.23}$$

$$G(u) = -\frac{\gamma}{u}\exp\left\{-\gamma\left(\frac{1}{u} - 1\right)\right\}\delta(u), \tag{3.24}$$

$$G'(u) = \frac{\gamma}{u^2}\left[\left(1 - \frac{\gamma}{u}\right)\delta(u) - u\delta'(u)\right]\exp\left\{-\gamma\left(\frac{1}{u} - 1\right)\right\}. \tag{3.25}$$

In order to evaluate the weights of the three terms, they are calculated for a 90-m-long platform located in Europe, by assuming the ratio $d_c/d_0 = 2$. Results are plotted in Fig. 3.9 in dimensionless form.

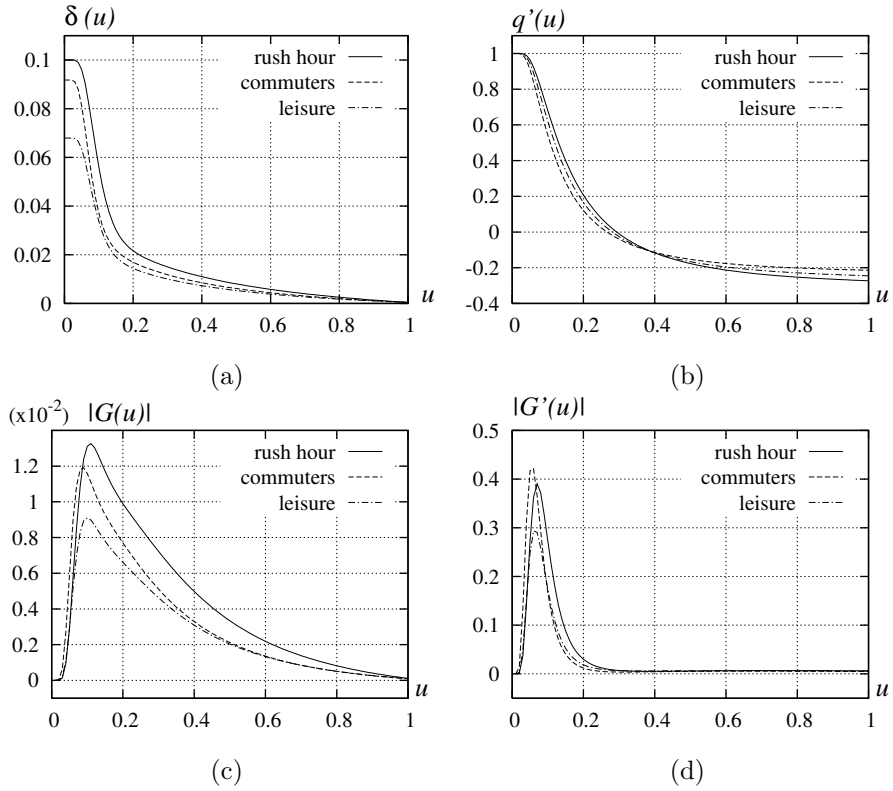

Figure 3.9. Space dislocation (a), convective term (b) and diffusive terms (c)-(d)

3.4 Crowd-to-Structure action: the force model

The scheme in Fig. 3.1 shows that the Crowd-to-Structure interaction takes place in two ways. On one hand, the mass M is constantly updated by adding the pedestrian mass M_c to the structural mass M_s; on the other hand, a force model is proposed to determine the lateral force exerted by pedestrians on the footbridge deck (Venuti and Bruno, 2007b).

The force model has the aim of giving due weight to some important features of the crowd-structure interaction phenomenon, that so far have not been taken into account, that is:

- the dependence of the pedestrian force on the two-way interaction between two systems, the crowd and the structure, which can be described by two variables, the pedestrian density and the footbridge lateral vibration;
- the possibility of a inhomogeneous distribution of the crowd along the deck due to bottlenecks, congested traffic or other non-linear traffic phenomena;
- the existence of two kinds of synchronization, as recently pointed out by Ricciardelli (2005) and Venuti et al. (2005), one between the pedestrians and the structure and the other among the pedestrians. The latter takes place when the relative movement of the pedestrians is constrained because of high crowd density;
- the presence of different frequency components in the overall force;
- triggering of the lock-in phenomena and the resulting self-limited oscillations.

It is worth recalling the hypothesis, presented in §3.3.3, that pedestrians react to the deck oscillations with a time delay τ. Therefore, all the variables describing the deck motion that are introduced in this section refer to the time $t - \tau$.

The model is conceived on the basis of a macroscopic description of crowd dynamics, which means that the pedestrians are not viewed as single individuals but as clusters characterized by a mean walking velocity and a mean step frequency. Nevertheless, an adaptation of the model to a microscopic or statistical description of the crowd is possible.

The proposed force model can be ascribed to the category of time-domain models. It is based on the assumption that the force exerted by a number n of pedestrians walking along a portion of the bridge span is given by the sum of three components:

$$F = F_{ps} + F_{pp} + F_s, \tag{3.26}$$

where F_{ps} is the term due to the synchronization between the pedestrians and the structure, F_{pp} is due to the synchronization among pedestrians and F_s is the part due to uncorrelated pedestrians.

F_{ps} has the same frequency f_s as the excited lateral structural mode, while the other two terms have the same frequency f_{pl} as the lateral pedestrian footstep. f_{pl}, which is half the walking frequency f_p, is assumed to vary as a function of the walking velocity v, as stated in §3.3 (Fig. 3.5), that is:

$$f_{pl} = (0.35v(u)^3 - 1.59v(u)^2 + 2.93v(u))/2. \tag{3.27}$$

It is worth stressing that the pedestrians who walk with a step frequency equal to f_{pl} are the ones not synchronized to the structure, that is, they are not sensitive to the deck lateral motion. This is the reason why the velocity v in Eq. (3.27) is only a function of u: in other words the term $g(\zeta)$ is not taken into account in the expression

of v.

Each term of the overall force is weighted on the basis of phenomenological considerations, by means of three weights, n_{ps}, n_{pp} and n_s, that can be considered, respectively, as the number of pedestrians in the cluster that are synchronized with the structure, synchronized to each other and uncorrelated:

$$\begin{aligned} n_{ps} &= nS_{ps} \\ n_{pp} &= nS_{pp}(1 - S_{ps}) \\ n_s &= n - n_{ps} - n_{pp} \end{aligned} \tag{3.28}$$

where S_{ps} and S_{pp} are the synchronization coefficients, which both vary in the [0 1] range. Thanks to the distinction of pedestrians in three categories, the model is able to represent the triggering of lock-in: even though no one is synchronized with the structure, the presence of a high crowd density results in a lateral force that triggers the lateral vibration of the bridge.

S_{ps} represents the degree of coupling between the crowd and the structure. This is a function of two variables: the structure lateral acceleration and the ratio $f_r = f_{pl}/f_s$, where f_r is defined in the [0 2] domain: the lower bound depends on the minimum value of f_{pl} (f_{pl} =0), when the walking velocity is null; the upper bound was obtained from the laboratory tests reported by Pizzimenti (2005), according to which pedestrians are not influenced by structural oscillations under 0.6 Hz and the maximum recorded lateral walking frequency is 1.1 Hz. The variation of S_{ps} versus ζ (Fig. 3.10a) is given by a fitting of the Dallard et al. (2001) experimental data, by means of the interpolating function:

$$S_{ps}(\zeta) = 1 - e^{-b(\zeta - \ddot{z}_c)}. \tag{3.29}$$

Pedestrians start to synchronize with the structure for values of ζ higher than $\ddot{z}_c$, and they are completely synchronized when ζ reaches the maximum value $\ddot{z}_M$. $S_{ps}(f_r)$ is supposed to have a normal distribution, with a variance that grows when ζ increases. This means that, for increasing values of ζ, the pedestrians who walk with a step frequency that is different from f_s gradually become involved in the synchronization phenomenon. For $\zeta = \ddot{z}_M$, everyone is synchronized with the structure, whatever the value of f_r (Fig. 3.10b). $S_{ps}(f_r)$ is defined as:

$$\begin{aligned} S_{ps}(f_r) &= e^{[-\eta(f_r-1)^2]}, \\ \eta(\zeta) &= 50e^{(-20\zeta/\pi)}. \end{aligned} \tag{3.30}$$

The synchronization coefficient $S_{ps}(\zeta, f_r)$ is given by the product of equations (3.29) and (3.30).

The coefficient S_{pp} (Fig. 3.11) represents the degree of synchronization among pedestrians and, because of the lack of experimental data, it has been defined in a qualitative way as a function of the crowd density u [ped/m^2]:

$$S_{pp}(u) = \frac{1}{2}\left\{1 + erf\left[a\left(u - \frac{u_{sync} + u_c}{2}\right)\right]\right\}, \tag{3.31}$$

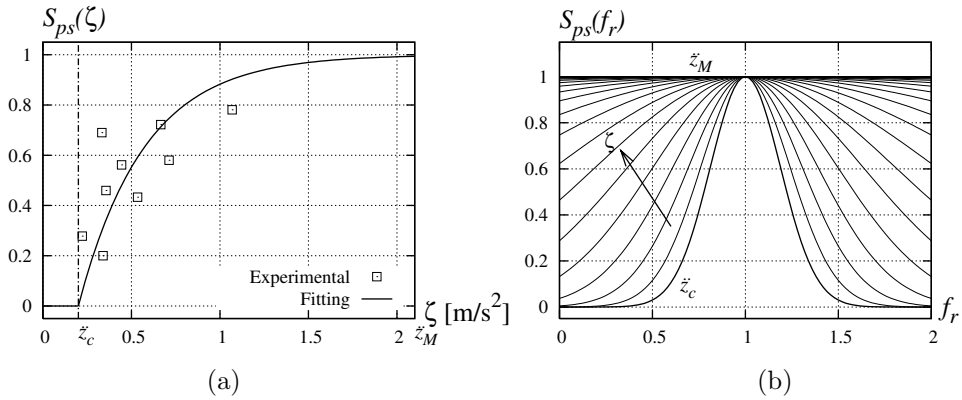

Figure 3.10. S_{ps} versus ζ (a) and f_r (b)

where a=3.14 and u_{sync} is the density that corresponds to the total synchronization of pedestrians. Its value is estimated to be 1.8 ped/m^2, according to the maximum densities recorded on crowd events (e.g. Fujino et al., 1993).

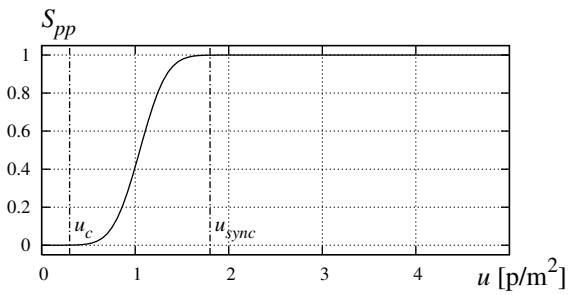

Figure 3.11. S_{pp} versus u

It is worthwhile pointing out that the proposed laws for the synchronization coefficients S_{ps} and S_{pp} can be interpreted as cumulative density functions of an exponential and a Gaussian probability density function, respectively. From this point of view, the model can be adapted to a statistical description of the phenomenon as soon as a greater amount of data is available.

The first component of the total force, F_{ps}, can be written, according to Pizzimenti (2005), as the sum of a component in-phase and another 90° out-phase with respect to the structure lateral displacement. The in-phase component can be seen as 180° out-phase of the acceleration, while the other can be seen as in-phase with the lateral velocity:

$$F_{ps} = n_{ps}[\bar{F}(\zeta)sin(2\pi f_s t + \pi) + \bar{F}(\nu)cos(2\pi f_s t)] \tag{3.32}$$

where ν is the envelope of the deck lateral velocity time history.

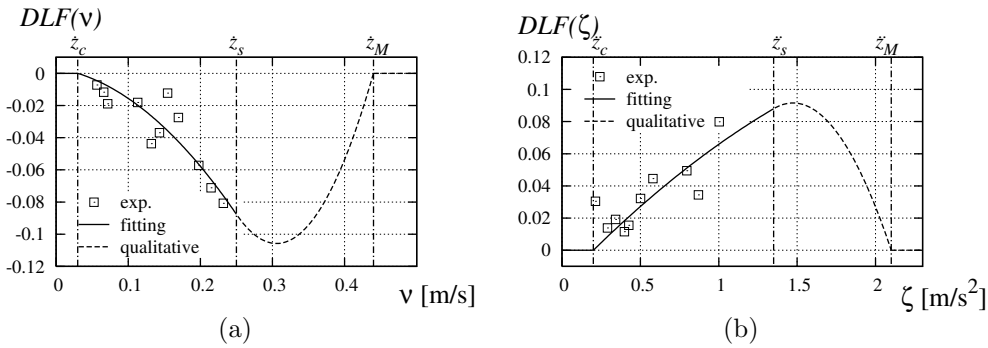

Figure 3.12. DLFs of the components in phase with ν (a) and ζ (b)

The amplitudes of the two components (Fig. 3.12) are defined by means of piecewise functions. The first branch comes from a quadratic fitting of the experimental data concerning the medium Dynamic Load Factors (DLFs) of the in-phase and out-of-phase components (Pizzimenti, 2005). The data corresponding to DLFs close to zero for non null ν or ζ, and to ν or ζ above their serviceability limit (that is, $\dot{z}_s$=0.25 m/s and $\ddot{z}_s$=1.35 m/s^2, Nakamura, 2003) have been discarded. The second branch is defined qualitatively, based on the following assumptions:

- the DLFs reach their maximum when the velocity and the acceleration exceed their serviceability limit;
- the DLFs decrease to zero when the velocity and the acceleration reaches maximum values, above which pedestrians stop walking, i.e. $\dot{z}_M$=0.44 m/s and $\ddot{z}_M$=2.1 m/s^2 (Nakamura, 2003). This trend also guarantees that the amplitude of F_{ps} is self-limited as is the overall structural response.

It should be pointed out that the threshold values suggested by Nakamura (2003) are based on a very limited number of observed cases. In particular, the maximum velocity and acceleration refer to those recorded on the Millennium Bridge, while the serviceability values are based on the field tests performed on the M-bridge in Japan. Recalling that the ratio between the acceleration and the velocity amplitudes depends on the natural frequency of vibration f_s (i.e. $|\zeta/\nu| = 2\pi f_s$), it is clear that the threshold values on the velocity and on the acceleration are simultaneously reached only for a particular frequency.

The second force component, F_{pp}, is defined as:

$$F_{pp} = n_{pp}\bar{F}_s sin(2\pi f_{pl} t) \tag{3.33}$$

where $\bar{F}_s$ is the medium amplitude of the force exerted by a single pedestrian in the case of a motionless deck, whose DLF=0.04 (Živanović et al., 2005).

Finally, the component F_s is determined according to the model proposed by Matsumoto et al. (1978), who found that the force due to n uncorrelated pedestrians is $\sqrt{n}$ higher than the force due to a single pedestrian. Therefore, F_s becomes:

$$F_s = \sqrt{n_s}\bar{F}_s sin(2\pi f_{pl} t). \tag{3.34}$$

Chapter 4

Computational approach

The solution of the mathematical model described in Chapter 3 is obtained by means of computational simulation performed in the space and time domains. This Chapter is devoted to the description of the Matlab code, specifically developed to simulate crowd-structure interaction.

4.1 Partitioned simulation strategies

The partitioned analysis of the coupled system allows the two-solver approach outlined in Fig. 4.1 to be used: a Computational Crowd Dynamics (CCD) solver for the PDE governing the Crowd subsystem and a Computational Structural Dynamics (CSD) solver for the ODE governing the Structure subsystem. In other words, the coupled system is decomposed into two fields, the Crowd and the Structure, that are computationally treated as isolated entities. Interaction effects are viewed as forcing effects that are communicated between the individual components using prediction, substitution and synchronization techniques (the latter only if the fields are separately stepped in time) (Park et al., 1999).

Fig. 4.2 shows the flowchart of the computational code. The code has been conceived in order to perform different types (#) of simulation, that could involve the complete model or just some of its parts:

1. crowd dinamics only;
2. crowd dynamics with imposed $\ddot{z}$;
3. structural dynamics with imposed F;
4. crowd-structure interaction without crowd added mass M_c;

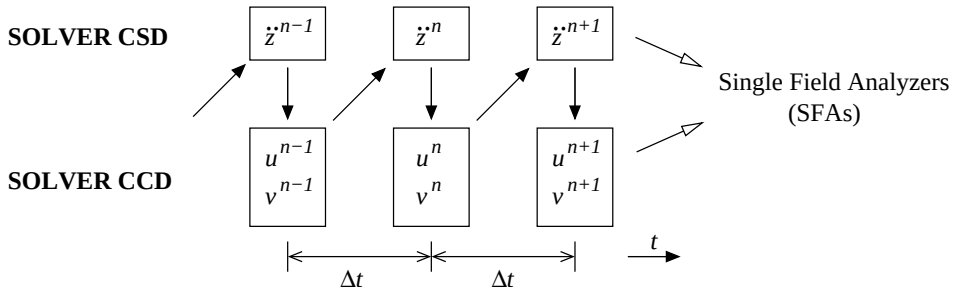

Figure 4.1. Scheme of the two-solver approach strategy

5. complete crowd-structure interaction.

Each part of the code will be discussed in the next sections.

4.2 Space and time grids

As stated in §2.2.4, the differential partitioning of the coupled system allows different discretization grids to be chosen for each subsystem. Some *a-priori* considerations about the computational grids can be drawn. The crowd and structural dynamics have quite different space and time scales. As far as the space discretization step Δx is concerned, the pedestrian traffic phenomena in fact require a dense computational grid because of the possibility of the occurence of high density gradients. On the other hand, the frequency of one of the first lateral modes usually falls in the lock-in region for the structures of interest: hence, a coarser grid can be used to describe the corresponding mode shape. For these reasons, non-matching space meshes are generated in the crowd field (subscript c) and structural field (subscript s), and this allows for a relevant reduction of the computational costs of the modal analysis. If the structure is modelled by means of a 3D MDOF model, only the deck nodes are retained for data interpolation between non-matching grids: space distributed variables (e.g. u) are treated by means of a standard quadratic interpolation while conservative interpolation (Farhat et al., 1998; Jiao and Heath, 2004) is used for the crowd added mass M_c. Furthermore, the step Δx_c should satisfy the continuity assumption of the model. It follows that it has a lower bound equal to the depth occupied by one pedestrian in a condition of congested traffic, i.e. $\underline{\Delta x_c} = d_0$.

A similar problem arises for the time discretization step Δt. The characteristic time of the structure, that is, the period of oscillation of interest T_s, is much smaller than the crowd characteristic time T_c, defined in §2.2.2. It follows that the structural field requires a finer time grid in order to fully describe the dynamics of the structure. Bearing this in mind, a common time step Δt is used for the simulation of both

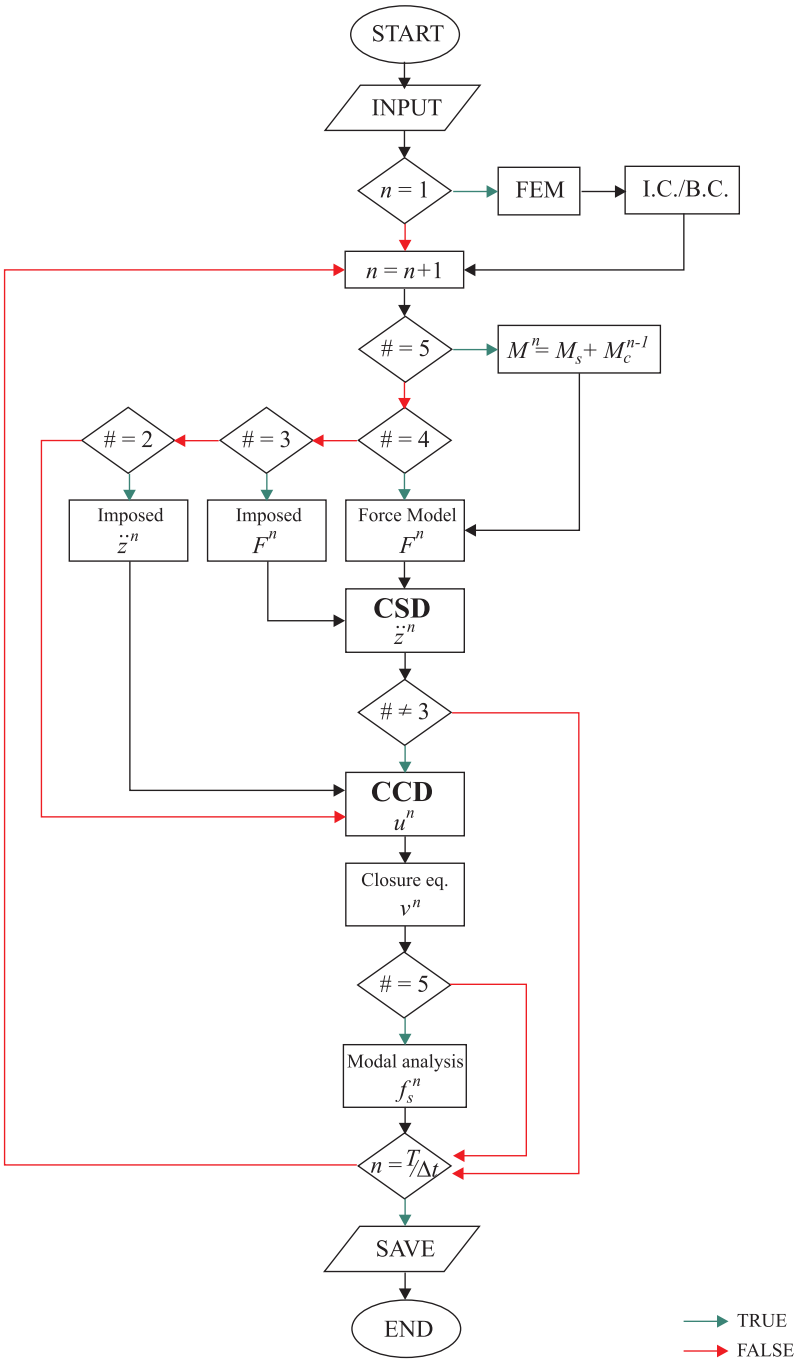

Figure 4.2. Flowchart of the computational code

phenomena, and its value is discussed in §4.3.

The notation used in the next Sections is as follows:
$h = \Delta x =$ space step
$k = \Delta t =$ time step
$x_j = jh = j$th point in the space grid
$t^n = nk = n$th instant of time.

4.3 Computational Structural Dynamics (CSD) solver

The Finite Element Method is employed for the space discretisation of the 3D structural field. As far as the advancement in time is concerned, the CSD solver employes a step-by-step integration method to solve the non-linear ODE that describes the multi-degree-of-freedom (MDOF) Structure subsystem (Eq. 2.12). The Constant Average Acceleration (CAA) method, which is one of the Newmark Beta methods, is chosen since it is widely used in practice, because it has the advantage of being unconditionally stable. The scheme is implemented using an incremental formulation, so that the procedure can be applied either to linear or non-linear analysis (Clough and Penzien, 1987).

The basic concept of a integration method is expressed by the following equations:

$$\begin{aligned} \dot{\mathbf{s}}_1 &= \dot{\mathbf{s}}_0 + \int_0^k \ddot{\mathbf{s}}(\tau)d\tau \\ \mathbf{s}_1 &= \mathbf{s}_0 + \int_0^k \dot{\mathbf{s}}(\tau)d\tau \end{aligned} \tag{4.1}$$

which express the velocity and displacement vectors at the end of the time step. The CAA method assumes the acceleration to be constant during the time step, leading to a linear variation of the velocity and a quadratic variation of the displacement (Fig. 4.3).

In the Newmark formulation, Eqs. (4.1) are expressed as follows:

$$\begin{aligned} \dot{\mathbf{s}}_1 &= \dot{\mathbf{s}}_0 + (1-\gamma)k\ddot{\mathbf{s}}_0 + \gamma k\ddot{\mathbf{s}}_1 \\ \mathbf{s}_1 &= \mathbf{s}_0 + k\dot{\mathbf{s}}_0 + (1/2-\beta)k^2\ddot{\mathbf{s}}_0 + \beta k^2\ddot{\mathbf{s}}_1 \end{aligned} \tag{4.2}$$

where the factor γ controls the amount of artificial damping induced by the integration procedure, which is null if $\gamma = 1/2$. The CAA method is characterized by $\gamma = 1/2$ and $\beta = 1/4$.

The exposed implicit formulation has to be converted in a explicit form. The explicit incremental procedure of the CAA method is described in the following. First, the effective stiffness matrix within the time step k is defined as:

$$\tilde{\mathbf{K}} = \mathbf{K} + \frac{2}{k}\mathbf{C} + \frac{4}{k^2}\mathbf{M}, \tag{4.3}$$

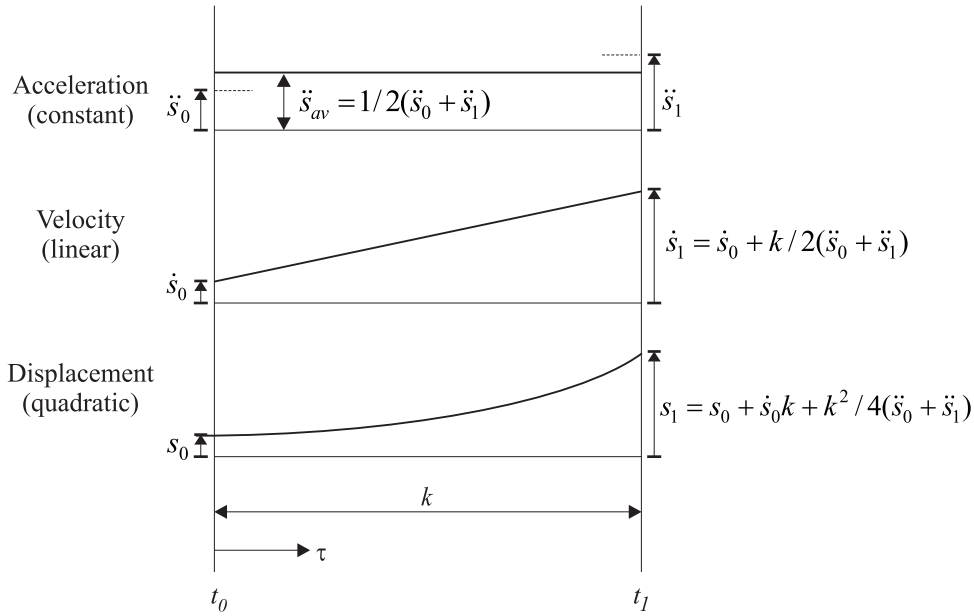

Figure 4.3. Motion based on constant average acceleration, after Clough and Penzien (1987)

while the incremental effective load vector is:

$$\Delta\tilde{\mathbf{F}} = \Delta\mathbf{F} + 2\mathbf{C}\dot{\mathbf{s}}_0 + \mathbf{M}\left[\frac{4}{k}\dot{\mathbf{s}}_0 + 2\ddot{\mathbf{s}}_0\right]. \tag{4.4}$$

Then the incremental displacement $\Delta\mathbf{s}$ is obtained by solving:

$$\tilde{\mathbf{K}}\Delta\mathbf{s} = \Delta\tilde{\mathbf{F}} \tag{4.5}$$

and the velocity increment is given by the following expression:

$$\Delta\dot{\mathbf{s}} = \frac{2}{k}\Delta\mathbf{s} - 2\dot{\mathbf{s}}_0. \tag{4.6}$$

Finally, the acceleration at the end of the time step is given by:

$$\ddot{\mathbf{s}}_1 = \mathbf{M}^{-1}(\mathbf{F}_1 - \mathbf{C}\dot{\mathbf{s}}_1 - \mathbf{K}\mathbf{s}_1). \tag{4.7}$$

As previously stated, the CAA method is unconditionally stable with respect to the size of the time step and, for this reason, is a very robust method that can be used for the step-by-step dynamic analysis of MDOF structural systems. On the other hand, the size of the time step influences not only the stability but also the

accuracy of the solution. A time step $k \leq 1/(20 f_{max})$ is recommended, where f_{max} is the highest natural frequency of vibration which significantly contributes to the structural response.

4.4 Computational Crowd Dynamics (CCD) solver

The CCD solver employes the Finite Difference Method to obtain the approximate solution to the non-linear PDE governing the crowd dynamics, that is rewritten in the form:

$$\frac{\partial u}{\partial t} + \frac{\partial}{\partial x} f(u) = 0, \tag{4.8}$$

where $f(u) = uv$ is the *flux function*. Eq. (4.8) holds for $t \geq 0$ and $0 < x < L$. In this case it is necessary to specify both the initial conditions (ICs) $u(x, 0)$ and the boundary conditions (BCs) at the inlet $u(0, t)$ and at the outlet $u(L, t)$. A Dirichlet BC is defined at the inlet, while a Von Neumann BC is imposed at $x = L$ ($\partial u/\partial x = 0$).

In this section some numerical methods for conservation laws are briefly reviewed, with reference to Leveque (1992)'s complete monograph. A finite difference method produces approximations U_j^n to the solution $u_j^n = u(x_j, t^n)$ of Eq. (4.8). Four different numerical schemes have been tested to establish the appropriate one: the Upwind (UP) and Lax-Friederichs (LF) schemes, which are first order ones; the Lax-Wendroff (LW) and MacCormack (MC) schemes, which use a two-step splitting procedure to achieve second order accuracy. The time derivative is replaced by a forward-in-time approximation, which means that the solution at time $n + 1$ only depends on the solution at the previous time n (explicit 2-level method). In general, it is possible to write:

$$U^{n+1} = \mathcal{H}_k(U^n), \tag{4.9}$$

where U^{n+1} is the vector of approximations U_j^{n+1} and $\mathcal{H}_k(U^n)$ is an operator that expresses the dependence of U_j^{n+1} at point j on several values from the vector U^n, depending on the *stencil* of the scheme (Fig. 4.4). In the following the mesh ratio k/h is assumed to be constant.

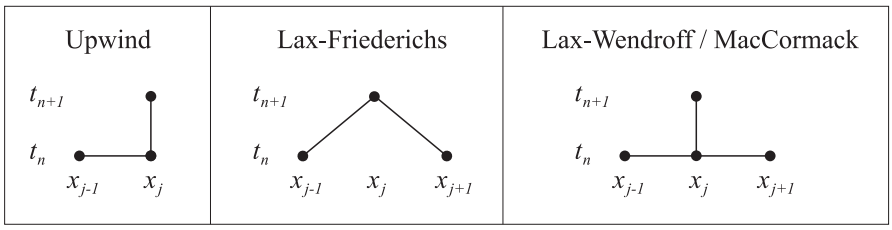

Figure 4.4. Stencils of the finite difference schemes

In order to guarantee convergence to the so-called *weak solution*, that is, the one which satisfies the integral form of the conservation equation (see A.1), the schemes are implemented in their conservation form:

$$U_j^{n+1} = U_j^n - \frac{k}{h}[G(U_{j-p}^n, U_{j-p+1}^n, \ldots, U_{j+q}^n) - G(U_{j-p-1}^n, U_{j-p}^n, \ldots, U_{j+q-1}^n)], \quad (4.10)$$

where G is called *numerical flux function*. In the simplest case, $p = 0$ and $q = 1$ so that G is a function of two variables and Eq. (4.10) becomes:

$$U_j^{n+1} = U_j^n - \frac{k}{h}[G(U_j^n, U_{j+1}^n) - G(U_{j-1}^n, U_j^n)]. \quad (4.11)$$

The UP scheme is defined as follows:

$$U_j^{n+1} = U_j^n - \frac{k}{h}[f(U_j^n) - f(U_{j-1}^n)]. \quad (4.12)$$

It should be pointed out that the upwind scheme becomes *downwind* when the propagation speed $s_p = f'(u)$ is negative.

The conservative form of the LF scheme is:

$$U_j^{n+1} = U_j^n - \frac{k}{h}[G(U_j^n, U_{j+1}^n) - G(U_{j-1}^n, U_j^n)], \quad (4.13)$$

where

$$G(U_j^n, U_{j+1}^n) = \frac{h}{2k}(U_j^n - U_{j+1}^n) + \frac{1}{2}[f(U_j^n) - f(U_{j+1}^n)]. \quad (4.14)$$

The two II Order schemes are generalized to non-linear systems by using a two-step procedure. The LW scheme takes the form:

$$\begin{aligned} U_{j+1/2}^{n+1/2} &= \frac{1}{2}(U_j^n + U_{j+1}^n) - \frac{h}{2k}[f(U_{j+1}^n) - f(U_j^n)] \\ U_j^{n+1} &= U_j^n - \frac{h}{k}[f(U_{j+1/2}^{n+1/2}) - f(U_{j-1/2}^{n+1/2})], \end{aligned} \quad (4.15)$$

while MC is:

$$\begin{aligned} U_j^* &= U_j^n - \frac{h}{k}[f(U_{j+1}^n) - f(U_j^n)] \\ U_j^{n+1} &= \frac{1}{2}(U_j^n + U_j^*) - \frac{h}{2k}[f(U_j^*) - f(U_{j-1}^*)]. \end{aligned} \quad (4.16)$$

Local truncation error

The local truncation error $L_k(x,t)$ is a measure of how well the difference equation models the differential equation locally. It can be obtained by replacing the approximate solution U_j^n in the difference equations by the true solution $u(x_j, t_n)$. For a

general 2-level method, the local truncation error is defined by:

$$L_k(x,t) = \frac{1}{k}[u(x,t+k) - \mathcal{H}_k(u(\cdot,t);x)], \tag{4.17}$$

where $u(\cdot,t)$ denotes the function of x alone obtained by fixing t. The method is of order p if, for all sufficiently smooth initial data with compact support, there is some constant C_L such that

$$\|L_k(\cdot,t)\| \leq C_L k^p \quad for\ all\ k < k_0, t \leq T. \tag{4.18}$$

If the procedure is applied, as an example, to the LF scheme, it can be found that L_k linearly depends on k, therefore the scheme is said to be first-order accurate. It should be pointed out that L_k is the local order of the method, but it results that, for smooth solutions, the global error is of the same order, provided the method is stable.

Stability

According to Courant, Friederichs and Lewy, the necessary condition for stability of a numerical scheme in the form (4.10) is:

$$\left| s_p \frac{k}{h} \right| \leq 1. \tag{4.19}$$

Eq. (4.19) is called CFL condition and the first term is the Courant number. If the propagation speed s_p is not constant, the CFL condition becomes:

$$k \leq \frac{h}{sup\,|s_p(x,t)|}. \tag{4.20}$$

4.4.1 Grid effects on a model equation

In order to study the qualitative behaviour of the approximate solutions, the four numerical schemes reported in the previous section are tested on a non linear hyperbolic model equation, the Burgers equation (see A.3), with Heaviside ICs

$$u(x,0) = \begin{cases} u_l & x < 0.2 \\ u_r & x > 0.2 \end{cases} \tag{4.21}$$

for which the analytical solution is available (Riemann problem) (Leveque, 1992) in two cases: $u_l > u_r$ (shock wave) and $u_l > u_r$ (rarefaction wave). All the variables are expressed in dimensionless form.

Fig. 4.5 shows a comparison between the exact and approximate solutions at t=0.5, obtained with the different numerical schemes and the same discretization in

time and space (Δt=1/1000, Δx=1/320). The first-order schemes show a diffusive effect while the second-order schemes show unphysical oscillations, especially upstream to the discontinuity: both effects are typical and are related to the local truncation error of the schemes.

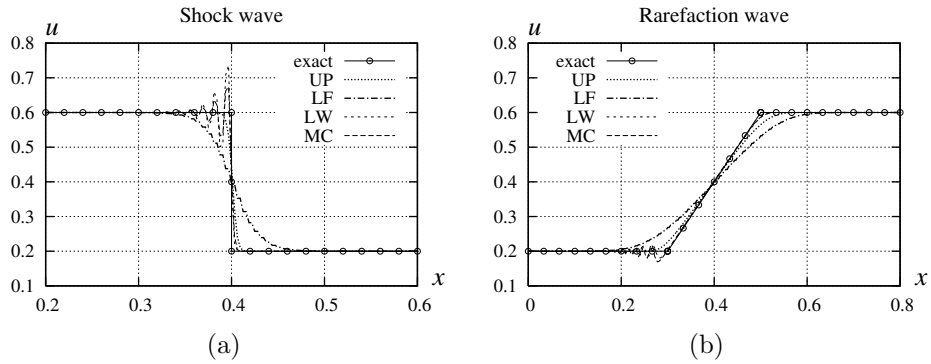

Figure 4.5. Comparison between the exact and approximate solutions of the Riemann problem

A parametric study on space discretization is then performed for each numerical scheme in the case of shock waves. The space step is systematically refined in the range [Δx_c=1/640;1/40], with a ratio of two between two successive grid sizes. The accuracy of each scheme is evaluated by means of three parameters measured in x=0.4 and t=0.5: i. the phase error between the approximate and exact solution expressed as $\epsilon_{ph} = (u_{approx} - u_{exact})/(u_l - u_r)$; ii. the diffusion evaluated by $\epsilon_d = (\partial u/\partial x)^{-1}$; iii. the maximum oscillation of the solution, which is typical of second-order schemes, calculated as $\epsilon_o = (u_{max} - u_l)/(u_l - u_r)$ (Fig. 4.6). An error threshold of 5% is fixed in order to determine the optimal space step Δx_c for each method. Fig. 4.6-c shows that the LF and MC schemes do not satisfy the imposed limit on oscillations, therefore they are discarded for the applications proposed in this work. It is worth pointing out that the Burgers equation always involves the forward propagation of the initial discontinuity, therefore it is not suitable to model all the different flow regimes. A proper choice of the numerical scheme and of the discretisation grid should be carefully evaluated for the specific simulation.

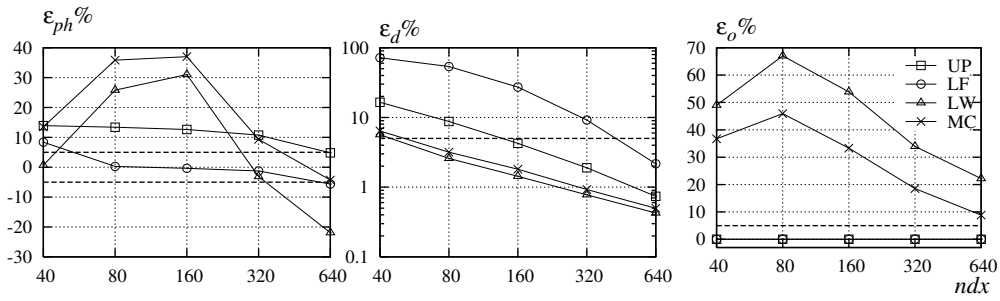

(a) (b) (c)

Figure 4.6. Evaluation of the accuracy of the numerical schemes ($t = 0.5, x = 0.4$)

Chapter 5

Applications and results

5.1 Crowd dynamics on a motionless platform

This section discusses the simulations of crowd dynamics on a motionless platform. Two kinds of simulations are performed, corresponding to two different boundary conditions at the inlet (Fig. 5.1):

1. a compact group of pedestrians that cross the initially empty bridge (BC1);
2. a smaller group of pedestrians that follows a higher density cluster (BC2).

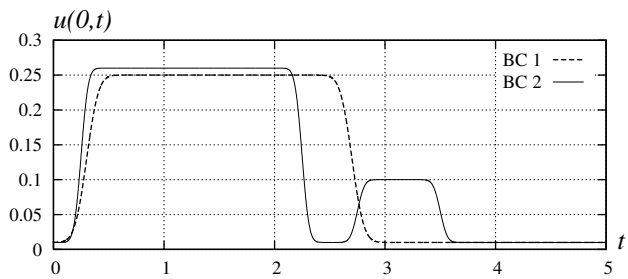

Figure 5.1. Boundary condition on the density at the inlet

The benchmark is an ideal 90-m-long footbridge located in Europe. The chosen closure equation is the revisited Kladek formula in its dimensionless form (Eq. 3.22).

The aim of the first set of simulations is to test the sensitivity of crowd behaviour to different travel purposes: rush-hour (R), commuters (C) and leisure (L). Each condition corresponds to a different value of γ and of the free speed v_M. All

the simulations are performed both in the non-dislocated ($v = v(u(x,t))$) and in the dislocated case ($v = v(u(x+\delta,t))$).

Fig. 5.2 reports the density and velocity space distributions at $t = 2.5$ for the non-dislocated case. As expected, in the R condition, which is characterised by the highest value of γ, pedestrians walk faster and fill the deck more quickly. The comparison with the dislocated case is reported in Fig. 5.3 for the R case at $t = 3$. The space dislocation δ is proportional to the walking velocity v and its main effect can be seen in terms of diffusion, that is, a smoother space distribution.

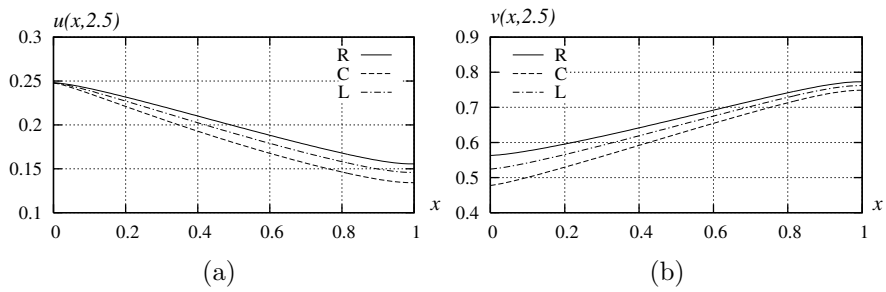

Figure 5.2. u and v space distribution at $t = 2.5$ in the non-dislocated case

The second simulation (BC2) has been performed in leisure conditions and Fig. 5.4 reports the density distribution for different instants of time:

- at $t = 1$ the first group of pedestrians is gradually filling the deck span;
- at $t = 2.5$ all the pedestrians of the first group have entered the bridge and some of them have already left;
- at $t = 3$ the smallest group enters the bridge;
- at $t = 4$ the smallest group has reached the pedestrians in front and the groups are no longer distinguishable.

The effects of the space dislocation once more have a diffusive nature.

5.2 Application of the force model

The properties of the force model described in §3.4 have been evaluated by means of a sensitivity study on the two main variables, ζ in the $[0\ \ddot{z}_M]$ m/s^2 interval and u in the $[0\ u_M]$ ped/m^2 range. The simulations are performed assuming a deck acceleration time history with constant amplitude ζ:

$$\ddot{z} = \zeta cos(2\pi f_s t). \tag{5.1}$$

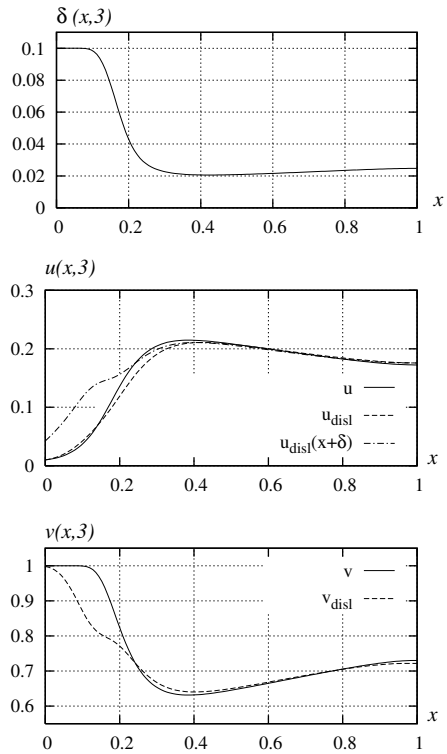

Figure 5.3. Comparison between the dislocated and non-dislocated simulation

This type of simulation can be compared to an experimental test on a moving treadmill, except that the single pedestrian is substituted by a cluster of pedestrians.

The sensitivity study has been performed by referring to two case-studies, the T-bridge and the south span of the London Millennium Bridge, since they are fully documented. Therefore, the closure equation has been characterized for the two cases as for the geographic area and the travel purpose, that is: Asia and rush hour traffic for the T-bridge (TB); Europe and leisure traffic for the Millennium Bridge (MB). A summary of the input data is reported in Table 5.1.

Fig.s 5.5a-c-e and 5.6a-c-e show the weights of the force components, scaled with respect to the number of pedestrians n, versus ζ and u. The following considerations can be made for both the case-studies:

- n_{ps} is much more sensitive to the deck acceleration ζ, than to the crowd density u and grows monotonically as ζ increases and as u decreases; it reaches the highest value for $\zeta > \ddot{z}_s$, whatever the value of u (Fig.s 5.5a and 5.6a);

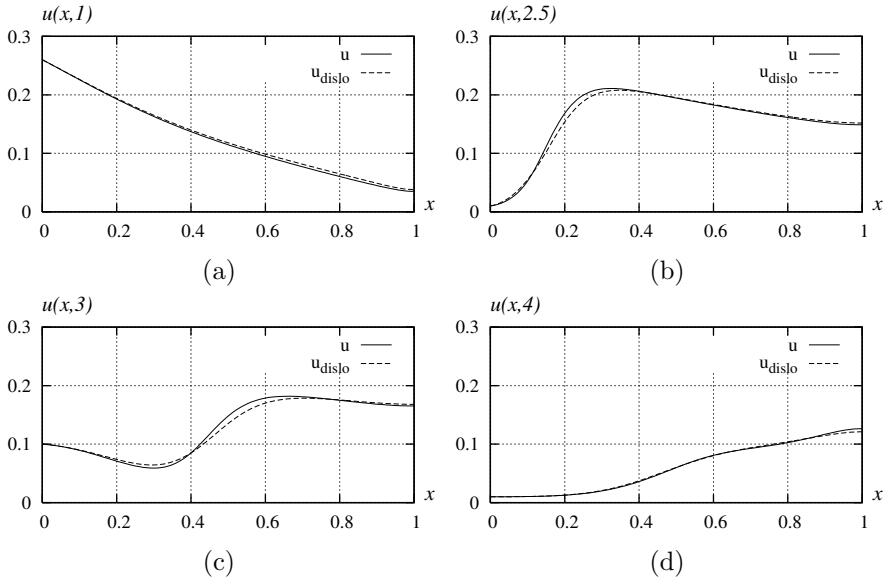

Figure 5.4. Space distributions of u for BC2

Table 5.1. Input data

	v_M [m/s]	u_M [p/m^2]	γ	u [p/m^2]	ζ [m/s^2]	f_s [Hz]
TB	1.48	7.7	$0.273u_M$	0.8÷2.0	0.34	0.9
MB	1.18	6.0	$0.245u_M$	1.3÷1.5	1.50	0.8

- n_{pp} has the opposite trend to n_{ps}: it grows as u increases and as ζ decreases. For $u > u_{sync}$ (S_{pp}=1), n_{pp} is complementary to n_{ps} (Fig.s 5.5c and 5.6c);

- n_s is obtained from subtraction of the other two terms, therefore it reaches the maximum value when ζ and u are under their critical values and is null for $\zeta > \ddot{z}_s$ and $u > u_{sync}$, when all the pedestrians are synchronized (Fig.s 5.5e and 5.6e).

A colour map of the three weights in the u-ζ plane (Fig. 5.7) can be obtained for each structure, in order to quickly estimate, in the preliminary design phase, which kind of synchronization will play the main role.

Fig.s 5.5b-d-f-h and 5.6b-d-f-h represent the amplitudes a of the three force terms (in N/m^2) and of the overall force F, which is expressed in terms of its root

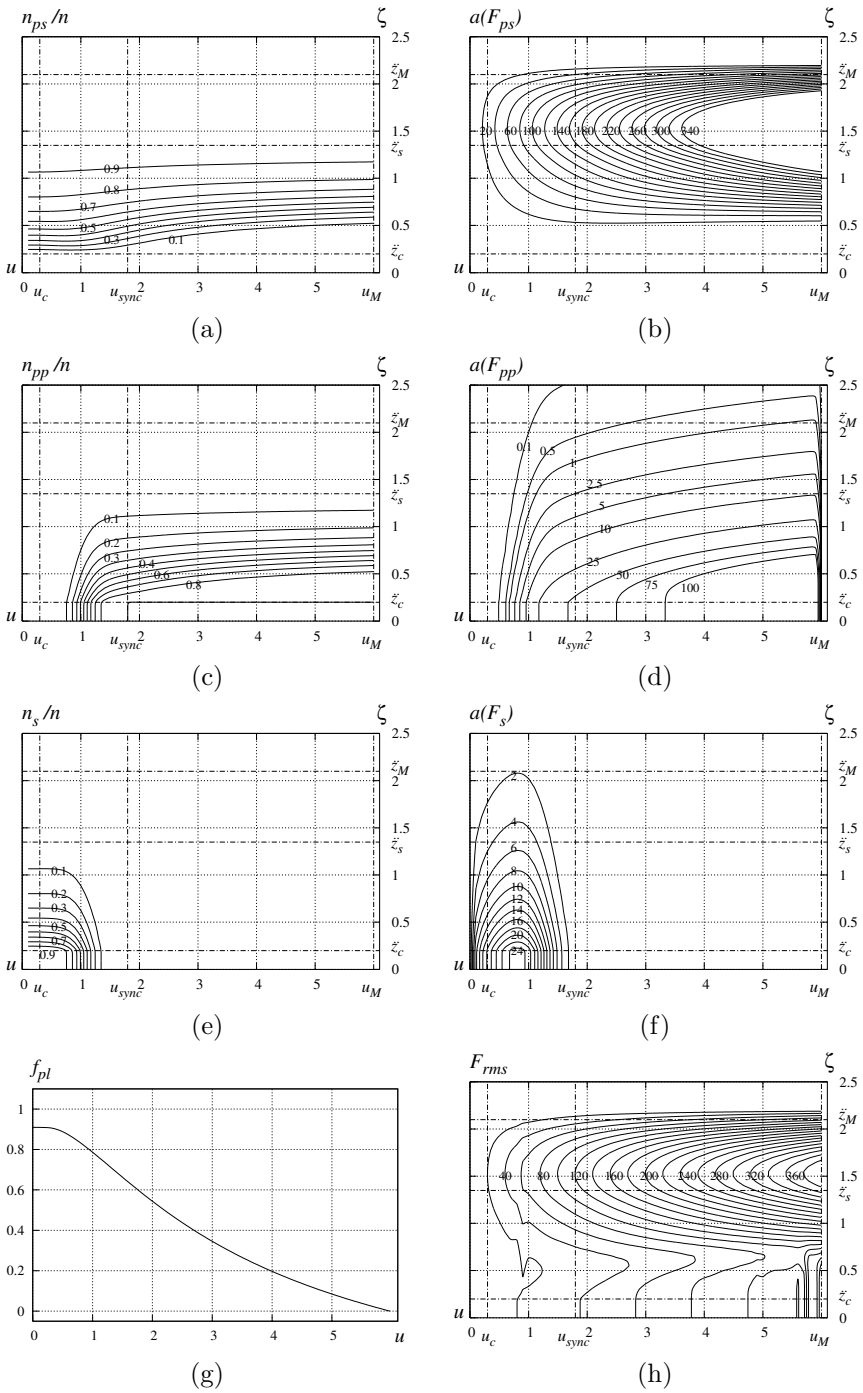

Figure 5.5. Millennium Bridge

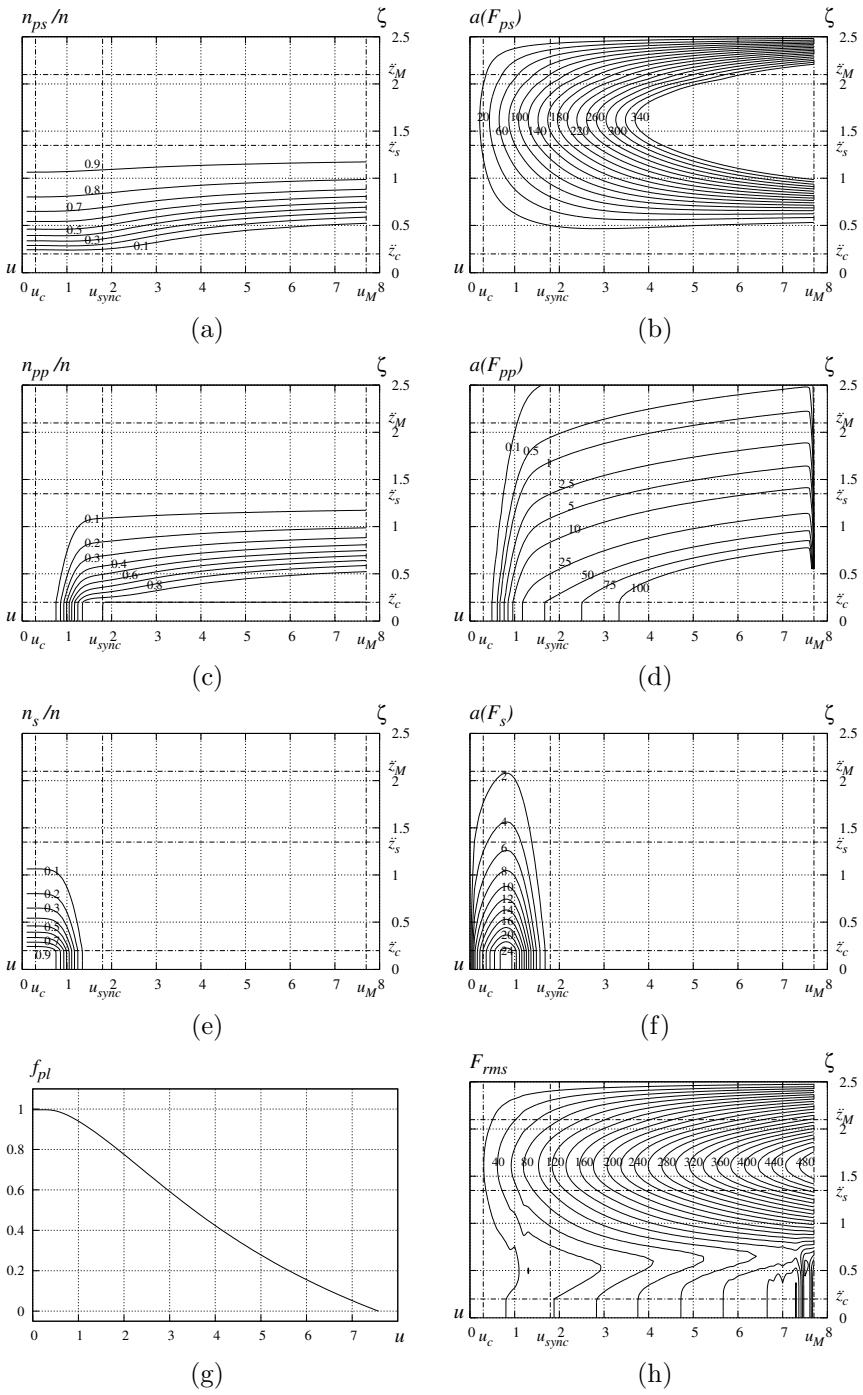

Figure 5.6. T-bridge

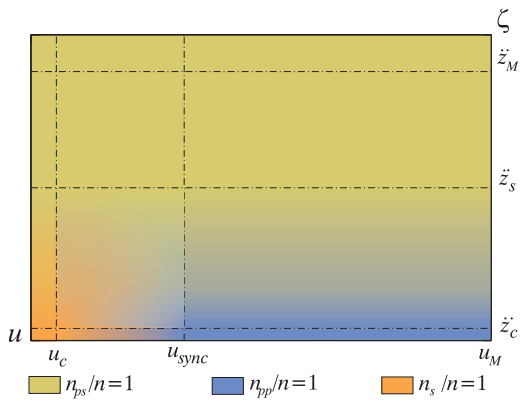

Figure 5.7. Colour map of the pedestrian synchronization

mean square (rms) value (F_{rms}), versus ζ and u. Some common features can be recognized in both cases:

- the evolution of F_{ps} versus ζ is influenced by both n_{ps} and by the distributions of the DLFs (see Fig. 3.12), which determine its non monotonic trend and its self-limited nature with respect to ζ. The dependence of F_{ps} on u is almost linear, i.e. its amplitude grows linearly as the number of pedestrians increases (Fig.s 5.5b and 5.6b);

- the amplitude of F_{pp} has the same evolution as n_{pp}, since it comes from the product of n_{pp} and the constant $\bar{F}_s$. It is worthwhile pointing out that F_{pp} goes abruptly to zero when f_{pl}=0, that is, for $u = u_M$: this means that the F_{pp} component is self-limited with respect to u (Fig.s 5.5d and 5.6d). A similar consideration can be drawn for F_s, which also has a non monotonic evolution versus u (Fig.s 5.5f and 5.6f);

- the evolution of F_{rms} versus u and ζ is not trivial, since it comes from the sum of periodic signals with different frequencies and it therefore cannot be determined by simply summing the three component amplitudes (Fig.s 5.5h and 5.6h).

The main difference between the two case-studies emerges in the F_{ps} diagrams. For the reasons explained in §3.4, F_{ps} becomes null for a value of ζ that is higher than $\ddot{z}_M$, depending on the value of f_s. As an example, Fig. 5.8 plots the amplitudes of the two F_{ps} components for the T-bridge: both the component in phase with the acceleration $\bar{F}(\zeta)$ and the one in phase with the velocity $\bar{F}(\nu)$ are null when ζ and

ν reach their the maximum values, but in the T-bridge case the limit values are non simultaneoulsy obtained (i.e. for $\nu = \dot{z}_M$, $\zeta = 2.5$ m/s^2).

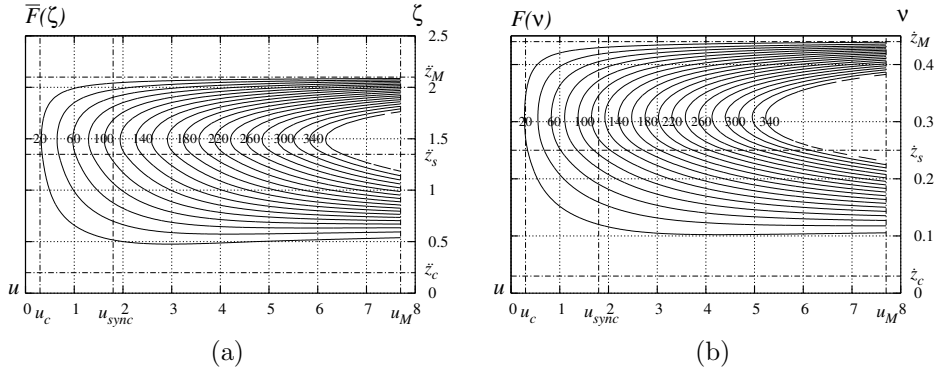

Figure 5.8. Amplitude of the F_{ps} components in phase with ζ and ν for the T-bridge

The amplitudes of the force components can also be analysed with respect to their frequency content (Fig. 5.9). Fig.s 5.9a-b are obtained for fixed ζ (the values reported in Table 5.1), while Fig.s 5.9c-d are obtained by fixing the crowd density $u = 1.4$ ped/m^2 for both cases (average value of the measured crowd conditions). The term F_{ps} evolves in time with a constant frequency equal to f_s; the component F_{pp}, instead, has a frequency f_{pl} which depends on u (see Fig.s 5.5g and 5.6g) and is constant when u is fixed (Fig.s 5.9c-d). When u is under its critical value, f_{pl} is at its maximum value, while, as u grows, the walking velocity decreases and f_{pl} decreases in turn. In the MB case, the deck acceleration, which is much higher than in the TB, causes the component F_{ps} to prevail on F_{pp} for a fixed density (Fig. 5.9a); on the TB the situation is opposite. The amplitudes of the forces for fixed u are, instead, very similar for the two cases since they have been obtained for the same value of u: the slightly differences are due to different closure equations and different values of f_s.

Table 5.2 provides a deeper insight into the other results obtained with the model. The correspondence between the simulated results and the actual data can clearly be seen by looking at the force frequency content. In the case of the T-bridge, the estimated step lateral frequency f_{pl} (0.86 Hz) is very close to the deck lateral frequency (0.9 Hz), therefore the two components F_{pp} and F_s also excite the first lateral mode. As for the Millennium bridge, since f_{pl} is very far from f_s, it can be stated that the overall force is mainly due to the synchronization between pedestrians and the structure. Finally, let us consider the number of synchronized pedestrians. Even though both events are characterized by high crowd density, as the two structures have different slenderness, the Millennium bridge shows higher oscillations than the T-bridge, which means a greater number of pedestrians synchronized with the structure. Since only a few pedestrians are captured in the structure-induced syn-

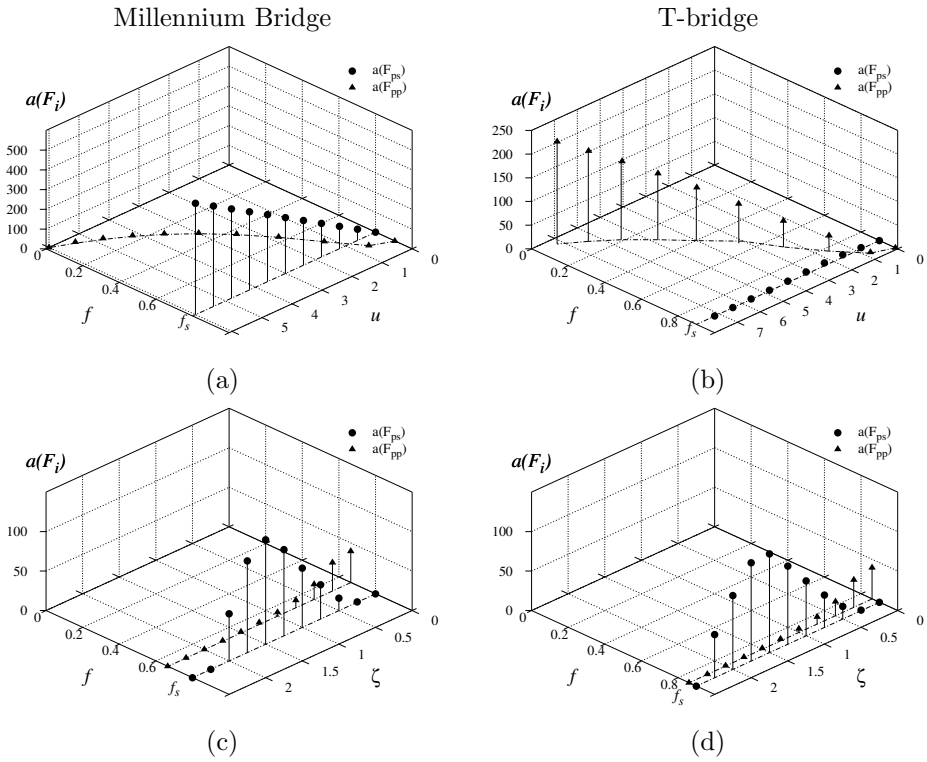

Figure 5.9. Amplitudes of F_{ps} and F_{pp} versus f, u and ζ

chronization on the T-bridge, the crowd density plays a leading role in determining the overall force.

Table 5.2. Results obtained with the proposed force model (forces in [N/ped])

Benchmark	$a(F_{ps})$	$a(F_{pp})$	$a(F_s)$	f_{pl}	F_{rms}	n_{ps}/n	n_{pp}/n
MB	94.3	0.87	1.09	0.66	67.0	0.97	0.03
TB	3.44	19.0	5.10	0.86	17.46	0.33	0.63

The single force per pedestrian [N/ped] obtained with the model is, finally, compared to that predicted with the force models proposed by Fujino et al. (1993), Nakamura and Kawasaki (2006) and Dallard et al. (2001) (Table 5.3). It should be pointed out that, since the cited models do not distinguish between the two types of

synchronization, the predicted force is considered to be only due to the pedestrian-structure synchronization and it is therefore compared to the term F_{ps}.

Table 5.3. Comparison between the proposed force model and those found in literature (forces in [N/ped])

Model	TB	MB
Fujino et al. (1993)	7	n.a
Nakamura and Kawasaki (2006)	4.7	n.a.
Dallard et al. (2001)	n.a.	89.5
Proposed	3.44	94.3

First, it is should be noticed that each model in literature is based on the data recorded on a particular footbridge and it can not therefore be extended to all other structures. For instance, Nakamura and Kawasaki (2006) observed that the model they proposed for the T-bridge only agreed with that of Dallard et al. (2001) for deck lateral velocities under 0.015 m/s. The proposed model, instead, has a more general validity, since it is not based on one single event but on the phenomenological description of the components of the coupled system in their fundamental constitutive laws. The amplitudes of the term F_{ps} predicted by the proposed model are very similar to those estimated by Nakamura and Kawasaki (2006) for the T-bridge and by Dallard et al. (2001) for the Millennium bridge, respectively: this fact highlights the wide applicability of the model.

5.3 Complete computational simulation on the T-bridge (Japan)

5.3.1 Description of the case study

The proposed model has been tested by simulating a crowd event on the T-bridge (Toda Park Bridge, Toda City, Japan, 1989). The T-bridge (Fig. 2.8) was chosen since it has been extensively described by Fujino and coworkers in several papers (Fujino et al. 1993, Nakamura 2003, Nakamura and Kawasaki 2006, Nakamura and Fujino 2002) and particular attention has been devoted to the description of the crowd conditions during the events. In the following, only some characteristics are recalled. The T-bridge is a cable-stayed footbridge with a two-span continuous steel box girder, a two-plane multistay cable system with 11 stays per plane and a 61.4 m-high tower made of reinforced concrete. The total bridge length L is about 180 m and

the road deck width B is 5.25 m. The girder is fixed longitudinally and transversely at the tower position. Concrete was poured inside the box girder on the side span to reduce the up-lift force at the end support. The bridge mass is 800 kg/m^2 and the damping ratio around 0.7%. The footbridge connects a boat race stadium to a bus terminal. Therefore, at the end of boat races the bridge is crossed by a great number of pedestrians, sometimes more than 20000, who leave the stadium to reach the bus terminal. In these situations, lateral vibrations of the girder of up to 1 cm were recorded.

Structural model

The FE modelling of cable-stayed bridges is not a simple task and different modelling strategies are possible. In order to reduce the degrees of freedom and simplify the dynamic analysis, a single-girder (spine) model is used (Ren and Peng, 2005), that is, the bridge deck is modelled using a single central spine with offset rigid links to provide cable anchor nodes. The deck stiffness is assigned to the spine elements and the deck translational mass (lumped mass approach) is assigned to the spine nodes. The towers and the deck are modelled with elastic beam elements and the cables with truss elements (Fig. 5.10).

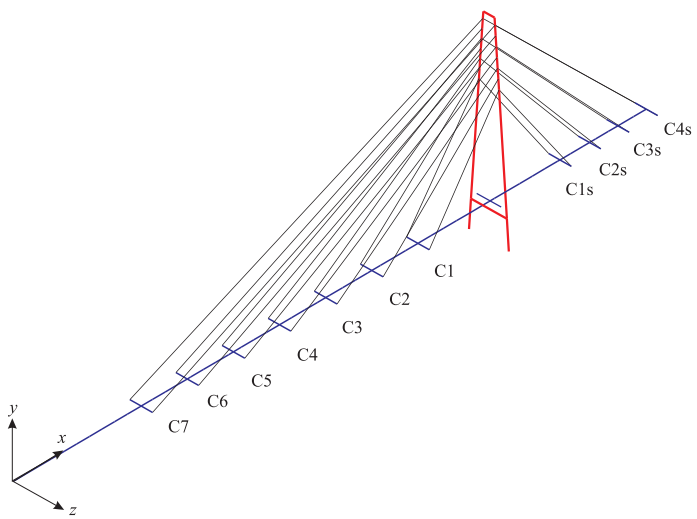

Figure 5.10. The FE model of the T-bridge

Each cable is modelled using a single truss element and the non-linear behaviour is taken into account by introducing an effective axial modulus of elasticity (Warnitchai

et al., 1995):

$$E_{eq} = \frac{E}{1+\lambda^2/12} \qquad \text{and} \qquad \lambda^2 = \frac{E(\rho L)^2}{T^3}, \tag{5.2}$$

where E is the cable modulus of elasticity, L is the horizontal projection of the cable length, ρ is the cable weight per unit length, A the cross-section area and T the prestress. The properties of the structural members are summarized in Table 5.4.

Table 5.4. Properties of the structural members

Component	Area [cm^2]	ρ [Kg/m]	E (10^5) [MPa]	I_z [m^4]	I_y [m^4]	T [KN]
C1	14.24	11.6	2.10	–	–	428
C2	14.24	11.6	1.99	–	–	451
C3	14.24	11.6	1.98	–	–	387
C4	21.17	18	1.73	–	–	290
C5	21.17	18	1.58	–	–	278
C6	28.09	24	1.61	–	–	425
C7	41.95	35	1.97	–	–	1790
C1s	41.95	35	1.93	–	–	451
C2s	41.95	35	1.87	–	–	451
C3s	41.95	35	1.79	–	–	451
C4s	41.95	35	2.00	–	–	3000
Deck main span	1340	4840	2.10	0.2175	0.68	–
Deck side span	1340	8200	2.10	0.2175	0.68	–
Tower	39600	9900	0.345	1.597	1.07	–

The FE model has been validated by comparing the natural frequencies and mode shapes of the footbridge with those reported by Fujino et al. (1993) and with those obtained through a commercial FE software, Ansys v.10 (Fig. 5.11). It can be observed that the first lateral frequency obtained using the developed FE model is higher (1.05 Hz) than the one obtained by Fujino et al. (0.9 Hz). Nevertheless, it should be noticed that the dominant frequency of the girder vibration recorded on the T-bridge was about 1 Hz when loading was small (Fujino et al., 1993), and decreased to about 0.93 Hz when the deck was congested and the vibration amplitude reached its maximum value (Nakamura and Fujino, 2002). Therefore, the obtained lateral frequency agrees with the deck behaviour in a non congested crowd condition, while the added pedestrian mass is obtained from the solution of the mass conservation equation (3.2). Moreover, Fujino et al. (1993) observed that some cables vibrate with

a frequency close to 1 Hz. In order to take into account the local motion of the cables, each cable should be described as a multi-element cable, with a consequent increase in the number of DOFs and required computational costs (Warnitchai et al., 1995). Since this kind of modelling is not the scope of this work, the inertial contribution of the vibrating cables has been taken into account by adding an estimated equivalent modal mass to the deck nodes that provide cable anchorages, as suggested by Fujino et al. (1993). In such a way, the first lateral frequency decreases from 1.05 to 0.97 Hz.

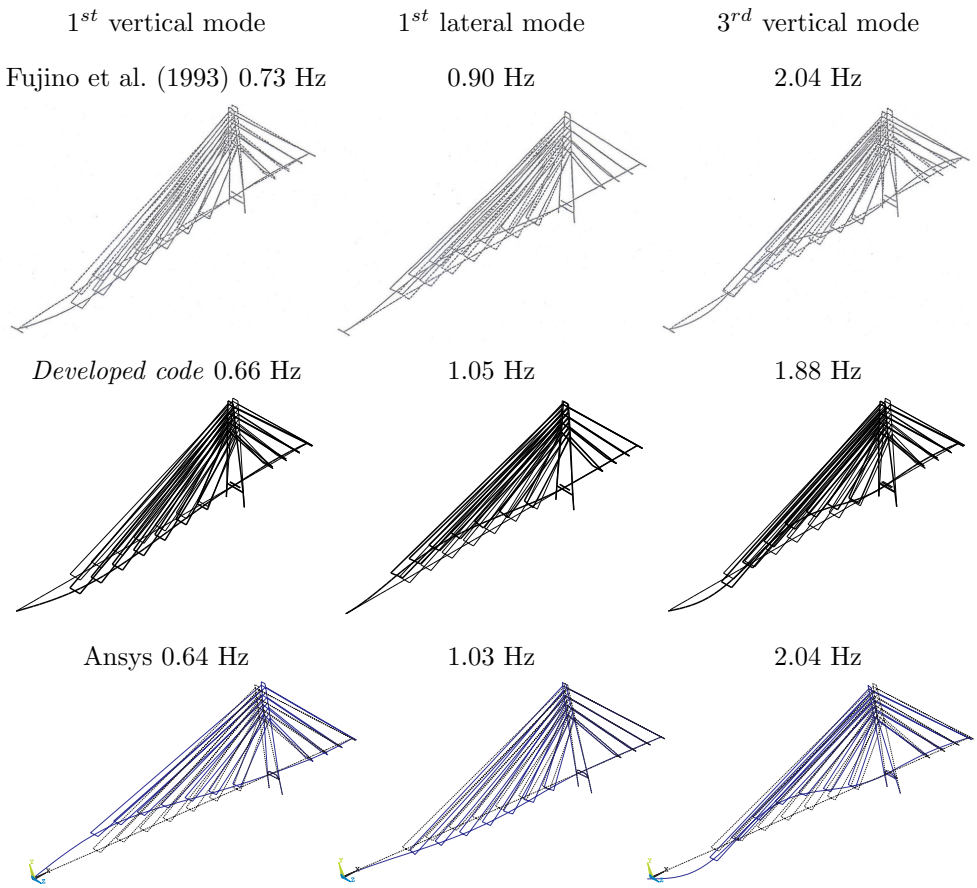

Figure 5.11. Comparison between the frequencies obtained with the developed code, Ansys and those reported by Fujino et al. (1993)

Crowd condition along the deck

The different crowd conditions recorded on the T-bridge have been described in a qualitative way in several papers. The most crowded event was reported by Fujino et al. (1993), when more than 20000 people left the stadium and crossed the bridge in about 20 minutes. In the most congested situation, about 2000 people walked simultaneously on the bridge. Less crowded situations are described in other papers (Nakamura 2003, Nakamura and Kawasaki 2006, Nakamura and Fujino 2002): a maximum number of around 12000 people crossed the bridge in 12 to 20 minutes, with a crowd density varying between 0.8 and 1.5 ped/m^2.

The simulated condition represents an average of the events reported in literature. The initial condition on the density is $u(0,x) = 0.01$ ped/m^2, while the boundary condition at the inlet $u(t,0)$ (Fig. 5.12) has been built in order to allow about 14000 pedestrians to pass over the bridge in 23 minutes, with a maximum density of 1.33 ped/m^2. It is worth pointing out that the incoming density shows a steady-state regime bounded between two transient ones, which correspond to the start and the end of the stadium evacuation. It should be noticed that the density decreases in a smoother way than the initial increase. This is due to the assumption that the stadium evacuation abruptly starts at the end of the boat race with a sudden increase in the crowd density, while the complete evacuation is expected to take a longer time.

The speed-density relation has been adapted for the case of Asia and rush-hour traffic, that is, $u_M = 7.7$ ped/m^2, $v_M = 1.48$ m/s and $\gamma = 0.273u_M$ (Venuti and Bruno, 2007a) (Fig. 5.13a). Fig. 5.13b graphs the flow-density diagram $q - u$, where $q = vu$, and shows the capacity density u_{ca}, which corresponds to the maximum flow. It is worthwhile recalling that, for $u > u_{ca}$, the crowd flow enters the congested regime.

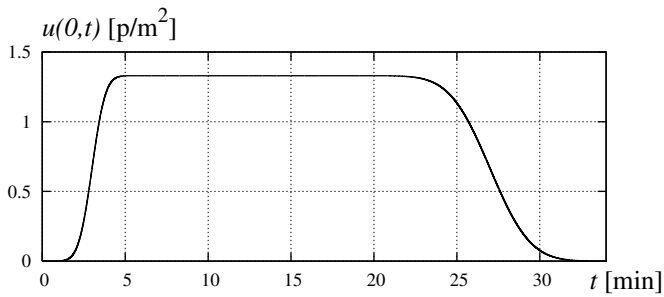

Figure 5.12. Boundary condition on the density at the inlet

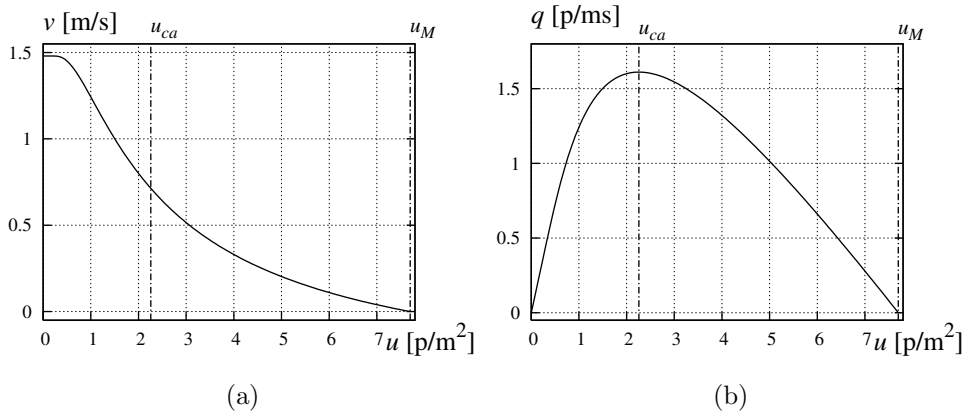

(a) (b)

Figure 5.13. Speed-density (a) and flow-density (b) relations

5.3.2 Simulation of an actual event

The proposed approach allows the evolution in space and time of both subsystems to be described. Fig. 5.14 reports the time-space distributions of some main variables obtained through the computational simulation: the crowd density u, the envelope of the deck lateral acceleration ζ and the force components, expressed in [N/m]. In order to retain only the large time-scale fluctuation, Fig.s 5.14c-f graph the envelope of the variable maxima. It is worth pointing out that ζ has to be considered delayed in time by a quantity τ, according to the hypothesis reported in §3.3.3.

The overall evolution in time of u is mainly due to the imposed boundary condition at the inlet. In other words, the crowd dynamics is not affected by non-linear traffic phenomena due to a crowd density above the capacity value u_{ca} or to the effects of excessive lateral acceleration of the deck, that is, $\zeta \geq \ddot{z}_M$.

When ζ exceeds the threshold of motion perception $\ddot{z}_c$, some pedestrians synchronize with the structure (Eq. 3.28), so that F_{ps} is not null and has a space distribution that matches the deck deformed shape (Fig. 5.14c). As a consequence, the number of pedestrians synchronized to each other decreases, causing a decay of F_{pp} (Fig. 5.14d). Otherwise, if $\zeta \leq \ddot{z}_c$, F_{pp} follows the same trend as u. F_s follows from the other two components: it has an increase when both F_{ps} and F_{pp} are null, that is, when $u \leq u_c$ and $\zeta \leq \ddot{z}_c$ (Fig. 5.14e). Fig. 5.14f clearly shows that the resulting total force F is mainly due to the F_{pp} component, since the magnitude of F_{ps} is small in the case-study.

Looking at the time-space distribution of the crowd density (Fig. 5.14a), five crowd regimes have been identified:

- Regime I 'advancing front':

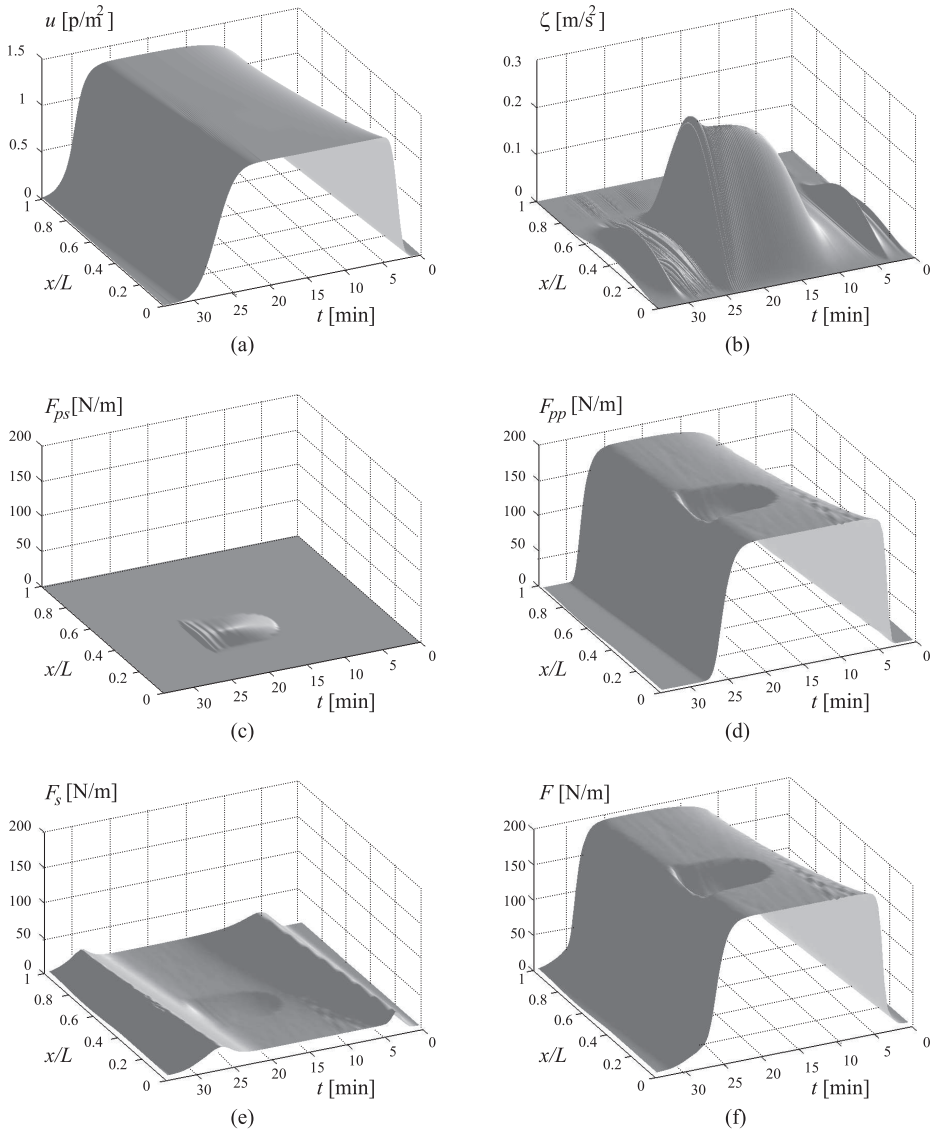

Figure 5.14. Space-time distributions of the main variables

- Regime II 'filling gradient'
- Regime III 'uniform crowd'

- Regime IV 'vacating gradient'
- Regime V 'leaving front'

The upper limit of regime I and the lower bound of regime V correspond to the maximum and minimum difference between the crowd density at the outlet and at the inlet $\Delta u = u(L,t) - u(0,t)$ (Fig. 5.15) respectively. The boundaries of regime III have been determined as the time window with a mean value of u along the span equal to 99% of the maximum mean density $\bar{u}$ and a standard deviation of less than $0.01\bar{u}$.

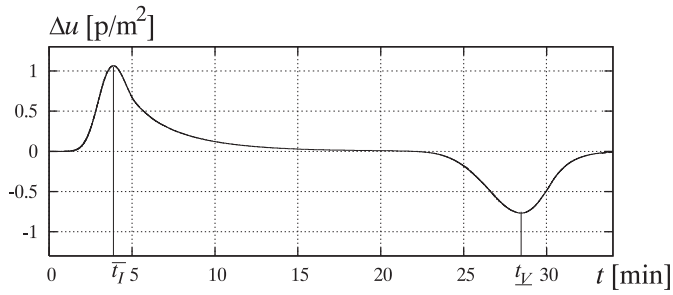

Figure 5.15. Δu time history

The five regimes are highlighted in Fig. 5.16, which plots the isolines of the crowd density and deck acceleration evolution. First, it can be noticed that the uniform crowd regime also corresponds to the highest values of the deck response ($\zeta > \ddot{z}_c$), which almost reaches the steady-state condition in the same period of time. Second, regimes I and V are characterized by two local maxima of the structural response that can be related to the well-known travelling load effects and can be better understood referring to the instantaneous fields reported in Fig.s 5.17a-b. The ζ local maximum around $t = 2.97$ min is mainly due to the F_s component, whose distribution excites the structural first mode. The F_{pp} component is negligible since the crowd density is below u_c in a large portion of the footbridge span. A similar but specular situation occurs at $t = 30.4$ min. In the time interval 27-29 min, the second lateral mode is mainly excited (Fig. 5.17c). In this case, F_{pp} prevails on F_s along the shorter span, where the density still remains high.

A deeper insight into the effects of crowd density and deck acceleration on the force F is given in the graphs in Fig. 5.18, which plots the matrix R of the coefficients of the space correlation of the force for each regime. Each term of the matrix R is defined as follows:

$$R(i,j) = \frac{C(F_i, F_j)}{\sqrt{C(F_i, F_i)C(F_j, F_j)}}, \tag{5.3}$$

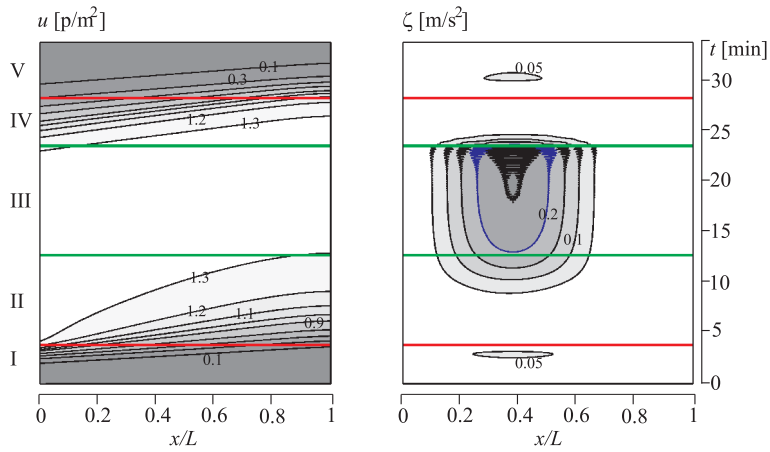

Figure 5.16. Crowd regimes

where $F_i = F(x_i, t)$ and $F_j = F(x_j, t)$ are the forces applied in two generic points of the deck space grid and C is the covariance matrix, defined as:

$$C(F_i, F_j) = E[(F_i - \mu_i)(F_j - \mu_j)], \tag{5.4}$$

where E is the expected value and $\mu_i = E\, F_i$. As expected, the highest space correlation occurs in regime III, where the crowd is almost uniform along the span. The transient regimes II and IV show a totally uncorrelated force, due to the space variation of the step frequency f_{pl} induced by the crowd density space distribution. Regimes I and V, which are characterized by the highest gradients of u, have higher values of correlation in the span portion where the density is very low, that is, the shorter span in regime I and the first quarter of the main span in regime V.

Finally, the results of the computational simulation are compared to the measurements reported by Fujino et al. (1993) for five time windows (Fig. 5.19). The time windows reported by Fujino et al. (1993) do not match the five regimes defined above, but have been defined with a similar objective, that is, to qualitatively identify the different flow regimes that characterize the event. As for the structure results, the figure reports the time history of the lateral deck displacement in the node corresponding to the position of the installed accelerometers (Fujino et al., 1993), the first lateral frequency of the structure f_s averaged over the period and the dominant frequency f, obtained through a PSD of the signal in the considered period. As far as the crowd results are concerned, the instantaneous spatial distributions of the crowd density are reported, as well as the mean walking frequency f_{pl}.

Looking at the results, a very good agreement between the simulation and the recorded data is evident. The maximum amplitude of the lateral deck displacement, of about 9 mm, matches the measured data very well. The maximum percentage of

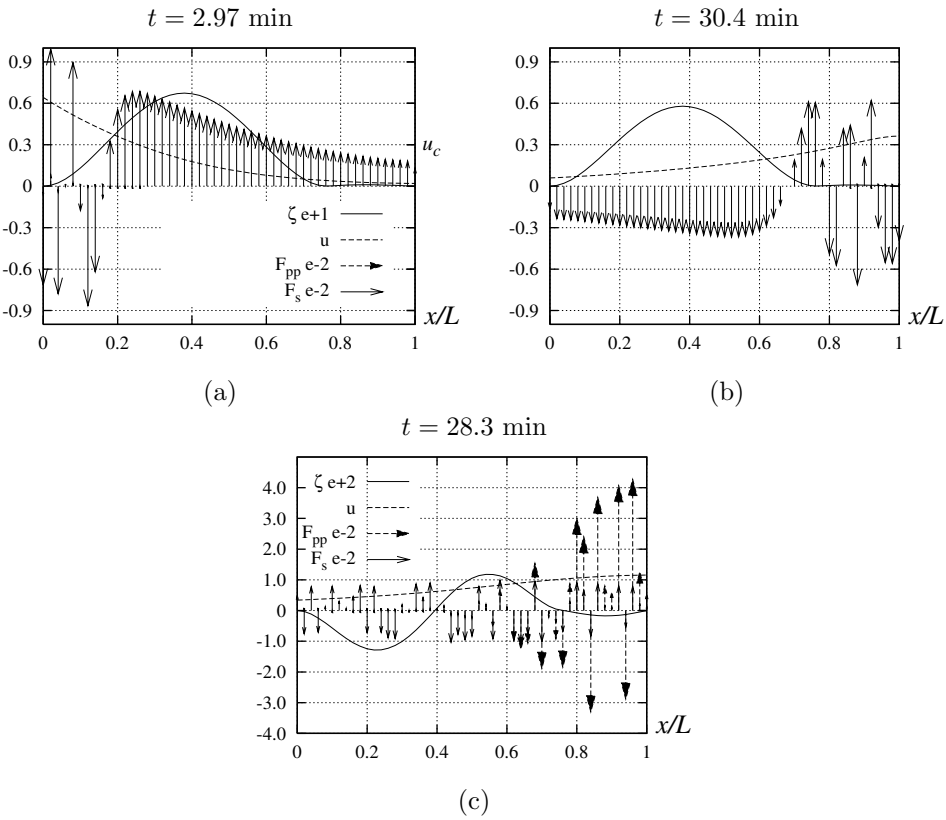

Figure 5.17. Instantaneous fields: crowd density u [ped/m^2], deck lateral acceleration ζ [m/s^2], force components F_{pp} and F_s [N]

pedestrians synchronized to the structure is about 21%, which is in very good agreement with the observation data of Fujino et al. (1993), who estimated a percentage equal to 20%. Similar considerations can be made for all the considered variables. It is worth pointing out that the dominant frequency of the deck vibration is always closer to the walking frequency than to the structure lateral frequency. This means that the force components due to synchronized-to-each-other or uncorrelated pedestrians are dominant with respect to the one due to pedestrians synchronized to the structure, as is also shown in Table 5.5. This outcome qualitatively confirms the results of the force model application to the T-bridge discussed in §5.2. It is worthwhile noting that the values of the force components obtained through the simple application of the force model (i.e. for a given ζ or u) in §5.2 differ from the ones reported in Table 5.5 obtained from a complete simulation: this highlights the complexity of the coupled behaviour of the system.

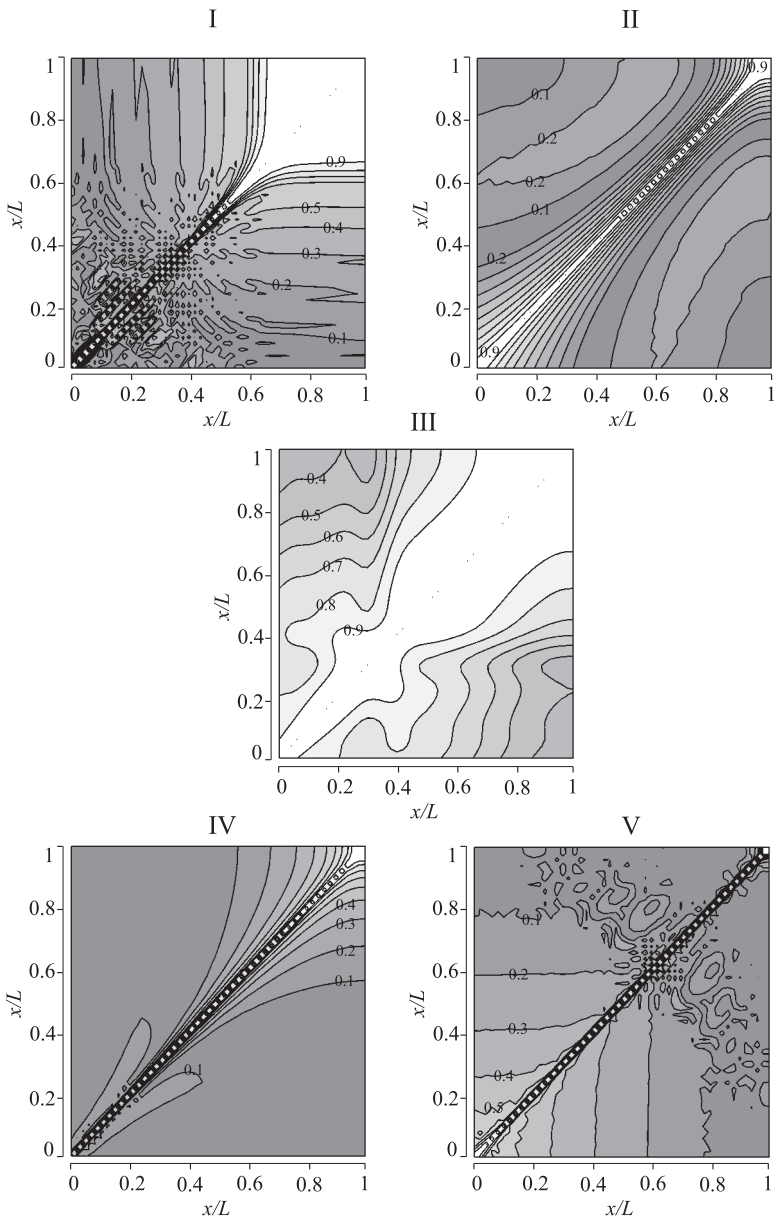

Figure 5.18. Coefficients of space correlation for the five regimes

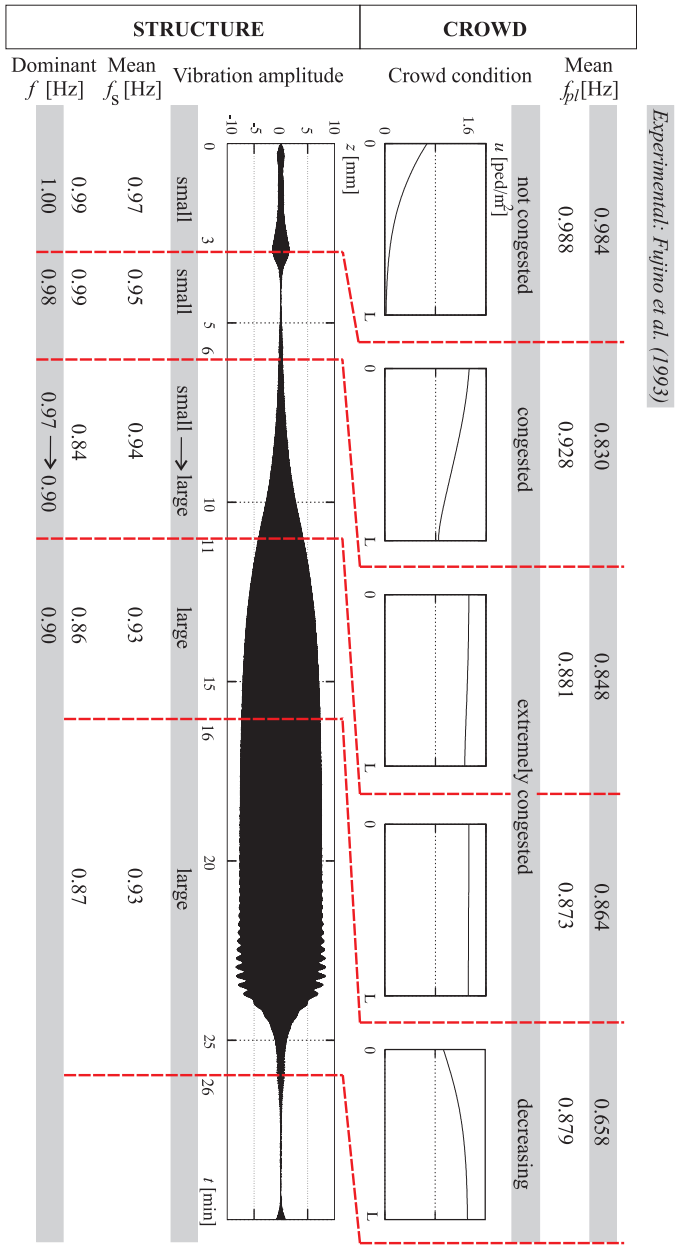

Figure 5.19. Comparison between the simulation results and the data reported by Fujino et al. (1993)

Table 5.5. Maximum amplitudes of the force components [N/ped] at between 16 and 23 minutes

F	F_{ps}	F_{pp}	F_s	n_{ps}/n	n_{pp}/n	n_s/n
28.8	1.1	26.9	2.1	0.21	0.9	0.13

5.3.3 Sensitivity studies on the model parameters

Sensitivity study on the interacting terms

The computational approach offers not only the opportunity to simulate mechanical systems in real conditions, but also to evaluate their behaviour under unphysical states in order to separate the effects of each component of a coupled interacting system. Bearing in mind this goal, the same benchmark was subjected to a sensitivity analysis on the model interacting terms. In practice, the various interacting terms were "turned off" in the complete model by successive addition, in order to perform the following simulations, which are summarized in Fig. 5.20:

1. complete Crowd-Structure Interaction, introduced in §5.3.2;
2. constant overall mass, that is, the structural mass M_s is retained while the crowd added mass M_c is discarded;
3. the sensitivity to the deck vibration is not taken into account in the Structure-to-Crowd interaction term, that is, $v = v(u)$, instead of $v = v(u, \ddot{z})$;
4. the sensitivity to the deck vibration is not taken into account in the Crowd-to-Structure interaction term, that is, $S_{ps} = 0$ and consequently $F_{ps} = 0$;
5. a combination of cases 3 and 4, i.e. the deck vibration effects are completely discarded;
6. the influence of the density u in the lateral force is not considered, that is, $S_{pp} = 0$ and consequently $F_{pp} = 0$ so that all the pedestrians are uncorrelated.

The structural responses obtained from the six configurations are compared in Fig. 5.21. The maximum values of the main parameters are summarized in Table 5.6. These values are the maximum ones obtained in the period of time from 16 to 23 minutes, which roughly corresponds to the steady state.
The following considerations can be made:

- the maximum amplitude of the deck displacement is reached with a complete crowd-structure-interaction simulation. The change in the footbridge modal

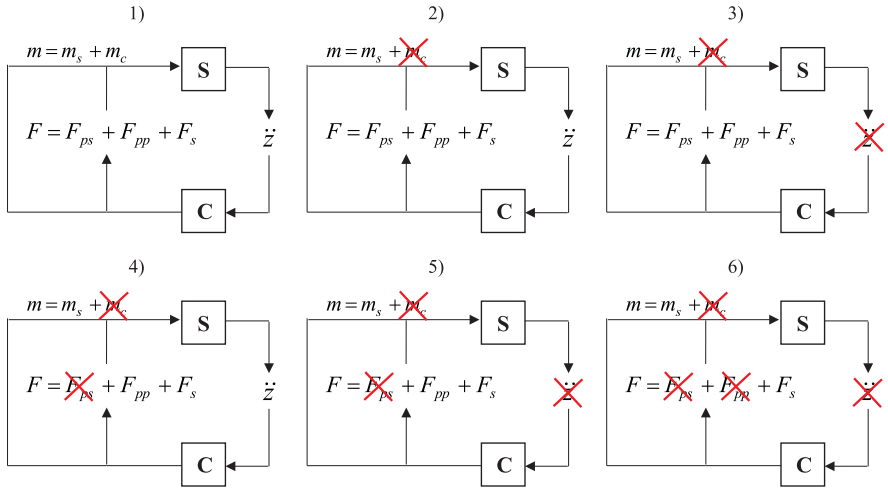

Figure 5.20. Scheme of the performed simulations

Table 5.6. Maximum values of the main variables at between 16 and 23 minutes

Simulation	z [mm]	$\ddot{z}$ [m/s^2]	F [N/ped]	n_{ps}/n	n_{pp}/n	n_s/n
1	9.3	0.28	28.8	0.21	0.9	0.11
2-5	6.2	0.19	28.8	0	0.89	0.12
6	1.3	0.04	6.0	0	0	1

properties, due to the crowd added mass, causes the first lateral frequency to be closer to the walking frequency (Fig. 5.22). As a consequence, the pedestrian-structure synchronization increases and the vibration in turn grows;

- the simulations from 2 to 5 give identical results. The absence of the crowd added mass causes the deck lateral acceleration $\ddot{z}$ to never exceed the critical value $\ddot{z}_c$. Therefore, S_{ps} is always null, v is only dependent on u and the four simulations are, in fact, the same as simulation 5;

- when all the pedestrians are forced to be uncorrelated (simulation 6), the maximum vibration amplitude is 1.3 mm. This is in line with the result obtained by Fujino et al. (1993) in their pioneering work: the application of a simplified single-DOF model of the T-bridge, with an applied force due to uncorrelated pedestrians, produced a vibration amplitude of 1 mm;

- the first and the last five minutes of the response are almost equal in all the six cases. This is due to the fact that the pedestrians are always uncorrelated in those periods since the crowd density is below u_c.

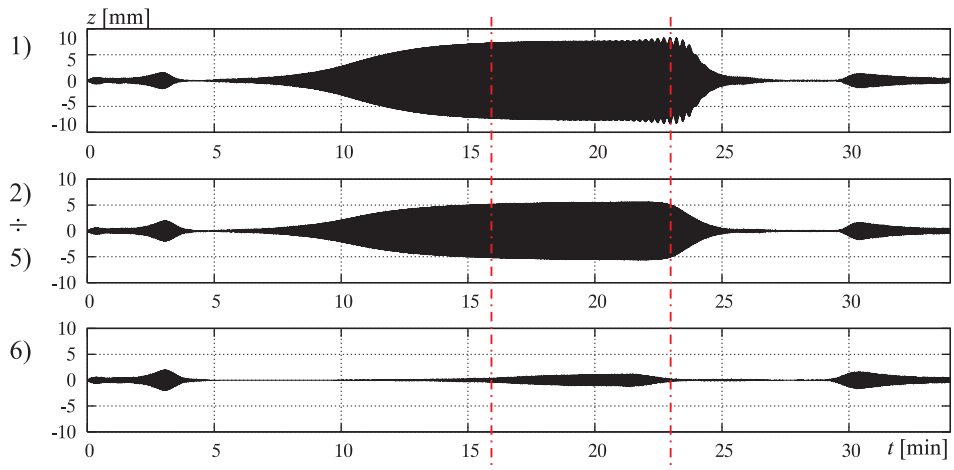

Figure 5.21. Deck displacement in the six different simulations

As far as the crowd system is concerned, simulations 2-6 present the same evolution in time and space of the crowd density, since the walking velocity is not sensitized to the deck lateral acceleration. The space distributions of u, v and ζ are compared in Fig. 5.23 in two instants of time. It can be noticed that, in the portion of the deck span in which $\zeta > \ddot{z}_c$, the walking velocity v is smaller in case 1 than in cases 2-6, because v is reduced by the deck lateral acceleration according to Eq. (3.4). Conversely, according to the fundamental relation (3.2), the crowd density increases in the same span portion shifted by a quantity due to the dislocation in space discussed in §3.3.3.

The sensitivity study highlights the leading role of the pedestrian added mass, which is about 11.6% of the deck weight, on the overall structural behaviour. The simulations without the added mass M_c (2-5) follow the qualitative trend of the observed structural response, but the vibration amplitude is underestimated by about 33%. In the case of the T-bridge, the amplitude of the lateral force exerted by pedestrians is mainly due to the synchronization among pedestrians: if the synchronization is neglected, that is, all the pedestrians are uncorrelated, the obtained vibration amplitude is further underestimated by about 90% of the recorded value, as already pointed out by Fujino et al. (1993).

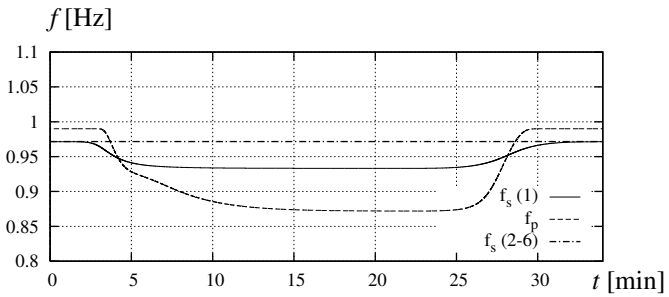

Figure 5.22. Evolution in time of the structural frequency f_s and of the walking frequency f_p

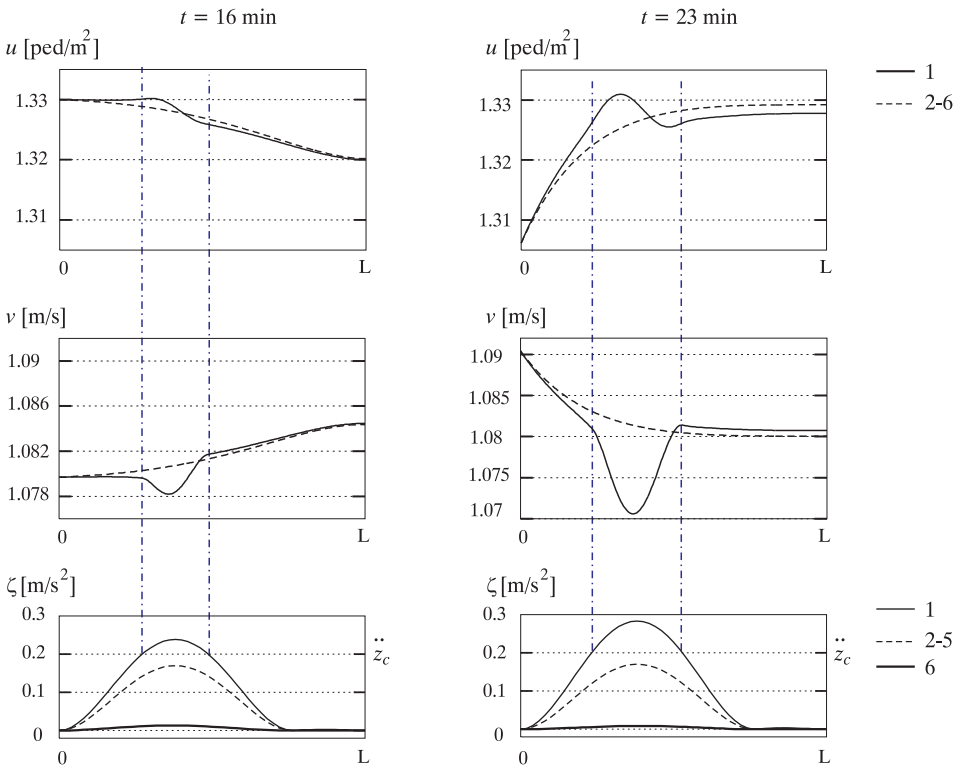

Figure 5.23. Crowd density, velocity and deck acceleration in two istants of time

Sensitivity study on the closure equation

The complete simulation described in §5.3.2 has been repeated with different closure equations in order to test the sensitivity of the model to different travel purposes or geographic areas. The revisited Kladek formula has been characterized each time by varying the coefficient γ and the values of u_M and v_M for the following combinations: Asia-rush hour (AR), Asia-commuters (AC), Asia-leisure (AL) and USA-leisure (UL), which correspond to a progressive decrease of v for $u > 0.8$ p/m^2 (Fig. 5.24a). The first case (AR) refers to the condition that actually occurred on the T-bridge and which is described in §5.3.2. The substitution of the four fundamental laws in Eq. (3.10) leads to the $f_p - u$ relations represented in Fig. 5.24b.

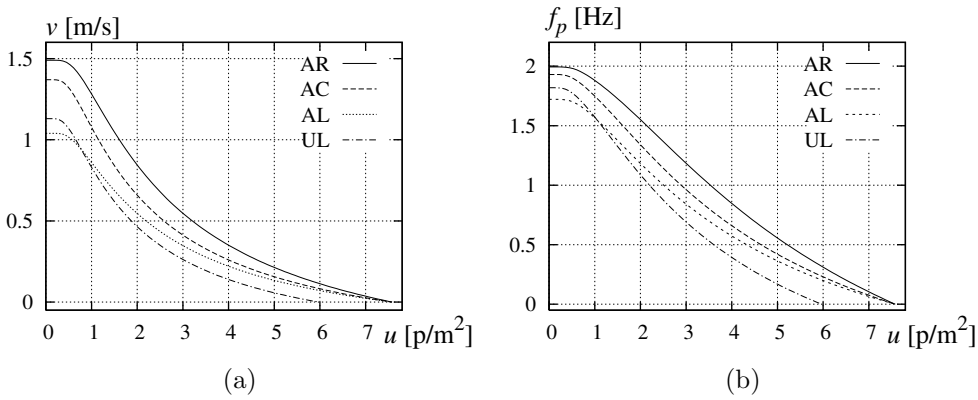

Figure 5.24. $v(u)$ and $f_p(u)$ relations

The five regimes described in §5.3.2 have been identified for the four cases. Fig. 5.25 graphs Δu for the four cases; the density space distribution corresponding to the boundaries of regimes I and V are represented in Fig. 5.26.

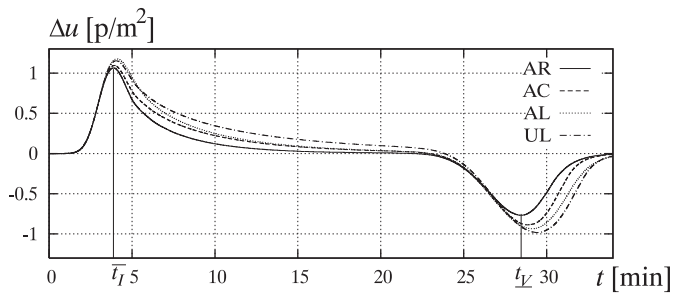

Figure 5.25. Δu time history

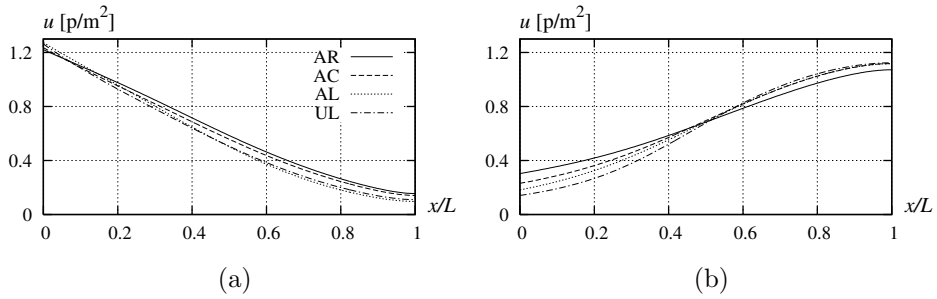

Figure 5.26. Spatial distribution of u at the upper boundary of regime I (a) and lower boundary of regime V (b)

Fig. 5.27 shows the time-space distribution of some of the main variables for the four cases.

The regimes are also represented in Fig. 5.28, which plots the deck acceleration time histories in $x/L = 0.3$, corresponding to the node monitored by Fujino et al. (1993). First, it can be noticed that the gradual decrease in the pedestrian velocity from AR to UL causes longer I and II regimes and a consequent progressive shortening of regime III. The main consequence can be seen in the deck response, which is gradually shifted in time and decreases: the lock-in threshold $\ddot{z}_c$ is only exceeded in the first case AR.

A deeper insight into the simulated phenomena is provided by Fig.s 5.29-5.31, which graph the space distribution of u, f_r and F in the instants of time that are representative of each regime. The following considerations can be made:

- at $t = t_I$, the four cases present similar distributions of u and F (Fig. 5.29a). The latter shows a higher space correlation in the portion of the span where f_r is constant (see Fig. 5.18). The different deck responses can be explained by looking at the f_r diagram: the highest motion corresponds to the value of f_r that is closest to unity (AC), which means that the force is almost resonant with the first lateral mode of the deck;

- at $t = t_{II}$, the crowd is in the transient condition of gradually filling the deck span (Fig. 5.29b). In all cases, the slight monotonic variation of f_r in space shows its effects on the space distribution of F. This time, AR has the closest f_r values to 1 and, therefore, the highest deck vibration;

- at $t = t_{III}$, the uniform crowd condition reflects on f_r, which is almost constant throughout the span (Fig. 5.30a). Two instants of time are represented in the AR case, in order to highlight the influence of the deck acceleration on the density distribution for $0.2 < x/L < 0.4$ at $t = t_{III,b}$;

- regime IV is specular to regime II as well as regime V is specular to regime I.

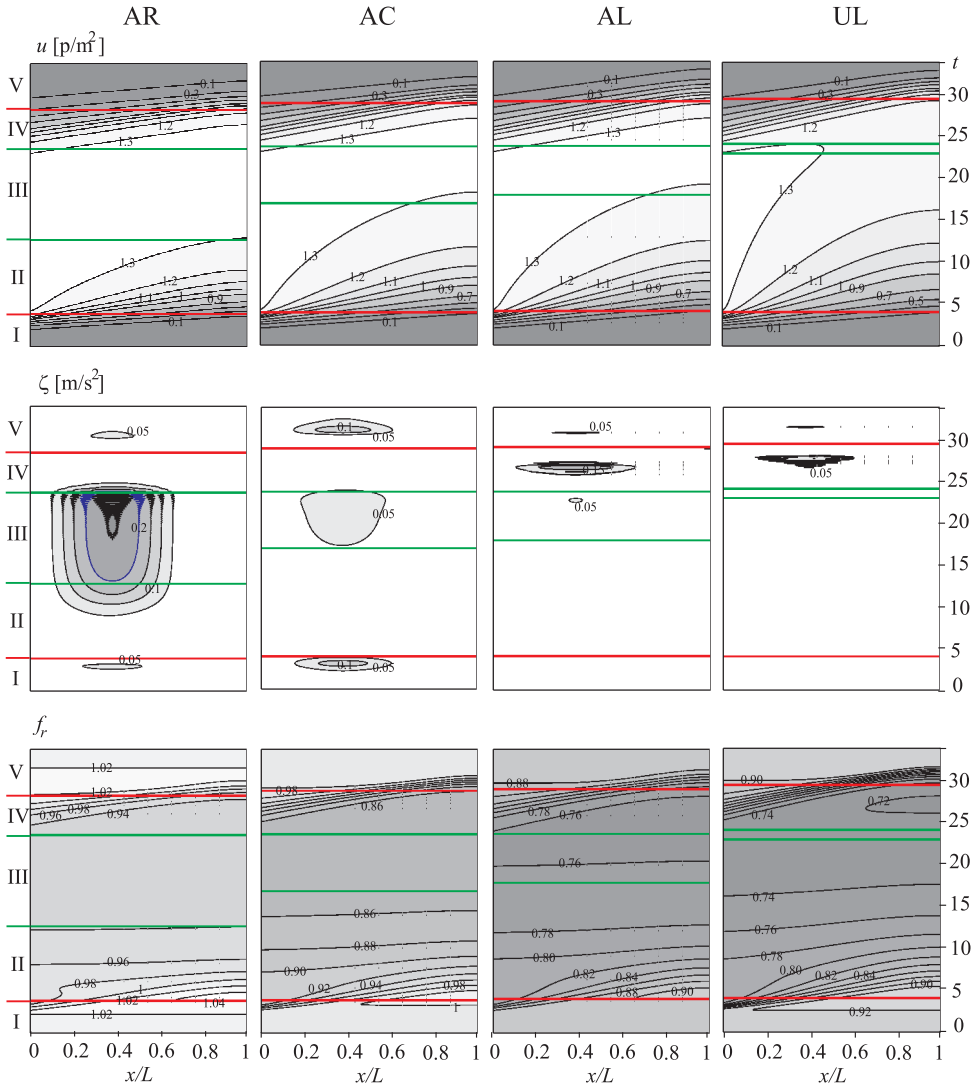

Figure 5.27. Evolution in space and time of the main variables

The sensitivity study on the closure equation shows that different crowd travel purposes can lead to quite different structural responses. In particular the case with rush-hour traffic causes a deck vibration amplitude which is almost three times the amplitude obtained in leisure traffic conditions in the same geographic area. For

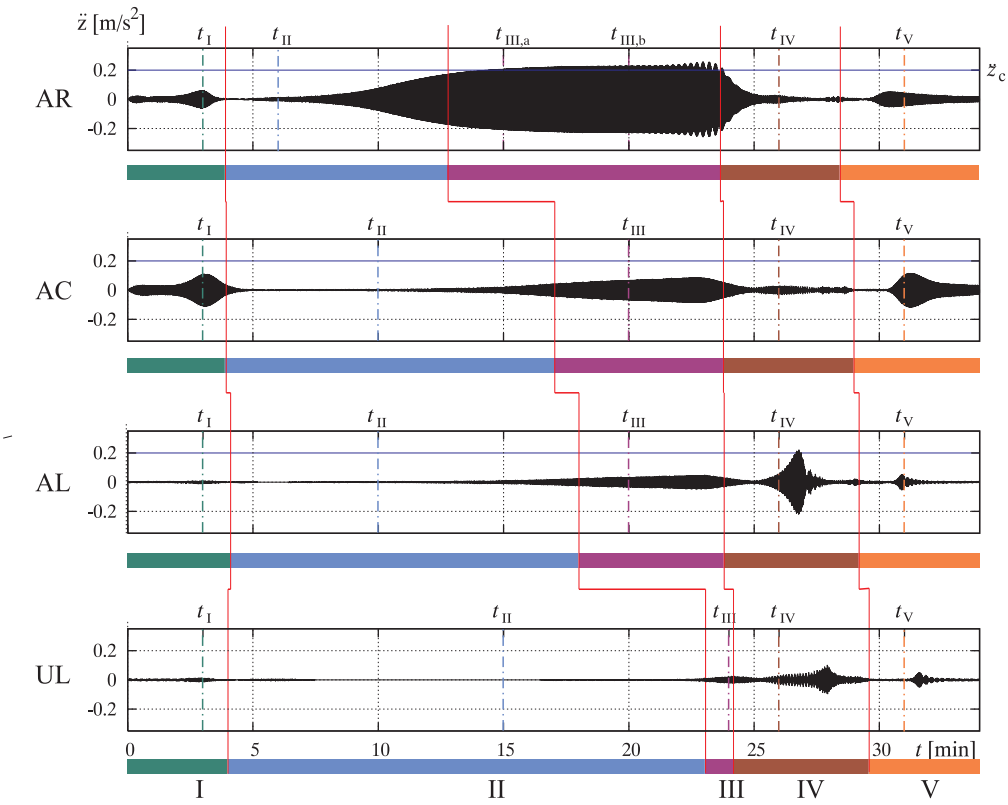

Figure 5.28. Time hystories of the deck lateral acceleration

this reason the footbridge should be designed according to the most likely pedestrian traffic type during the lifetime of the bridge (FIB, 2005).

Sensitivity study on the crowd boundary conditions

The third sensitivity study was performed on the crowd BCs at the inlet, by varying the maximum value reached by the density u_h (Fig. 5.32). The $u_h = 1.33$ p/m^2 case corresponds to the condition simulated in §5.3.2.

First, it should be noticed is that the maximum amplitude of the deck lateral acceleration does not correspond to the case with the highest density $u_h = 2$ p/m^2 (Fig. 5.33). This can easily be explained by looking at the data in Table 5.7. Increasing values of u_h correspond to increasing amplitude of the total force, but also to a decrease in f_r due to the effect of the crowd added mass. As a consequence, when $u_h = 0.8$ p/m^2, the total force is an order of magnitude lower that in the case $u_h = 2$

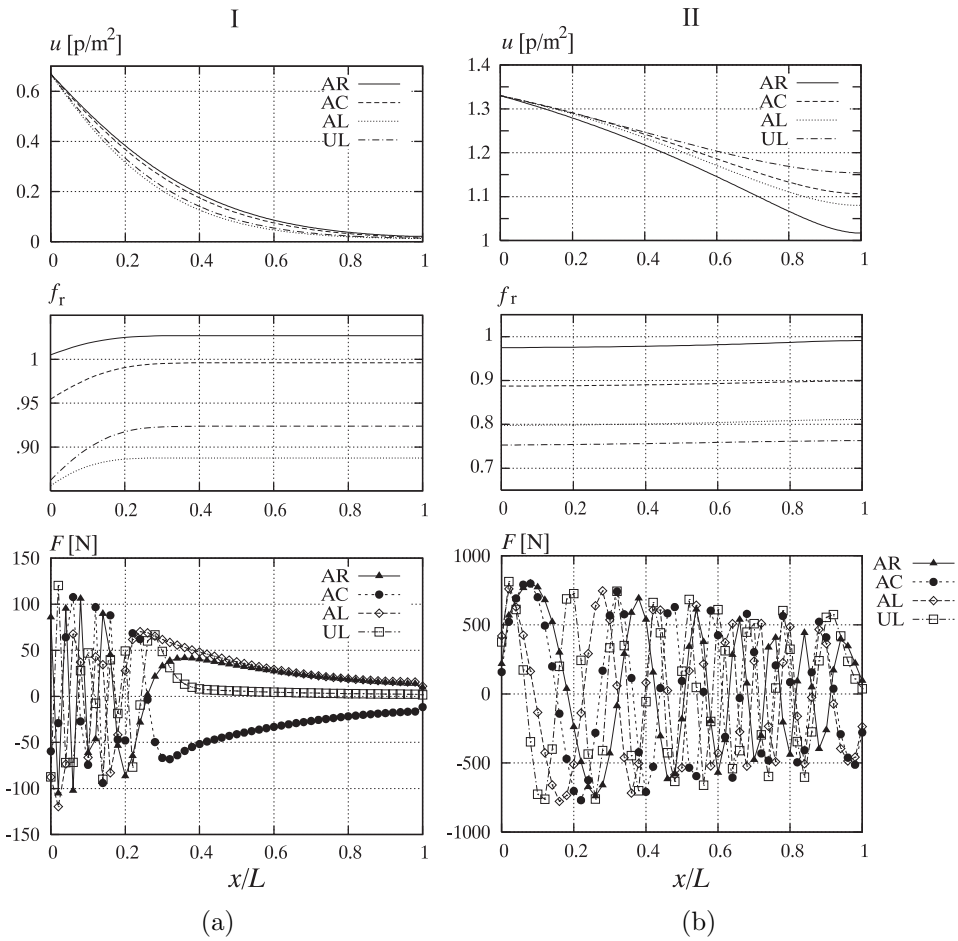

Figure 5.29. Space distribution of the main variables in regimes I (a) and II (b)

p/m^2, but the force is almost resonant with the deck first mode and, therefore, it induces the highest structural response (Fig. 5.34).

The almost steady-state response for $u_h = 2$ p/m^2 is due to the fact that, in the same time window, the crowd density exceeds the value u_{sync}, above which $S_{pp} = 1$. Therefore, all the pedestrians are synchronized to each other and walk with the same frequency, which is sufficiently far from f_s to prevent resonance (Fig. 5.35). The two local maxima at $t \approx t_A$ and t_B could be explained by looking at the space distributions of u, F and ζ in Fig. 5.36. The variables present similar but specular space distributions. The concentration of the crowd in the first half of the main span at $t = t_A$ and in the shorter span at $t = t_B$ is probably the reason for the higher deck

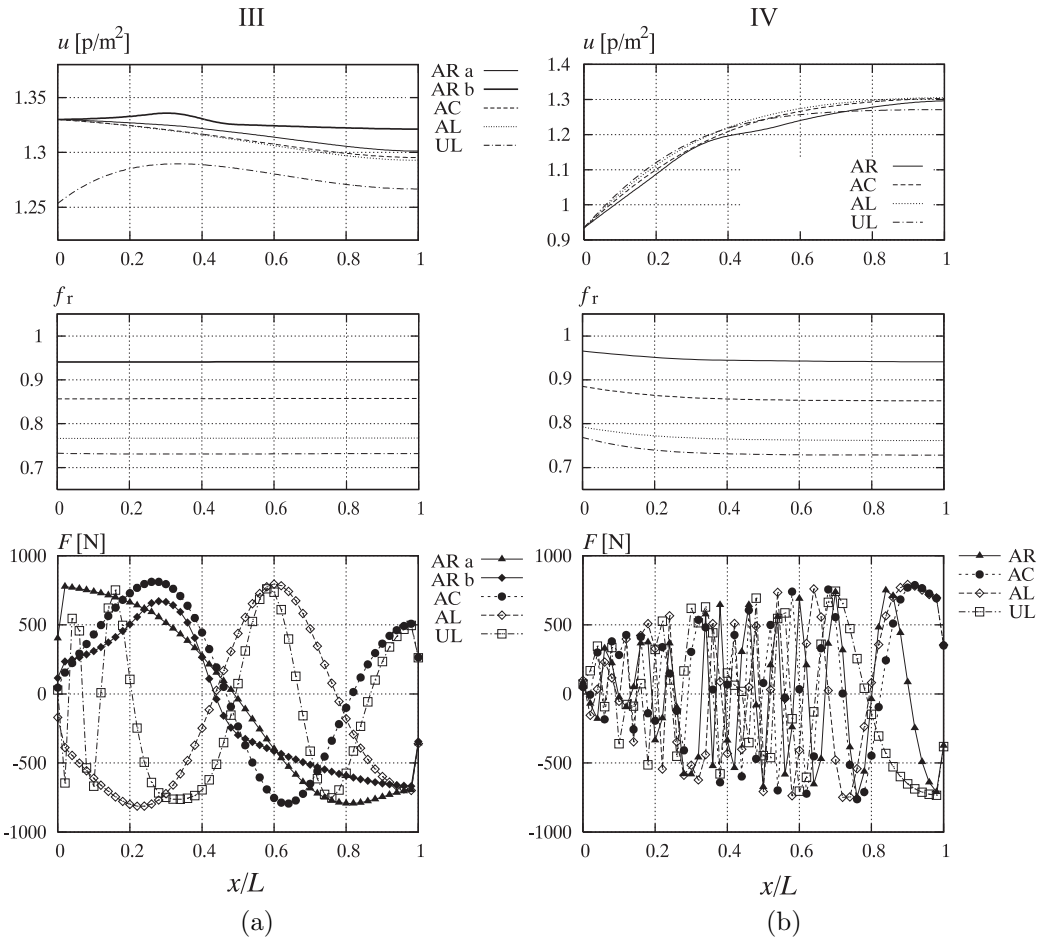

Figure 5.30. Space distribution of the main variables in regimes III (a) and IV (b)

Table 5.7. Mean values of the main variables between 15 and 20 minutes

u_h	[p/m^2]	2	1.3	0.8
f_r		0.85	0.93	1.01
$\|F\|$	[N]	1122	719	169
ζ_{max}	[m/s^2]	0.10	0.25	0.27

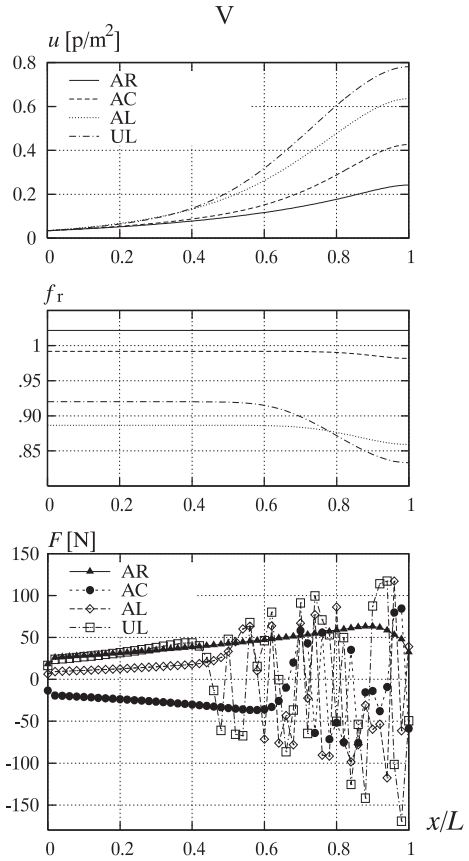

Figure 5.31. Space distribution of the main variables in regime V

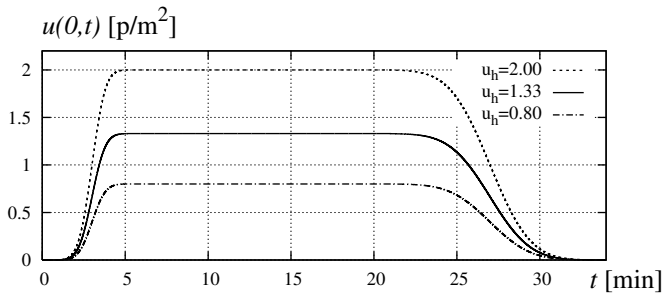

Figure 5.32. Boundary condition on the density at the inlet

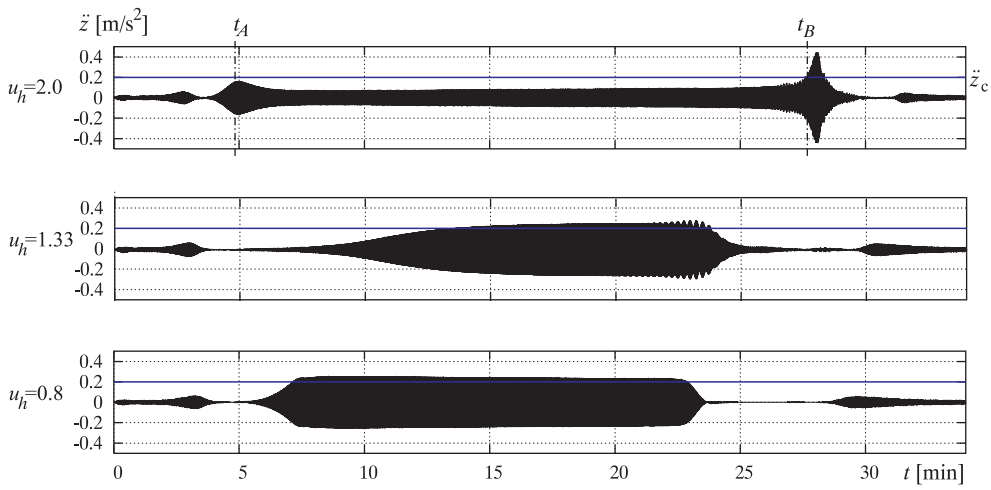

Figure 5.33. Time histories of the deck lateral acceleration in $x = 0.3L$

response: in other words, the two local maxima are due to the transient effect of the travelling load.

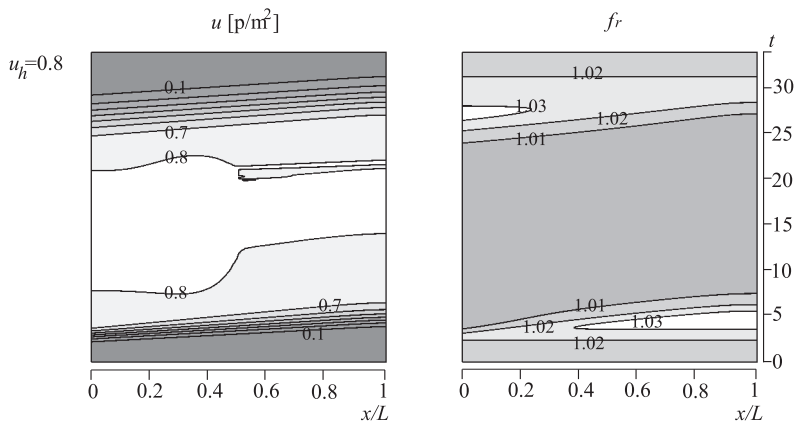

Figure 5.34. Evolution in time and space of u and f_r for u_h=0.8 p/m^2

This study once again demonstrates the non-linearity and complexity of the

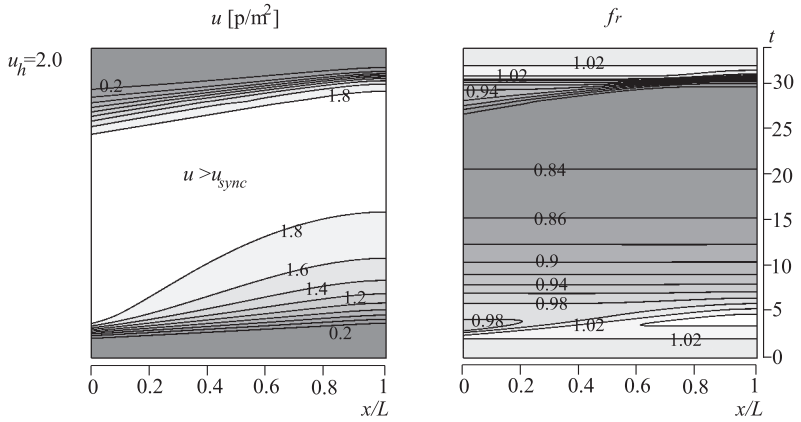

Figure 5.35. Evolution in time and space of u and f_r for u_h=2 p/m^2

coupled system. For the analysed case-study, in fact, the lowest structural response was obtained for the higher value of the crowd density. This is due to the effects of the crowd added mass, which changes the dynamical properties of the footbridge, and of the closure equation, which influences the lateral walking frequency: both factors have the effect of changing the ratio f_r.

Sensitivity study on the structural constraints

Finally, the influence of the structural constraints is explored by changing the way in which the deck is constrained at the tower position, according to the scheme reported in Fig. 5.37:

- A) the deck is not directly connected to the tower: an external constraint inhibits all the translations and the rotations around the y and x axes;

- B) the deck is fixed at the tower with two rigid links. This constraint models the actual condition of the T-bridge;

- C) the deck is not directly connected to the tower: an external constraint inhibits all the translations and the rotation around the x axis.

The itemizing order corresponds to a decreasing flexural stiffness of the deck in the $x - z$ horizontal plane.

Looking at the deck acceleration time histories (Fig. 5.38), it can be noticed

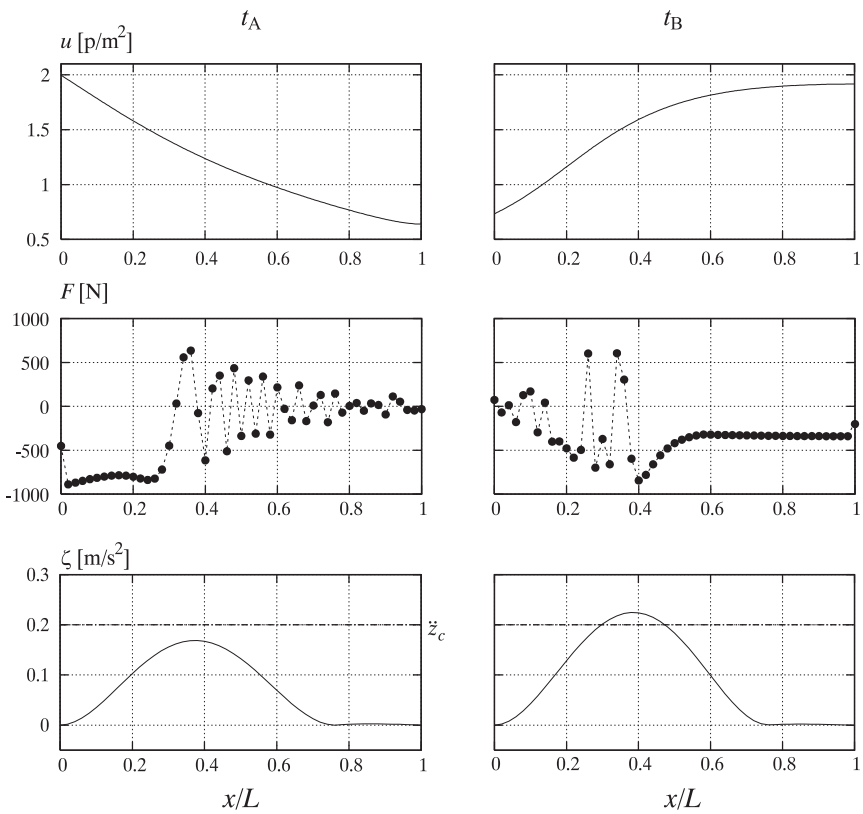

Figure 5.36. Space distribution of the main variables at $t = t_A$ (a) $t = t_B$ (b)

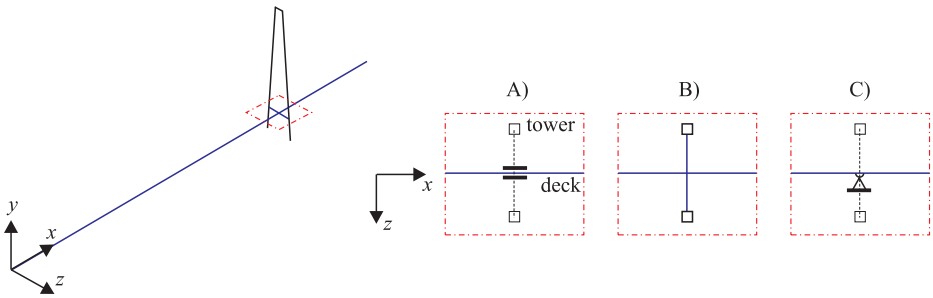

Figure 5.37. Scheme of the deck-tower constraint

that case A is qualitatively similar to case B. The higher structural stiffness of the first case can explain the lower response, which is always under the critical value $\ddot{z}_c$. On the contrary, the higher values of the acceleration local maxima at $t \approx 3$ and $t \approx 31$ min in case A are due to a closer f_r to unity than in case B and C (Fig. 5.39).

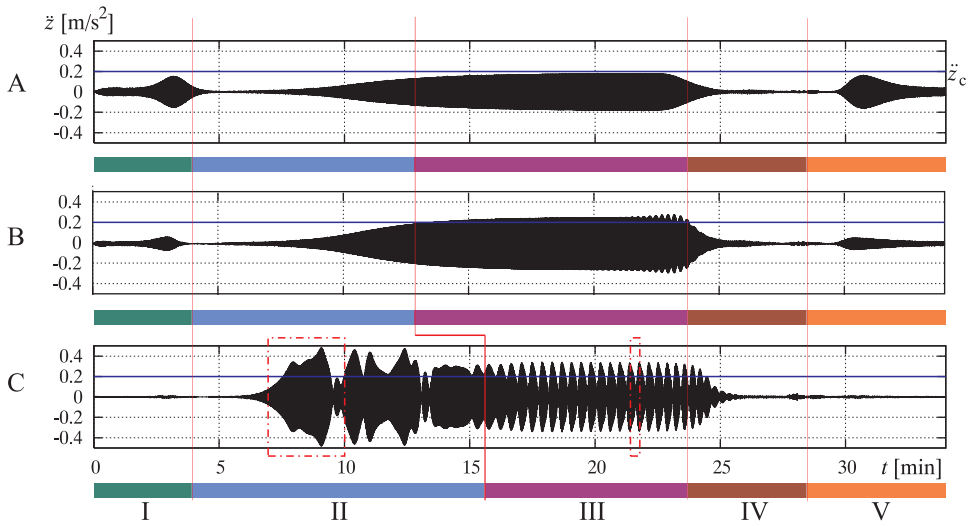

Figure 5.38. Time histories of the deck lateral acceleration

The structural response of case C is quite different from the other cases so far analysed. Once again, it is possible to identify a correspondence between the crowd regimes and the structural response. In particular, the deck response in regime II alternates lock-in and unlock phases, like the ones analyzed in Fig. 5.40. At $t = t_1$, the distributions of v and u are still not affected by the deck acceleration. As ζ increases, v decreases where $\zeta > \ddot{z}_c$, causing a local growth of the crowd density, which is clearly visible at $t = t_2$. The resulting loss of space correlation in the total force, due to local gradients of the step frequency, cause a decrement of the deck response. At $t = t_3$, the effects of ζ on u and v have almost disappeared and the deck acceleration again starts to increase.

The uniform crowd regime III corresponds to a deck response that clearly recalls the "beating" phenomenon, which is characteristic e.g. of the response of an undamped SDOF system subjected to harmonic loading (Clough and Penzien, 1987). The natural frequency $f_s = 0.87$ Hz in fact slightly differs from the frequency of the leading force component F_{pp}, that is, $f_{pl} = 0.83$ Hz. Therefore, the deck response varies with an average frequency equal to $(f_s + f_{pl})/2$, while the amplitude varies with a rate equal to the difference between the two frequencies $(f_{pl} - f_s)/2$, that is, with

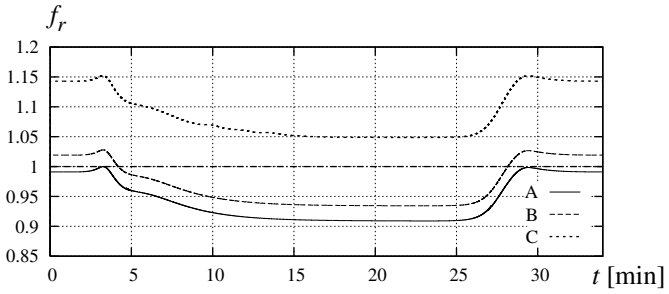

Figure 5.39. Evolution in time of f_r in $x/L = 0.3$

a period equal to 47 seconds.

A deeper insight into the simulated phenomena is provided by the time histories of the main variables in Fig. 5.41 for a characteristic time-scale of about 24 s in $x = 0.3L$. The time history of the deck acceleration is useful to interpret the other diagrams. When $\zeta > \ddot{z}_c$, the crowd velocity v proportionally decreases, while u increases. The effects of ζ are also visible in the percentages of synchronized pedestrians: n_{ps} grows with ζ and is null when the acceleration is below the critical value, while n_{pp} has a complementary evolution. As already pointed out for the previous simulations, the synchronisation among pedestrians plays a leading role. This is confermed by the evolution of the force components: the amplitude of F_{ps} is negligible with respect to F_{pp}, both because $n_{ps} < n_{pp}$ and because the $DLFs$ corresponding to the reached deck acceleration and velocity are smaller than the DLF of a motionless pedestrian (§3.4, Fig. 3.12).

As expected, the different ways in which a structure is constrained cause a change in its dynamic properties. Therefore, the footbridge can be less or more sensitive to the force exerted by walking pedestrians (according to the f_r ratio), with a consequent change in the structural response.

Concluding remarks

The results of the simulations commented on in this section highlight the major role played by the crowd added mass. In lightweight structures, the added mass has the main effect of changing the structural dynamic properties, that is, the natural frequencies, with the effect of making both the structure less, or more, sensitive to the lateral force exerted by pedestrians and the pedestrians less, or more, likely to synchronize to the structure. Therefore, as already pointed out in recent guidelines (e.g. FIB 2005), the mass of pedestrians has to be considered together with the mass of the structure in the overall dynamical system.

The structural response is also very sensitive to the crowd travel purpose.

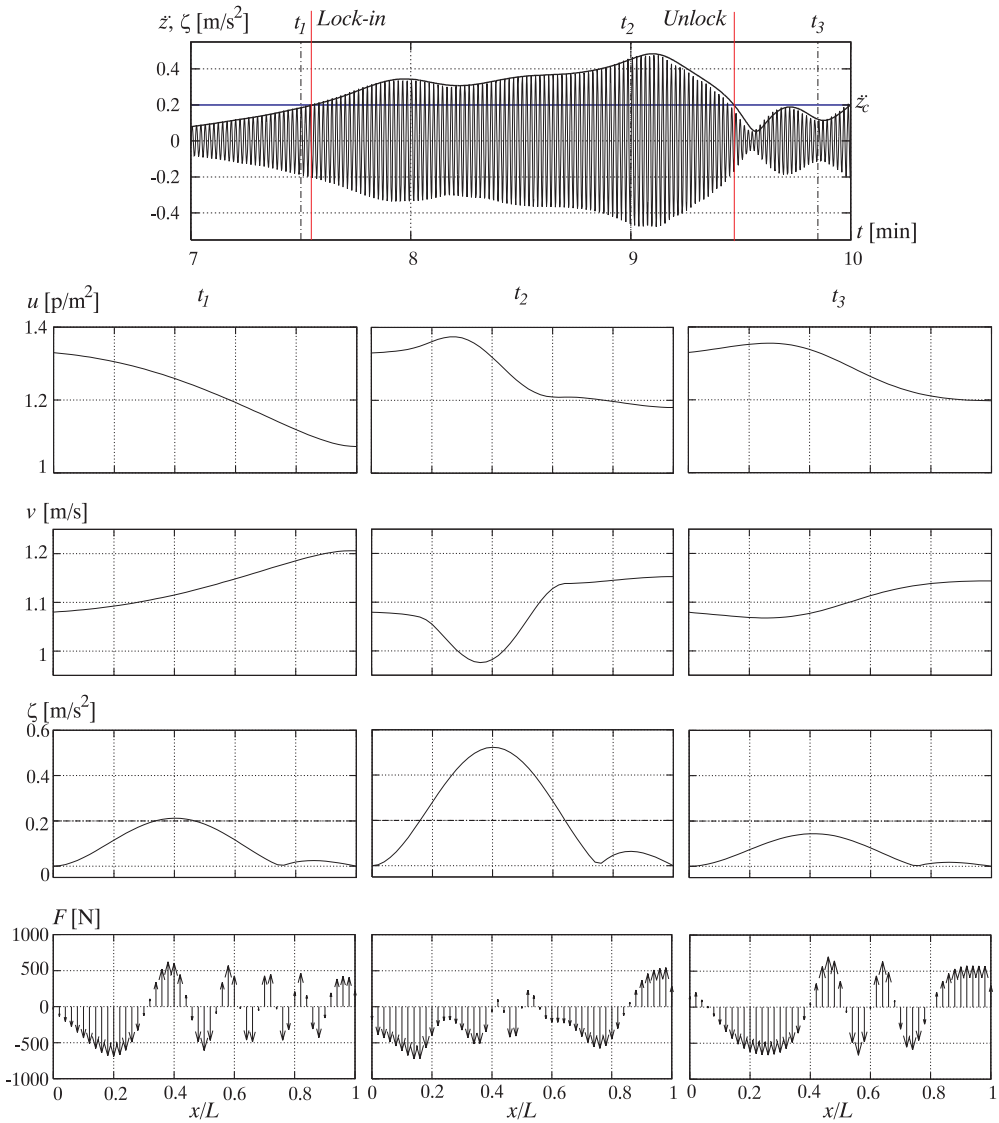

Figure 5.40. Istantaneous fields in regime II

Therefore, in the conceptual design phase, it is important to plan the kind of pedestrian traffic that is more likely to cross the footbridge (Schlaich, 2002) during its lifetime.

Quite surprisingly, a more crowded condition does not always correspond to

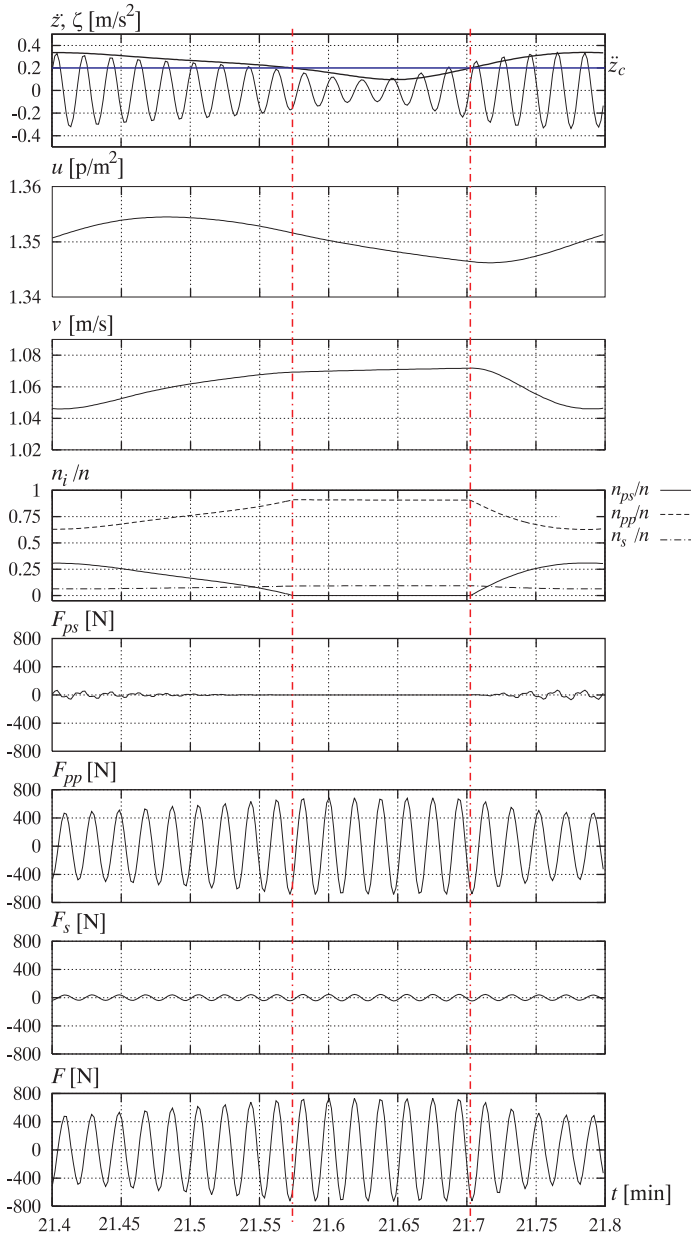

Figure 5.41. Regime III: time histories of the variables

higher deck vibrations. This result once more confirms the complexity of the coupled dynamical system. It also shows that simplified comfort criteria based on the limitation of the number of pedestrians crossing the bridge (e.g. Dallard et al., 2001) might not be effective in preventing the synchronous lateral excitation phenomenon.

Chapter 6

Conclusions

This work has tackled the problem of crowd-structure interaction in lively footbridges. The aim of the study was to develop a general modelling framework, that has been specifically characterized to simulate the synchronous lateral excitation on footbridges, in order to provide an accurate description of the most relevant features of the phenomenon and to represent a solid background for reliable and useful design tools for engineers.

The model is based on the partitioned approach, widely used in the modelling of multiphysics systems, i.e. the complex coupled dynamical system is decomposed into two subsystems, the Crowd and the Structure, separately modelled and discretised, that interact with each other. One of the most original aspects of this approach to the problem of human-induced vibration is that the crowd is not simply considered as a load, but as a dynamical system that is governed by specific laws and evolves in time and space.

The modelling of crowd dynamics has been developed in the framework of first order macroscopic modelling, which refers to the derivation of an evolution equation for the mass density, regarded as a macroscopic quantity of the flow which is assumed to be continuous. The mass conservation equation is closed by a constitutive law that links the crowd velocity to the density. A great effort has been devoted to the determination of a suitable relation, in order to sensitise the pedestrian velocity not only to the crowd density, but also to the lateral motion of the footbridge deck and to other parameters, such as the travel purpose and the geographic area. In addition, a space dislocation and a time-delay have been introduced into the closure equation to account for non-equilibrium conditions due to space gradients in the density distribution and deck response effects on crowd density, respectively.

Finally, the modelling term that provides the crowd-to-structure action has been handled by proposing a load model of the lateral action of the pedestrians. The aim of this model was to take into account some features of the synchronous lateral

excitation phenomenon, which so far has not been completely understood or modelled: the existence of two kinds of syncronization, the first between the pedestrians and the structure (lock-in) due to the deck lateral motion and the second among the pedestrians, due to high crowd density; the triggering of the lock-in and the self-limitation of the force when excessive oscillations prevent pedestrians from walking; the presence of different frequency components in the overall force.

The model has been implemented in an *ad hoc* computational code, which has been used to perform simulations of ideal or actual events. The simulation of the event recorded on the T-bridge in Japan and the parametric studies on the model parameters have in particular given relevant results from the engineering point of view. First of all, the results of a simulation of the actual event on the T-bridge gave a good correspondence to the measured data reported in literature. In addition, the sensitivity studies performed on the same benchmark allowed some important aspects to be highlighted: the crowd added mass plays a leading role in the behaviour of the dynamical system and should not be disregarded; the structural response is not linearly dependent on the number of pedestrians crossing the bridge; the structural response is very sensitive to the closure equation adopted in crowd dynamics, i.e. to the mean biometric and psychological features of the crowd.

The proposed crowd-structure interaction model has the advantage of providing a general framework that can be characterized in each of its parts to simulate a specific problem. The characterization of the model for the synchronous lateral excitation phenomenom is based both on the data obtained from literature and on the original modelling of some "constitutive laws" of the pedestrian behaviour. These laws can certainly be improved as soon as new experimental data are available.

The developed code provides a useful tool both to reproduce real events that have occurred on footbridges and to simulate different crowd scenarios and structural behaviour in the conceptual design phase. The development of a simplified revision of the code for the design of footbridges is one of the first research perspectives, in order to attain a version that will be easier to use and more widely applied. Other future developments of this work could be the extension of the model to vertical excitation and the tuning of the proposed laws by means of *ad hoc* conceived experimental tests or simulations of other case-studies.

Appendix A

The derivation of the mass conservation equation

A.1 Integral and differential forms

The one-dimensional mass conservation equation is derived in its integral and differential form (Leveque, 1992). As an example, let us consider the flow of a gas in a tube, where density and velocity of the gas are assumed to be constant across each section of the tube. Let x be the distance along the tube and $u(x,t)$ the density at point x and time t. The total mass in any given section from x_1 to x_2 is given by:

$$\int_{x_1}^{x_2} u(x,t)dx. \tag{A.1}$$

The walls of the tube are impermeable, therefore any change in the mass in the considered section is only due to gas flowing across the endpoints x_1 or x_2. The rate of flow, or **flux** of gas is given by:

$$q(x,t) = u(x,t)v(x,t), \tag{A.2}$$

where $v(x,t)$ is the velocity of the gas at point x and time t. The rate of change of mass in $[x_1, x_2]$ is given by the difference in fluxes at x_1 and x_2:

$$\frac{d}{dt}\int_{x_1}^{x_2} u(x,t)dx = u(x_1,t)v(x_1,t) - u(x_2,t)v(x_2,t). \tag{A.3}$$

Eq. (A.3) represents one integral form of the conservation law. Another form can be obtained by integrating this in time from t_1 to t_2:

$$\int_{x_1}^{x_2} u(x,t_2)dx = \int_{x_1}^{x_2} u(x,t_1)dx + \int_{t_1}^{t_2} u(x_1,t)v(x_1,t)dt - \int_{t_1}^{t_2} u(x_2,t)v(x_2,t)dt, \tag{A.4}$$

where Eq. (A.4) gives an expression for the mass in $[x_1, x_2]$ at time $t_2 > t_1$ in terms of the mass at time t_1 and the total flux at each boundary during the considered time period.

The differential form of the conservation law is derived assuming that $u(x,t)$ and $v(x,t)$ are differentiable functions. Then, replacing the following expressions in Eq. (A.4):

$$\begin{aligned} u(x,t_2) - u(x,t_1) &= \int_{t_1}^{t_2} \frac{\partial}{\partial t} u(x,t)dt \\ u(x_2,t)v(x_2,t) - u(x_1,t)v(x_1,t) &= \int_{x_1}^{x_2} \frac{\partial}{\partial x}(u(x,t)v(x,t))dx \end{aligned}$$

gives:

$$\int_{t_1}^{t_2}\int_{x_1}^{x_2} \left\{ \frac{\partial}{\partial t} u(x,t) + \frac{\partial}{\partial x}(u(x,t)v(x,t)) \right\} dx\, dt = 0. \tag{A.5}$$

Since this must hold for any section $[x_1, x_2]$ and over any time interval $[t_1, t_2]$, the integrand in Eq. (A.5) must be identically zero, i.e.,

$$u_t + (uv)_x = 0, \tag{A.6}$$

which is the differential form of the mass conservation equation. It can be solved alone only if the velocity $v(x,t)$ is known *a priori* or is a function of $u(x,t)$. In this case, the flux is a function of u only, that is, $uv = f(u)$, and Eq. (A.6) becomes a scalar conservation law for u:

$$u_t + f(u)_x = 0. \tag{A.7}$$

A.2 Scalar conservation laws

In the simplest case, the velocity v is known *a priori* and is constant, say $v(x,t) = a$ and $f(u) = au$. In this case Eq. (A.6) reduces to

$$u_t + au_x = 0, \tag{A.8}$$

which is called **linear advection equation**. If it is solved for $t \geq 0$ with initial data $u(x,0) = u_0(x)$ for $-\infty < x < \infty$ (Cauchy problem), then the solution is simply:

$$u(x,t) = u_0(x - at). \tag{A.9}$$

As time evolves, the initial data propagates unchanged with velocity a. The solution $u(x,t)$ is constant along each ray $x - at = x_0$, which are called the **characteristics** of the equation.

The main property of the solution $u(x,t)$ at any point $(\bar{x},\bar{t})$ is that it depends on the initial data u_0 at a single point, namely the point $\bar{x}_0$ such that $(\bar{x},\bar{t})$ lies on the characteristic through $\bar{x}_0$. The set $\mathcal{D}(\bar{x},\bar{t}) = \{\bar{x}_0\}$ is called **domain of dependence** of the point $(\bar{x},\bar{t})$. The size of this set has a bound of the form $\mathcal{D} \subset \{x : |x-\bar{x}| \leq a_{max}\bar{t}\}$. Conversely, initial data at a point x_0 can influence the solution only within some cone $\{x : |x - x_0| \leq a_{max}t\}$ of the $x - t$ plane, called **range of influence** of the point x_0 (Fig. A.1). Summarizing, hyperbolic equations have finite progation speed, that is, information can travel with velocity at most a_{max}.

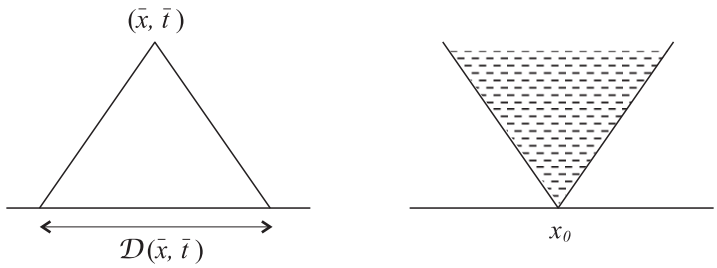

Figure A.1. Domain of dependence and range of influence

A.3 Burgers' equation

In the previous sections we made reference to linear equations. Lets now consider the non-linear scalar equation, given by Eq. (A.7) with $f(u) = \frac{1}{2}u^2$, that is, $v(u) = \frac{1}{2}u$:

$$u_t + \left(\frac{1}{2}u^2\right) = 0. \tag{A.10}$$

Eq. (A.10) can be rewritten in a quasi-linear form, recalling that $f(u)_x = f'(u)u_x$:

$$u_t + uu_x = 0. \tag{A.11}$$

This equation is called Burgers' equation or "'inviscid Burgers' equation"', since the equation studied by Burgers also includes a viscous term. It looks like an advection equation, with the advection velocity equal to the value of the avected quantity u. The characteristic are straight lines and u is constant along each characteristic.

It is interesting to study the Burgers' equation together with piecewise constant initial data having a single discontinuity: this is known as the **Riemann problem**:

$$u(x,0) = \begin{cases} u_l & x < 0 \\ u_r & x > 0 \end{cases} \tag{A.12}$$

The following two cases are possible.

Case I: Shock wave: $u_l > u_r$.
There is a unique weak solution, that is:

$$u(x,t) = \begin{cases} u_l & x < s_d t \\ u_r & x > s_d t \end{cases} \tag{A.13}$$

where

$$s_d = (u_l + u_r)/2 \tag{A.14}$$

is the **shock speed**, the speed at which the discontinuity travels. The characteristics in the two regions where u is constant go into the shock as time advances (Fig. A.2). More generally, the shock speed for scalar problems is given by:

$$s_d = \frac{f(u_l) - f(u_r)}{u_l - u_r} \tag{A.15}$$

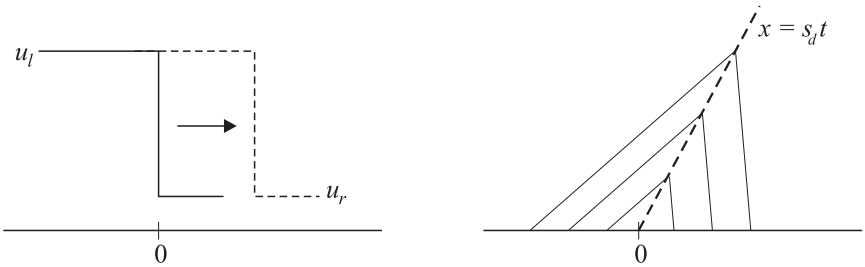

Figure A.2. Shock-wave

Case II: Rarefaction wave: $u_l < u_r$.
In this case there are infinite weak solutions. One weak solution is again (A.13) with (A.14). Characteristics go out of the shock (Fig. A.3) and this solution is not stable to perturbations, that is, if a small amount of viscosity is added to the equation, the solution completely changes.
Another weak solution is the rarefaction wave:

$$u(x,t) = \begin{cases} u_l & x < u_l t \\ x/t & u_l t \leq x \leq u_r t \\ u_r & x > u_r t \end{cases} . \tag{A.16}$$

This solution is stable to perturbation (Fig. A.4) and satisfies the entropy conditions.

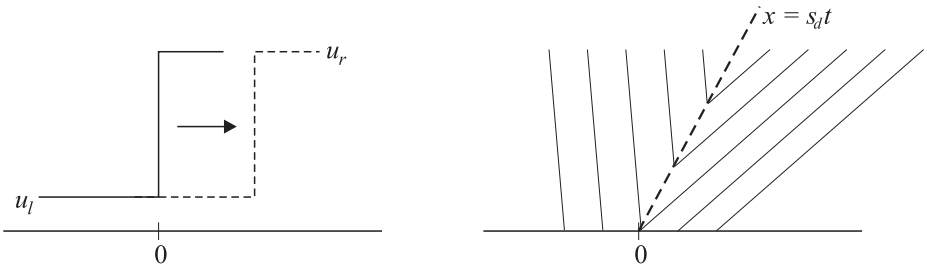

Figure A.3. Entropy-violating shock

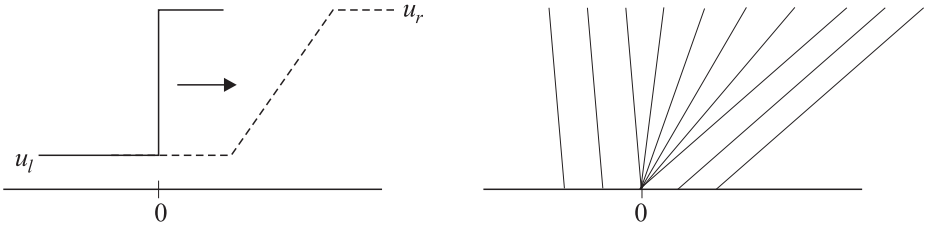

Figure A.4. Rarefaction wave

Bibliography

T. P. Andriacchi, J. A. Ogle, and J. O. Galante. Walking speed as a basis for normal and abnormal gait measurements. *Journal of Biomechanics*, 10:261–268, 1997.

H. Bachmann. Lively footbridges - a real challenge. In *Proceedings Footbridge 2002*, Paris, 2002.

H. Bachmann and W. Ammann. Vibration in structures induced by man and machines. In *Structural Engineering Documents*, volume 3a. IABSE, Zurich, 1987.

C. Barker. Some observations on the nature of the mechanism that drives the self-excited lateral response of footbridges. In *Proceedings Footbridge 2002*, Paris, 2002.

C. E. Bauby and A. D. Kuo. Active control of lateral balance in human walking. *Journal of Biomechanics*, 33:1433–1440, 2000.

A. Belli, P. Bui, A. Berger, A. H. Geyssant, and J. H. Lacour. A treadmill ergometer for three-dimensional ground reaction forces measurement during walking. *Journal of Biomechanics*, 34:105–112, 2001.

N. Bellomo and V. Coscia. First order models and closure of mass conservation equations in the mathematical theory of vehicular traffic flow. *C.R. Mecanique*, 333:843–851, 2005.

N. Bellomo, M. Delitala, and V. Coscia. On the mathematical theory of vehicular traffic flow i. fluid dynamic and kinetic modelling. *Math. Models Methods Appl. Sci.*, 12(12):1801–1843, 2002.

N. Bellomo, A. Marasco, and A. Romano. From the modelling of drivers' behaviour to hydrodynamic models and problems of traffic flow. *Nonlinear analysis RWA*, 3: 339–363, 2003.

M. L. Bertotti and N. Bellomo. Boundary value steady solutions of a class of hydrodynamic models for vehicular traffic flow. *Mathematical and Computer Modelling*, 38:367–383, 2003.

J. E. Bertram and A. Ruina. Multiple walking speed-frequency relations are predicted by constrained optimization. *J. theor. Biol.*, 209:445–453, 2001.

V. Blue and J. Adler. Emergent fundamental pedestrian flows from cellular automata microsimulation. *Transportation Research Board*, 1644:29–36, 1998.

I. Bonzani and L. Mussone. From experiments to hydrodynamic traffic flow models. I - Modelling and parameter identification. *Mathematical and Computer Modelling*, 37:109–119, 2003.

S. Buchmueller and U. Weidmann. *Parameters of pedestrians, pedestrian traffic and walking facilities, Report no. 132*. ETH, Zürich, 2006.

R. Clough and J. Penzien. *Dynamics of structures*. McGraw-Hill, New York, 1987.

W. Daamen. *Modelling passenger flows in public transport facilities*. PhD thesis, Delft University of technology, Department transport and planning, 2004.

W. Daamen and P. Hoogendoorn. Free speeds distribution for pedestrian traffic. In *TRB 2006 Annual meeting*, 2006.

P. Dallard, T. Fitzpatrick, A. Flint, S. Le Bourva, A. Low, R. M. Ridsdill, and M. Willford. The London Millennium Footbridge. *The Structural Engineer*, 79 (22):17–33, 2001.

M. Delitala and A. Tosin. Mathematical modeling of vehicular traffic: a discrete kinetic approach. *Math. Mod. Meth. Appl. Sci.*, 17:901–932, 2007.

A. Ebrahimpour and L. L. Fitts. Measuring coherency of human-induced rhythmic loads using force plates. *ASCE Journal of Structural Engineering*, 122:829–831, 1996.

A. Ebrahimpour, A. Hamam, R. L. Sack, and W. N. Patten. Measuring and modelling dynamic loads imposed by moving crowds. *ASCE Journal of Structural Engineering*, 122:1468–1474, 1996.

Z. Fang, S. M. Lo, and J. A. Lu. On the relationship between crowd density and movement velocity. *Fire Safety Journal*, 38:271–283, 2003.

C. Farhat, M. Lesoinne, and P. LeTallec. Load and motion transfer algorithms for fluid/structure interaction problems with non-matching discrete interfaces: Momentum and energy conservation, optimal discretization and application to aeroelasticity. *Comput. Methods Appl. Mech. Engrg.*, 157:95–114, 1998.

FIB. *Guidelines for the design of footbridges, Bullettin no. 32*. FIB Féderation International du Béton, Lausanne, 2005.

J. J. Fruin. *Pedestrian planning and design*. Elevator World Inc., 1987.

Y. Fujino, B. M. Pacheco, S. Nakamura, and P. Warnitchai. Synchronization of human walking observed during lateral vibration of a congested pedestrian bridge. *Earthquake Engineering and Structural Dynamics*, 22:741–758, 1993.

H. Grundmann, H. Kreuzinger, and M. Schneider. Dynamic calculations of footbridges. *Bauingenieur*, 68:215–225, 1993.

D. Helbing. Traffic and related self-driven many-particle systems. *Rev. Mod. Phys.*, 73:1067–1141, 2001.

D. Helbing. A mathematical model for the behaviour of pedestrians. *Behavioural Science*, 36:298–310, 1991.

D. Helbing and P. Molnár. Social force models for pedestrian dynamics. *Physical Review E*, 51(5):4282–4286, 1995.

D. Helbing, A. Hennecke, V. Shvetsov, and M. Treiber. Micro and macro simulation of freeway traffic. *Mathematical and Computer Modelling*, 35:517–547, 2002.

L. F. Henderson. On the fluid mechanics of human crowd motion. *Transportation Research*, 8:509–515, 1974.

S. P. Hoogendoorn and P. H. L. Bovy. A gas-kinetic model for pedestrian flows. *Transportation Research Record*, 1710:28–36, 2000.

S. P. Hoogendoorn and P. H. L. Bovy. Pedestrian route-choice and activity scheduling theory and models. *Transportation Research Part B*, 38:169–190, 2004.

R. L. Hughes. A continuum theory for the flow of pedestrians. *Transportation Research Part B*, 36:507–535, 2002.

ISO 10137. *Bases for Design of Structures Serviceability of Buildings Against Vibrations.* Geneva, Switzerland, 1992.

X. Jiao and M. Heath. Common-refinement-based data transfer between non-matching meshes in multiphysics simulations. *Int. J. Numer. Meth. Engng*, 61: 2402–2427, 2004.

W. Leutzbach. *Introduction to the Theory of Traffic Flow.* Springer, 1988.

R. J. Leveque. *Numerical methods for conservation laws.* Birkhauser, Zurich, 1992.

K. Masani, M. Kouzaki, and T. Fukunaga. Variability of ground reaction forces during treadmill walking. *J. Appl. Physiol.*, 92:1885–1890, 2002.

Y. Matsumoto, T. Nishioka, H. Shiojiri, and K. Matsuzaki. Dynamic design of footbridges. *IABSE Proceedings*, (P17/78):1–15, 1978.

A. McRobie, G. Morgenthal, J. Lasenby, and M. Ringe. Section model tests on human-structure lock-in. *Bridge Engineering*, 156(BE2):71–79, 2003.

S. Nakamura. Field measurement of lateral vibration on a pedestrian suspension bridge. *The Structural Engineer*, 81(22):22–26, 2003.

S. Nakamura and Y. Fujino. Lateral vibration on a pedestrian cable-stayed bridge. *Structural Engineering International*, 12(4):295–300, 2002.

S. Nakamura and T. Kawasaki. Lateral vibration of footbridges by synchronous walking. *Journal of Constructional Steel Research*, 62:1148–1160, 2006.

D. E. Newland. Pedestrian excitation of bridges - recent results. In *10th International Congress on Sound and Vibration*, Stockholm, 2003.

D. Oeding. Verrkhersbelastung und Dimensionierung von Gehwegen und anderen Anlagen des Fußgangerverkhers. *Strassenbau and Strassenverkherstechnik*, 22:36–40, 1963.

A. Pachi and T. Ji. Frequency and velocity of people walking. *The Structural Engineer*, 83(3), 2005.

K. C. Park and C. A. Felippa. Partitioned analysis of coupled systems. In *Computational Methods for Transient Analysis*, chapter 3, pages 157–219. T. Belytschko and T.J.R. Hughes, Amsterdam, 1983.

K. C. Park, C. A. Felippa, and C. Farhat. *Partitioned analysis of coupled mechanical systems, Report no. CU-CAS-99-06*. University of Colorado, 1999.

A. D. Pizzimenti. *Analisi sperimentale dei meccanismi di eccitazione laterale delle passerelle ad opera dei pedoni*. PhD thesis, Universitá degli Studi di Catania, Dottorato in Ingegneria delle Strutture XVII ciclo, 2005.

A. D. Pizzimenti and F. Ricciardelli. Experimental evaluation of the dynamic lateral loading of footbridges by walking pedestrians. In *6th International Conference on Structural Dynamics*, Paris, 2005.

A. D. Pizzimenti and F. Ricciardelli. The synchronization: the lessons of the wind engineering and their application to the crowd-structure interaction. In *8th Italian Conference on Wind Engineering*, Reggio Calabria, 2004.

I. Prigogine and R. Herman. *Kinetic Theory of Vehicular Traffic*. Elsevier, New York, 1971.

W. X. Ren and X. L. Peng. Baseline finite element modeling of a large span cable-stayed bridge through field ambient vibration tests. *Computers & Structures*, 83: 536–550, 2005.

F. Ricciardelli. Lateral loading of footbridges by walkers. In *Proceedings Footbridge 2005*, Venezia, 2005.

T. M. Roberts. Synchronised pedestrian excitation of footbridges. *Bridge Engineering*, 156(BE4):155–160, 2003.

M. Schlaich. Planning conditions for footbridges. In *Proceedings Footbridge 2002*, Paris, 2002.

Sétra. *Passerelles piétonnes. Évaluation du comportement vibratoire sous l'action des piétons.* Sétra, Paris, 2006.

A. Seyfried, B. Steffen, W. Klingsch, and M. Boltes. The fundamental diagram of pedestrian movement revisited. *J. Stat. Mech*, 10, 2005.

A. Seyfried, B. Steffen, and T. Lippert. Basics of modelling the pedestrian flow. *Physica A*, 368:232–238, 2006.

C. L. Vaughan. Theories of bipedal walking: an odyssey. *Journal of Biomechanics*, 36:513–523, 2003.

F. Venuti and L. Bruno. An interpretative model of the pedestrian fundamental relation. *C.R. Mecanique*, 335:194–200, 2007a.

F. Venuti and L. Bruno. Pedestrian lateral action on lively footbridges: a new load model. *SEI Journal*, 17(3), 2007b.

F. Venuti, L. Bruno, and N. Bellomo. Crowd-structure interaction: dynamics modelling and computational simulation. In *Proceedings Footbridge 2005*, Venezia, 2005.

S. Živanović, A. Pavic, and P. Reynolds. Vibration serviceability of footbridges under human-induced excitation: a literature review. *J. of Sound and Vibration*, 279: 1–74, 2005.

P. Warnitchai, Y. Fujino, and T. Susumpow. A non-linear dynamic model for cables and its application to a cable-structure system. *Journal of Sound and Vibration*, 187(4):695–712, 1995.

U. Weidmann. *Transporttechnik der Fussgänger, Ivt Report no. 90.* ETH, Zürich, 1993.

J. E. Wheeler. Prediction and control of pedestrian induced vibration in footbridges. *ASCE Journal of the Structural Division*, 108:2045–2065, 1982.

M. Willford. Dynamic actions and reactions of pedestrians. In *Proceedings Footbridge 2002*, Paris, 2002.

M. Yoneda. A simplified method to evaluate pedestrian-induced maximum response of cable-supported pedestrian bridges. In *Proceedings Footbridge 2002*, Paris, 2002.

J. Yoshida. Image analysis of human-induced lateral vibration of a pedestrian bridge. In *Proceedings Footbridge 2002*, Paris, 2002.